Spring 2005

Mechanisms of Cell Death Initiated in Herpes Simplex Virus Thymidine Kinase Expressing Colon Tumor Cells Treated with Ganciclovir and UCN-01

Christina Elizabeth Ahn
Old Dominion University

MECHANISMS OF CELL DEATH INITIATED IN HERPES SIMPLEX VIRUS THYMIDINE KINASE EXPRESSING COLON TUMOR CELLS TREATED WITH GANCICLOVIR AND UCN-01

by

Christina Elizabeth Ahn
B.A., May 1999, Austin College

A Dissertation Submitted to the Faculty of Eastern Virginia Medical School and Old Dominion University in Partial Fulfillment of the Requirement for the Degree of

DOCTOR OF PHILOSOPHY

BIOMEDICAL SCIENCES

EASTERN VIRGINIA MEDICAL SCHOOL AND OLD DOMINION UNIVERSITY
May 2005

Approved by:

Richard Drake (Director)

Richard Britten (member)

Richard Ciavarra (member)

O. John Semmes (member)

Stephen Beebe (member)

ABSTRACT

MECHANISMS OF CELL DEATH INITITATED IN HERPES SIMPLEX VIRUS THYMIDINE KINASE EXPRESSING COLON TUMOR CELLS TREATED WITH GANCICLOVIR AND UCN-01

Christina Elizabeth Ahn
Eastern Virginia Medical School and Old Dominion University, 2005
Director: Dr. Richard R. Drake

Metastatic colon carcinoma is the second leading cause of death from malignancy in the United States, and development of more effective treatments is essential. Heterologous expression of Herpes Simplex Virus Thymidine Kinase (HSVtk) in combination with the prodrug, ganciclovir (GCV), has shown great promise for the genetic therapy of many cancers, but most patients have had only a partial or minimal response to the therapy. After screening a panel of two drug combinations, our laboratory has shown that the combination of GCV and the protein kinase inhibitor UCN-01 (7-hydroxystaurosporine) enhances tumor cell death more effectively than either drug alone. However the molecular basis of this enhancement was unknown, and it was investigated by studying the effects on the cell cycle, DNA metabolism and damage signaling, and finally tested in the transgenic adenocarcinoma of mouse prostate (TRAMP) model. Colon tumor cells treated with GCV arrest in S-phase, and cells treated with the combination of UCN-01 and GCV also undergo S-phase specific cell death. However, UCN-01 treatments induced the disappearance of key mitotic proteins and had variable effects on the cell cycle.

Distinct immunofluorescence patterns, phosphorylation of histone H2AX, and elution out of agarose plugs after pulsed field gel electrophoresis were detected after UCN-01 treatment, and it was concluded that UCN-01 can cause DNA double strand breaks in treated cells. It was shown that this damage most likely resulted from UCN-01 interacting or damaging the DNA itself and was not simply due to inhibition of endogenous damage repair mechanisms.

Several HSV-TK active site variants were also studied for S-phase specific apoptosis, and it was determined that the more GCV incorporated into the DNA, the faster the S-phase arrest and the higher the levels of apoptosis were. However, a lower metabolizing variant was successful *in vivo*. GCV and UCN-01 studies *in vivo* revealed that each could reduce tumor burden; however, the combination did not show any enhanced effects.

Taken together, these results offer a significant contribution to molecular therapeutics by delineation of pathways involved in the drug response and evaluation of the treatment schemes *in vivo*.

This dissertation is dedicated to my husband Moon, my parents Tim and Dianne, and my sister Anne.

It is also dedicated in memory of Grandma Nellie, Aunt Zoe, Donna, and JoAnn. All were very special women in my life who lost their battle with cancer.

ACKNOWLEDGMENTS

I have benefited from the wisdom of many amazing family members, friends and colleagues, and so many have contributed greatly to the completion of this dissertation that I could not possibly fit all of their names here. I definitely need to thank my husband Moon for being a patient and excellent coach to get through this process. I extend many, many thanks to my major advisor Dr. Richard Drake for his mentorship that included overwhelming enthusiasm and inspiration for my research endeavors, an excellent environment to work in, and untiring editing efforts of my dissertation. I thank my committee members for their project advice and encouragement, and a special acknowledgment is due for Dr. Richard Britten for many invaluable research discussions. I am extremely grateful for the advice and support in life and science from Drs. Richard and Becky Gale, Katherine Goodbar, and Dr. Betty Stewart.

TABLE OF CONTENTS

Page

CHAPTER

Page

CHAPTER

LIST OF TABLES

LIST OF FIGURES

Figure Page

Figure Page

CHAPTER I

INTRODUCTION

Colon cancer pathway of pathogenesis

According to the American Cancer Society statistics, colon cancer is the 3rd most frequently diagnosed malignancy in the United States, and it is the 2nd leading cause of cancer related deaths. Even though many areas of research have advanced the treatment and improved the lives of patients, forty-two percent of the 134,560 newly diagnosed patients will die from colon cancer this year. Progress in understanding the etiology of colon cancer is being made using the inherited forms of this cancer as molecular models, but unfortunately, more than 80% of colon cancers are sporadic. Treatment regimes are still largely based on the use of 5-fluorouracil chemotherapies that have been in use for the last 40 years as reviewed by (1). It is now commonly believed that all cancers result from the accumulation of genetic alterations in cellular cancer causing genes. These alterations are thought to be driven by genetic instabilities. Colorectal cancer is a multifactoral disease, and while environmental factors are clearly relevant in the etiology of the condition, genetic factors have a significant input.

Over the last decade it has become clear that there are at least two major molecular pathogenic pathways leading to **colorectal cancer (CRC)**: 1) **microsatellite instability**, because of defects in DNA **mismatch repair (MMR)**; and 2) **chromosomal instability**, because of defects in the mitotic spindle

---

This manuscript follows the journal format of Cancer Research.

apparatus and other genes (2, 3). Approximately 85% of all CRCs are characterized by genomic instability and loss of normal karyotype, while the other 15% are typically from **hereditary nonpolypopsis colon cancer (HNPCC)** and have deficiencies in mismatch repair and have microsatellite instabilities as reviewed by (4). Interestingly, the pathological and clinical attributes of the cancers arising out of each of these two pathways are different in that high frequency microsatellite instability CRCs are more often located in the right colon, typically diploid, have high grade histology, and cause a prominent lymphoid reaction (5). This pathway also underlies most cases of **HNPCC** (6), and leads to cancers that display less aggressive growth characteristics causing fewer metastases and better overall survival. CRCs with chromosomal instabilities are characterized by widespread chromosomal deletions and translocations, whereas those with MSI have ubiquitous DNA mutations (7-9).

Pathogenic mutations in mismatch repair genes have been detected in a large percentage of families diagnosed with HPNCC, and **human mutL homolog 1 (hMLH1)** and **human mutS homolog 2 (hMSH2)** mutations occur in 90% of the mutations that have been identified so far. Mutations in other mismatch repair genes like hMSH6 and hPMS2 may be responsible for pathogenicity in the mutations not identified (10, 11). Microsatellite instability or replication error is seen in almost all CRC from patients with HPNCC, and in approximately 15-20% of sporadic CRC from patients with no reported family history (10). Besides point mutations, DNA methylation is also a well-known cause of the inactivation of MMR genes in HPNCC and sporadic CRC with

microsatellite instability. One small study of 37 Hungarian sporadic CRC patients revealed that the most prominent mismatch repair inactivation mechanism was the hMLH1 promoter hypermethylation. This suggests that may have a role in the pathogenesis of sporadic colorectal cancer (12).

Gene therapy for cancer treatment

There are many potential contributions of gene therapies for overcoming the vast obstacles of cancer treatment. Tumors are genetically unstable rendering them extremely adaptable to environmental changes and resistant to a variety of treatment schemes. Gene therapy could potentially restore DNA stability through transfer of normal cell cycle or DNA repair genes. Also, since tumors can acquire treatment resistance, gene therapies can be delivered to re-sensitize the tumors to treatments. Similarly, tumors that are not responsive to standard treatments because they consist of slowly dividing cells can be transduced by vectors that do not require cellular division for gene delivery and expression, such as adenovirus, herpesvirus, lentivirus, and chimeric vectors. Even tumors that have metastasized can be targeted by injectable vectors and genetic immunopotentiation strategies. Furthermore, better animal models are being created to fully understand the spontaneous nature of human tumors that varies significantly from *in vitro* studies (13). Thus, there are many gene therapy clinical trials attacking cancer from multiple fronts including: mutation compensation, molecular chemotherapy, genetic immunopotentiation and viral-mediated oncolysis (13).

HSV-tk/ganciclovir (GCV) gene therapy

The most common molecular chemotherapy system used to date to accomplish tumor cell killing has been the herpes virus thymidine kinase (HSVtk) gene combined with the pro-drug GCV. HSV-tk/GCV gene therapy has already shown initial clinical promise for glioma, mesothelioma, leukemia, and ovarian cancers (14-18). The rationale behind this system is the use of HSV-tk to selectively phosphorylate GCV to GCV-monophosphate. Cellular kinases further metabolize it to GCV-triphosphate, which becomes incorporated into the DNA and leads to cell death (19-23).

HSV-tk delivery/vectors

The most important step for the success for any gene therapy strategy is the development of an efficient vector system that is able to specifically deliver therapeutic genes into targeted cells (24). Gene transfer options include using nonviral systems such as liposomes or naked DNA or RNA injection, and mainly viral vehicles including retroviruses, adenoviruses, adeno-associated viruses, herpes viruses, and lentiviruses (13). Currently, many preclinical and clinical trials are using retroviral and adenoviral vectors containing the Herpes Simplex Virus Type-1 thymidine kinase gene (HSV-tk) in combination with the prodrug ganciclovir (GCV) (14-18). Imaging potential of HSV-tk gene therapy alive is very promising for future effective cancer treatments. Recently, a study was developed to use HSV-tk fused to the firefly luciferase gene for real-time noninvasive *in vivo* monitoring of the activity of the therapeutic gene in brain

tumor cells (25). It was determined that bioluminescence can be used reliably for repetitive quantification of HSV-tk/GCV therapeutic efficacy.

Problems with retroviruses as HSV-tK delivery systems

Worldwide gene therapy trials began to pause or halt after it was determined that two children developed leukemia after retroviral transduction of gene therapy. The two youngest recipients of the gene therapy to correct the mutation in X-linked severe combined immunodeficiency (XSCID) developed T-cell leukemia because the retrovirus inserted in front of LMO2, a known oncogene (26). The children reportedly responded well to chemotherapy, and are currently in clinical remission, however the whole ordeal has caused researchers in the gene therapy community to assess alternatives to using retroviruses for gene delivery.

The promise of adenoviruses

The most popular method of delivery for gene therapy has been using retroviruses, however, the use of adenoviruses is gaining popularity because they are highly efficient *in vivo*, high titres can be produced, tropism can be modified, and non-replicative vectors are available (13). Adenoviral delivery systems hold the promise of future gene therapy approaches because they are easily manipulated and targetable, and they remain epichromosomal, unlike retroviruses. This is important because it not only prevents a situation like what

happened in the X-SCID children, but the gene is not a permanent resident of the cell and will be cleared.

Recombinant adenoviruses and herpes viruses display high efficiency and stabilities *in vivo*, and their replication can be controlled. Despite these properties, use of adenoviruses currently has severe clinical limitations. It has been determined that ad-HSV-tk administered locally in mice could leak into the bloodstream and result in a high level of liver associated toxicity (27) and this have also been shown in an adenovirus mediated transfer of the HSV-tk gene in an ascites model of human breast cancer (28)

As mentioned above in the summary of clinical efficacy of HSV-tk, many attempts have been made to involve the immune system. For HSV-tk/GCV therapy, "the role of the immune system has been suggested since autopsy results showed a rapid and centralized hemorrhagic tumor necrosis after injection of HSV-tk modified tumor cells" (14). However, many groups have shown apoptosis induction with GCV treatment, and it has been thought that necrosis would be the only way to truly stimulate the immune system. Melcher *et al* in their 1999 review (29) concluded that enhancement of tumor killing by involvement of the immune system could be determined by a combination of factors, including: 1)the mechanism and levels of tumor cell cytotoxicity and 2) the local environment that exists within and immediately surrounding the dying tumor. Presumably, if an immune response is to be raised, the tumor cell killing must occur under specific circumstances in which the immune system can sense cell death, and this can be exploited in the design of effective therapies (29).

The immune response to HSV-tk/GCV therapy will be discussed further in relation to the *in vivo* bystander effect on page 9.

Mechanism of GCV-mediated Cell Killing

A precise mechanism for how GCV metabolites lead to tumor cell death has not been established, and there are likely many cellular processes that need to be characterized including apoptotic responses, DNA damage pathways, and regulation of the cell cycle. *In vitro*, GCV-TP has been shown to be a potent and preferential inhibitor of mammalian DNA polymerase delta (Ki=2 μM), while the K_is for DNA polymerase alpha and DNA polymerase epsilon were 80 μM and 140 μM respectively (30). In this same *in vitro* system, GCV-TP can incorporate into elongating DNA (30). This incorporation is not a chain termination, but it can significantly distort decamer duplex DNA(30). In cells expressing HSV-TK, GCV-TP is also incorporated into cellular DNA (19, 23). It has been postulated that all of these incorporation events could lead to enough DNA destabilization for strand breakage.

Thust *et al.* have determined in HSV-tk expressing CHO cells that genotoxicity and apoptosis are late events in the response of cells to GCV, indicating that the incorporation step of GCV is not decisive for triggering genotoxicity and apoptosis. In these CHO cells, a structural analog of GCV, penciclovir, could induce apoptosis with minimal genotoxicity, whereas GCV exerted higher levels of genotoxicity as revealed by sister chromatid exchange and clastogenicity assays (31). Furthermore, Tomicic *et al.* showed that GCV-

induced apoptosis was due to incorporation of the drug into the DNA resulting in replication-dependent formation of DNA double strand breaks and at later stages, cell cycle arrest at S and G2/M (32). Protection of cells against the genotoxic effects of GCV involved β-pol-dependent single nucleotide and β -pol dependent long-patch base excision repair (BER) (33). Using the β -pol inhibitor prunasin and the β -pol dependent short patch base excision repair inhibitor methoxyamine, these authors demonstrated that GCV incorporated into DNA could be subjected to repair.

Because GCV can cause severe DNA instability, Bcl-2 levels were observed to decrease as caspase 3 and caspase 9 activities increased in GCV treated CHO cells. Further disappearance of Bcl-2 was due to cleavage of that protein by caspase-9. Bcl-2 cleavage led to excessive cytochrome c release, dephosphorylation of BAD, cleavage of PARP, and finally DNA degradation (32). It appeared that in these cells, GCV-induced apoptosis was stimulated by activation of the mitochondrial damage pathway that is independent of p53. Caspase mediated cleavage of Bcl-2 can accelerate the apoptotic process, and this could explain the high potential of GCV to induce apoptosis (32). HSV-tk expressing glioma and colon tumor cells treated with GCV demonstrate a G1-S arrest, and melanoma cells have shown an arrest in S-G2 phase of the cell cycle (19, 21, 23, 34). Apoptosis occurred following the cell cycle arrest in these cells. Measurement of sister chromatid exchanges and chromosomal aberrations revealed GCV to be a very active agent classifying it as a strong clastogen (31, 35).

Bystander Effect

The bystander effect is the phenomenon that actually propelled HSV-tk gene therapy into clinical trials. Moolten *et al.* were the first to describe the bystander effect when they found that a 9:1 mixture of HSV-tk negative and HSV-tk positive cells plated at a high density was killed completely after GCV addition (36). The bystander effect is therefore defined as GCV-mediated death of HSV-tk expressing cells and adjacent HSV-tk negative cells (37, 38). The bystander effect is extremely attractive for gene therapies because it overcomes the many issues related to gene delivery efficiencies. A major mechanism for the transfer of GCV metabolites to neighboring cells was reported to be connexin43 (Cx43) mediated gap junctional intercellular communication (GJIC), and this transfer of GCV metabolites occurred within 2-4 hours of GCV addition (39). However, McMasters *et al.* determined that even cells transduced with connexin 43 did not improve overall bystander effect in all cell lines and that it would not be an effective gene therapy combination in all situations (40).

Cell to cell contact is not required for all cell lines to achieve significant bystander effect, and cytotoxicity tests have indicated that various cell lines have a full spectrum of bystander effects. Interestingly, SW620 cells were more sensitive to low concentrations of GCV (<1uM), accumulated higher levels of GCV triphosphate and higher levels of GCV incorporation in DNA compared to HT29 cells. This difference between SW620 and HT29 responding to GCV has been observed by other labs as well (39). GJIC has been implicated for many bystander situations, but this effect is not dependent on GJIC in every cell type.

This was further confirmed when Drake *et al.* showed that there can be connexin-independent ganciclovir-mediated killing conferred on bystander effect resistant cell lines by a HSV-tk expressing colon cell lines. In this study, GCV mono-, di-, and tri-phosphates could be detected in the culture medium of SW620.tk cells treated with GCV. These metabolites were most likely effluxed from the SW620.tk cells, indicating that some kind of mechanism independent of gap junctions exists for nucleotide uptake into neighboring cells (41).

Distant bystander effect

The efficiency of retroviral transduction of solid tumors for gene therapy purposes remains low, resulting in genetic modification of only a small fraction of the tumor cells. Therefore, properties of the bystander effect mentioned in the previous section, or any strategy that does not require all or most of the cells to be transduced, represents a significant advantage for therapy. In this context, the involvement of the immune system for effective tumor eradication is imperative; therefore, understanding how to manipulate therapy to promote anti-tumor responses by the immune system is a priority for gene therapy researchers. This has been assessed in many *in vivo* studies of HSV-tk/GCV therapies. In one study, one HSV-tk positive tumor was generated simultaneously with one or multiple HSV-tk negative tumors in different rat liver lobes such that there was no contact between the resulting tumors. Both the TK – and TK + tumors regressed after GCV treatment and showed infiltration with macrophages and T lymphocytes (42). The term **distant bystander** effect

involves anatomically separated tumors. Even in chemically induced rat mammary tumors, a distinct distant bystander effect occurred after treatment with HSVtk and GCV (43).

HSVtk/GCV therapy demonstrates local and distant bystander effects in a number of animal tumor models. In B16 melanoma tumor targeted by retrovirus HSV-tk vectors, cell killing was amplified locally due to the bystander killing effect. This *in vivo* killing of B16 cells in the lungs (melanoma metastes) may then elicit an antitumor immune response that appears to be at least partially dependent on T-cells since it does not occur in athymic mice (44). Treatment of HSV-tk expressing B16 cells appears to result mainly in necrotic cell death (45). Also, an HSVtk-mediated local and distant antitumor effect was observed in tumors of head and neck origin in athymic mice, and the anti-tumor effect was reduced when performed in SCID-mice (46). However, in murine hepatocellular carcinoma cells, the HSVtk gene therapy treatment can induce an immune response in immunocompetent mice, but not in nude mice suggesting that T-cell mediated immune responses may be a critical factor for achieving successful therapy results (47). It was hypothesized that the combination of the HSV-tk gene with a cytokine would enhance an overall immune response to treatment. Such cytokines tested include: IL-2, IL-4, IL-12, or GM-CSF (45).

The presence of natural killer (NK) cells within adenovirus/HSVtk and GCV treated tumors analyzed from an orthotopic mouse model of prostate cancer were identified. Furthermore, *in vivo* antibody depletion studies noted that inactivation of NK cells lessened the impact of HSV-tk and GCV on the

injected primary tumors and completely abrogated the induced systemic activities due to HSV-tk and GCV. In contrast, depletion of CD4+ and CD8+ T cells had no impact on either activity (48). Immunization of tumor bearing mice with syngeneic tumor cells prior to injection of HSVtk modified tumor cells prolonged mouse survival. However, unimmunized mice or mice immunized against HSVtk modified tumor cells showed little to no progress in survival (49).

HSVtk/GCV and multiple modality approaches

In vivo approaches

Unfortunately in previous clinical trials, a majority of the patients have experienced minor or no responses to HSV-tk/GCV therapy, while 5-10% have experienced curative or significant clinical responses. It is not clear why there are variable responses to treatment. This dilemma has prompted initiatives to improve the therapies using a variety of modalities. Clinical trials are in need of synergistic effective therapies, and several attempts are being made to evaluation combination therapies as shown in Table 1.

In vitro approaches

Immunotherapies could prove to be useful adjuvant therapies with HSV-tk/GCV gene therapy, and many other different approaches for the improvement of HSV-tk/GCV gene therapy *in vitro* have shown progress. A summary of that research is provided in the Table 2.

Table 1 *Summary of HSV-tk/GCV clinical trials using multiple modalities*

Combination	Gene delivery	Therapy delivery	Target cancer	Principle Investigator
Tumor vaccination with Her2/Neu	Retrovirus *in vitro*	Intraperitoneal	Ovarian	Scott Freeman
Radiation and surgery	Retrovirus *in vivo*	Intraperitoneal	Glioblastoma	Bernard Maria
Acyclovir and topotecan	Adenovirus *in vivo*	Intraperitoneal	Ovarian	Dirk G. Kirkpatrick
Mutigene vector: HSV-tk connexin-43 and TNFalpha	Herpes simplex virus	Intratumoral	Glioblastoma multiforme	L. Dade Lungsford
Chemotherapy and radiation	Adenovirus	Intratumoral	Locally advanced pancreatic cancer	Carlo Fernandez-del-Castillo

Table 2 *Summary of in vitro HSV-tkGCV combination approaches*

Combination approach	TK delivery mechanism	Cell lines/system	Results	Citation
TRAIL	Stable transfection	SH-EP neuroblastoma cells	Increase apoptosis and increase bystander effect	(53)
Tumor immunization		KBALB and PA-1 cells	Enhanced tumor killing	(49)
Topotecan	Adenoviral	Murine MC38 and human HT-29 Animal model	Effective in syngeneic and xenograft	(54)
Ionizing radiation	Adenoviral	Prostate cancer Animal model	↓ lung metastisis and ↑ in tumor immune cell infiltrate	(55)
Ionizing radiation	Adeno-associated virus(AAV)	Hela and HP-2 Xenografts nude mice head neck cancer	Effective and reduces toxicities of both therapies	(56)
Secondary Lymphoid tissue chemokines (SLC)	Bicistronic vector Stable transfection	B16 murine melanoma model	Enhanced antitumor and strong CTL recruitment	(57)
Hydroxyurea	Stable transfection	SW620 HT29 U251	Synergy	(58)
IL-2 and GM-CSF	Retroviral and adenoviral	Murine melanoma	Synergy	(59)
Butyrate	Stable	HCT116 SW620	Minor potentiation	(60)
Camptothecin	Stable	HCT116	Antagonistic	(60)
Taxol	Stable	HCT116 SW620	Antagonistic	(60)

Herpes Simplex Virus Thymidine Kinase Variants

Modifications of the wild type HSV-tk1 have been pursued as another way to improve HSV-tk suicide gene therapy. Black *et al* generated one TK variant that mediated markedly enhanced tumor cell killing *in vitro* and *in vivo* compared with wild type thymidine kinase. The variant was reported to have increased preference for phosphorylating GCV and ACV over the competing natural substrate, thymidine (50). Specific active site HSV-tk variants were generated and shown to increase tumor cell killing over the others prostate cancer model both *in vitro* and *in vivo* (51). Furthermore, Kelly E. Mercer, a previous graduate student in the Drake laboratory, designed, purified, and characterized 16 mutant HSV-tk enzymes and determined that variants Q7530 and N7530 were GCV specific kinases (52). All of the variants had lower deoxythymidine phosphorylation activities relative to GCV phosphorylation, and the Q7530.tk had higher GCV activity than wild type HSV-tk.

Furthermore, even though there are many reports in the literature demonstrating the antitumor activity of HSV-tk/GCV, information on the metabolism and cytotoxic mechanism is sparse. **Using a well-characterized second drug with HSV-tk/GCV could not only potentially improve clinical treatments, but it could also aid in delineating the molecular mechanism of HSV-tk/GCV cell killing.** Our lab had previously reported that colon tumor cell lines expressing HSV-tk treated with GCV and the staurosporine derivative, UCN-01 led to increased induction of apoptosis and cell killing rates compared with either drug alone (60).

UCN-01 (7-hydroxystaurosporine)

Staurosporine is a fungal metabolite isolated from *Streptomyces*, and it potently inhibits the activity of all protein kinase C (PKC) enzymes(61). Although staurosporine has been characterized as the "universal inducer" of apoptosis *in vitro* (62), animal trials have revealed its lack of clinical efficacy (63) . This has prompted efforts to design staurosporine derivatives demonstrating high efficacy *in vivo.* (As reviewed in (64)) UCN-01 is one such derivative (63), and has shown great clinical promise. UCN-01 is being used as a single agent for the treatment of cancers such as lymphoma and melanoma. (www.clinicaltrials.gov) However, since UCN-01 was found to have a prolonged pharmacological half-life due to its affinity for alpha-1-acid glycoprotein in the blood (65), the majority of these trials are using UCN-01 in combination with other chemotherapeutic drugs, and a summary of those trials is provided in Table 3.

Recently, Sparreboom *et al.* reported extensive binding of UCN-01 to alpha-1-acid glycoprotein (AAG) after obtaining pharmokinetic data from a group of 41 cancer patients receiving UCN-01 as a 72-hour intravenous infusion. This may partially explain the fact that UCN-01 has had a small volume of distribution and slow systemic clearance. Furthermore, it was determined that measurement of UCN-01 plasma concentrations is a poor representation of pharmacologically active fraction of unbound drug. (66)

Table 3 *Summary of UCN-01 clinical trials from actively recruiting through recently completed. (www.clinicaltrials.gov)*

Clinical Trial	Target cancer
Actively Recruiting as of November 2004	
UCN-01 and Fluordabine	Lymphoma and Leukmia
UCN-01 single agent	Relapsed T-cell Lymphomas
UCN-01 and Topotecan	Recurrent, Persistent, or Progressive Advanced Ovarian Epithelial, Primary Peritoneal, or Fallopian Tube
UCN-01 and Irinotecan	Advanced solid tumors
UCN-01 and carboplatin	Advanced Solid tumors
UCN-01 and prednisone	Lymphoma
UCN-01 single agent	Metastatic melanoma
UCN-01 and cisplatin	Advanced solid tumors
No Longer recruiting	
UCN-01 and Cytarabine	Refractory or Relapsed Acute Myelogenous Leukemia or Myelodysplastic Syndrome
UCN-01 and cisplatin	Advanced or metastatic solid tumors
UCN-01 and fludarabine	Chronic Lymphocytic Leukemia or Lymphocytic Lymphoma
Completed	
UCN-01 and Topotecan	Recurrent Ovarian Epithelial Cancer, Fallopian Tube Cancer, or Primary Peritoneal Cavity Cancer
UCN-01 and fluorouracil	Metastatic pancreatic cancer
UCN-01 and fluorouracil	Advanced or refractory solid tumors
UCN-01 and gemcitabine	Unresectable metastatic pancreatic cancer
UCN-01 and Fluorouracil and Leucovorin	Metastatic or unresectable solid tumors
UCN-01 single agent	Lymphoma and Leukemia
UCN-01 and Fluorouracil and Leucovorin	Dose Determination
UCN-01 continuous infusion single agent	Breast, lymphoma, and prostate cancers

UCN-01 molecular mechanism

UCN-01 can induce cell cycle arrest at the G1 checkpoint, but it can also abrogate cell cycle arrest induced by cytotoxic DNA damaging agents like cis-platin, araC, or ionizing radiation, UCN-01 has been shown to abrogate S or G2 cell cycle arrest and promote tumor cell death (64, 67). This property has been attributed to the fact that UCN-01 is a potent inhibitor of Chk1 (IC_{50}=5-11nM) but not Chk2 (IC_{50}>1000nm) (as reviewed by (68)). One function of Chk1 is to phosphorylate the cdc25c phosphatase at residue Ser216 (69, 70). The phosphorylated cdc25C is recognized by a 14-3-3 protein and forms a complex that is sequestered in the cytoplasm (69-71) that prevents premature cdc25c-mediated dephosphorylation (and activation) of cdk1/cyclinB. The phosphorylated form functions to maintain cells in G2 arrest following DNA damage (72). Thus, a current model is that the inhibition of Chk1 by UCN-01 in DNA damaged cells (i.e. G2 phase arrest) leads to activation of cdc25C phosphatase, subsequent dephosphorylation of cdk1/cyclinB, and accelerated tumor cell death due to abrogation of the G2 checkpoint and entry into mitosis (73-75).

UCN-01 is commonly categorized as a PKC or CDK (cyclin dependent kinase) inhibitor, but it is unlikely that interference with those protein classes are responsible for all the reported effects that UCN-01 has on cells. UCN-01 is a potent inhibitor of PDK1 (phosphatidlyinositol dependent kinase 1), and unlike its parent compound staurosporine, the 7-OH group generates direct and water-mediated hydrogen bonds with residues in the active site of PDK1 (76), and

therefore directly interferes with the PDK1-AKT survival signaling pathway (77). UCN-01 has also been shown to inhibit the RAF/MEK and AKT pathways in leukemia cells (78), and it has been reported to inhibit nucleotide excision repair in response to DNA damage caused by cisplatin by attenuating XPA and ERCC1 nucleotide excision repair proteins in chronic lymphocytic leukemia lymphocytes (79). In human ovarian tumor cells, UCN-01 inhibits the cisplatin-induced ubiquitination and shift of RNA polymerase II (RNAP II) from the hypophosphorylated IIa to the hyperphosphorylated IIo, without affecting basal levels of those forms of the RNAP II CTD (c-terminal domain). This suggests that UCN-01 is **inhibiting** some of the kinases involved in the conversion that is important for ubiquination of RNAP II and its subsequent degradation (80).

In colon cancer cells (HT-29), UCN-01 markedly reduced the expression of Bcl-X_L while enhancing the level of p38 MAPK, and the overexpression of Bcl-X_L significantly blocked the apoptosis induced by UCN-01 (81). Since UCN-01 can block the phosphotransferase activity of many kinases by preventing access of ATP to its binding site on the enzymes, several proteins exhibiting kinase activity involved in double strand break repair could also be inhibited by UCN-01. Currently, only the combination of UCN-01 and camptothecin has been shown to induce DNA double strand breaks in p53 mutant tumor cells, but not in normal p53 positive epithelial cells (82). UCN-01 has been shown to sensitize a lymphoma patient to a high dose chemotherapy cocktail, EPOCH II (etoposide, prednisone, vincristine, cyclophosphamide, doxorubicin) (83). In addition, multiple fresh surgical specimens obtained from gastric and colorectal cancer

patients also appear to be particularly sensitive to UCN-01 treatment, and this response to UCN-01 is more cytotoxic to conventional chemotherapies such as mitomycin and cisplatin (84). A summary of UCN-01 combination approaches that have been reported to enhance cell killing or tumor reduction is provided in Table 4.

The drugs in combination with UCN-01 have a full spectrum of mechanisms of enhanced cell killing. We have hypothesized that UCN-01 effects cell cycle, checkpoints, and cell death and DNA damage signaling mechanisms. In the remaining sections, an overview of those areas will be presented.

Cell cycle and DNA damage repair

Cell cycle checkpoint signaling networks monitor the successful completion of each event during eukaryotic cell cycle progression prior to proceeding into the next phase. Cells can temporarily arrest their metabolic activities associated with DNA replication of mitosis at these checkpoints to allow for repair of any damage, dissipation of exogenous cellular factors, or for the accumulation of essential nutrients and growth factors. The basic outline of cell cycle progression is as follows: G_1 is defined as the phase of the cycle where cells develop a metabolic state suitable for growth and division; S-phase is where the cells are committed to doubling their genomic information; G_2 phase is where the cells prepare for final checks before commitment to mitosis and subsequent division into two daughter cells. Signaling may also activate pathways leading to

Table 4 *Summary of UCN-01 combination approaches in vitro and in vivo*

Compounds combined with UCN-01 resulting in increased cell killing or tumor reduction	Cell line/ model	Citation
Gemcitabine	Human myeloid leukemia	(85)
Cisplatin	A549	(79)
Cisplatin	CHO	(86)
Cisplatin	Human breast cancer cells	(87)
Camptothecin	MDA-MB-231 HMEC HE6	(82)
Camptothecin	HT29 HCT116 MCF-7	(88)
Mitomycin C	A431 HCT116 MCF-7	(89)
Mitomycin C	A431 Murine Leukemia	(89)
Ara-C	U937 HL-60	(90)
Ara-C	HT-29	(91)
TRAIL	U937	(92)
17-AAG	U937 HL-60	(78)
MEK Inhibitors PD98059 And U0126	U937 HL-60	(93)
Nucleside analogs: gemcitabine ara-c, f-ara-A, FMdC	Leukemia	(85)
5-Fluorouracil	SK-GT5	(94)
4-HC UV	Normal and leukemic lymphocytes	(95)
Perifosine	PC-3 A549	(96)
Tamoxifen	Human breast cancer *in vitro* and *in vivo*	(97)
Radiation	Non-small cell lung carcinoma	(98)
Danazol and mifepristone	Hormone responsive breast cancer	(99)
ATF-2 derived peptides	Melanoma	(100)
GCV	SW620.tk	(60)

programmed cell death if the damage cannot be properly repaired. (as reviewed by (101))

A sophisticated DNA damage response pathway sensing aberrant DNA structures has evolved in mammalian cells to ensure their long-term survival. Activation of this pathway causes stimulation of DNA repair complexes, and cell cycle arrest, and if the damage cannot be repaired, the cell is committed to apoptosis. The eukaryotic strategy to handle damaged DNA can be split into three stages: the recognition of injured DNA, a period of damage assessment, regulated by checkpoints, and the implementation of the appropriate response- DNA repair or cell death. These responses are not activated in a linear fashion because damage recognition elicits multiple synchronous signals that can trigger both repair and apoptotic processes. (as reviewed in (102)).

Three robust DNA damage repair systems have evolved for the protection of eukarytotic cells including: nucleotide and base excision repair (NER and BER), mismatch repair (MMR), and double strand break (DSB) repair. Double strand breaks are the most lethal, as they are not all accurately repaired due to non-homologous end rejoining. In contrast, altered bases and single strand breaks are more readily repaired. Secondary effects of DNA damage can arise if the damage is not repaired leading to DNA fragmentation, deletions, and chromosomal rearrangements. (as reviewed in (102).

Excision Repair

Nucleotide excision repair (NER) is primarily used to excise bulky adducts crosslinked to the oligonucleotide, and oxidative DNA damage is also repaired by NER. This mechanism of repair is very flexible and it corrects damage that both distorts the DNA molecule and alters the chemistry of the DNA molecule. This repair involves damage recognition; binding of a protein complex at the damaged site; double incision of the damaged strand several nucleotides away from the site of damage; exicision of the damage followed by filling in by a DNA polymerase and ligation (103). Base excision repair (BER) is the main system for removing small base damages including oxidative DNA lesions. In contrast to NER, BER employs DNA lesion-specific glycoslyases to recognize and bind to the damaged site, and then they remove the base. The resulting abasic site is cleaved to remove the 5-1-deoxyribose phosphate and the one-nucleotide gap is closed by DNA polymerase (104, 105).

Mismatch repair (MMR)

The DNA mismatch repair system is involved in the correction of base/base mismatches and insertion/deletion loops arising during replication, and monitors closely the newly synthesized DNA strand for incorrect or mismatched bases which are removed and replaced by the correct equivalents (11). DNA excision repair and MMR overlap to some extent, and MMR is not only involved in the repair of chemical damage to DNA but is also involved in processing of recombination in intermediates. Both hMSH2 and hMLH1 (missing

in the HCT116 colon tumor cell line) have recently been shown to be a part of a super complex of BRCA-1 associated proteins also containing MSH6, ATM, NBS1, and MRE11, and this complex is believed to act as a DNA damage sensor and to participate in the recognition and repair of aberrant DNA structures (106, 107). Detection of this repair complex after DNA damage would also reveal the level of damage and potential mechanism of drug action.

Double Strand Breaks and associated repair mechanisms

Double strand breaks are a severe threat to the maintenance of genomic integrity. They can be produced endogenously by DNA replication, through processes such as V(D)J recombination and meiosis, some chemotherapeutic drugs, hydroxyl radicals, ionizing radiation, and unrepaired single strand breaks (as reviewed in (108)). If left unrepaired, DSBs can result in permanent cell cycle arrest, induction of apoptosis, or mitotic cell death caused by loss of genomic material. The two main strategies to repair DSBs are homologous recombination repair (HRR) and non-homologous end joining (NHEJ) (108).

Nonhomologous end joining (NHEJ)

The major pathway for repairing DSBs in mammalian cells is NHEJ which repairs broken DNA ends with little or no requirement for sequence homology. It involves the XRCC4 gene product (109), DNA ligase IV (110) and the DNA-protein kinase (DNA-PK) holo-enzyme (111), consisting of the DNA end-binding heterodimer Ku70/Ku80 and the catalytic subunit DNA-PKcs. Ku70 and Ku80

bind to free ends, DNA-PKcs associates with Ku-signals (112), NBS and Rad50 stimulates Mre11 exonuclease and they process the DSB, and finally XrCC4 binds to Ku and targets the ligase IV to the break (113). ATM and ATR share homology in their kinase domains with the DNA DSB repair protein DNA-Pk catalytic subunit (DNA-PKcs). In vertebrates, Ku serves as the DNA targeting subunit of DNA-PKcs which together forms the DNA-Pk holoenzyme. The catalytic subunit alone is ~465 kd, and the c-terminal domain shares homology with the catalytic domains of proteins in the phosphotidyl inositol 3-kinase-like family (PIKK). (as reviewed in (108))

Homologous recombination repair (HRR)

HR is an essential DNA damage repair pathway for cell survival, and it is involved in the repair of DNA double strand breaks and DNA lesions that occur at replication forks. It involves the genetic exchange between DNA sequences that share homology. A classical double strand break cuts the DNA strand leaving two free DNA ends that may both initiate recombination. Also, a double strand break can arise if a replication fork collides with an unrepaired DNA single strand break causing a collapsed replication fork, and these DSBs trigger HRR in mammalian cells even though they only have one free DNA end to initiate the repair. HRR has also been implicated in the repair of stalled replication forks that can occur without detectable DSBs (114).

DNA damage signaling

The sequestration of molecules by scaffold proteins is a familiar concept in the field of protein signaling and imposes order and substrate specificity on proteins that are common to several pathways. The existence of such regulatory supercomplexes within the nucleus would be a necessity given that crucial repair nucleases cannot be allowed to diffuse freely. Recently, the BASC, BRCA1 associated genome surveillance complex, has been described as a supercomplex of tumor suppressors and DNA repair proteins (115). Detection of these foci, which suggests a DNA damage protein supercomplex response, would help delineate the signalling pathway that potentially indicates double strand breaks.

Breast Cancer 1 (BRCA1)

BRCA1 is the 220kd protein product of Breast Cancer susceptibility gene1, and it is a major target of a DNA damage response. The DNA dependent kinases ATM and ATR are known to phosphorylate BRCA1 in response to ionizing radiation. BRCA1 has been shown to function in genomic stability by controlling homologous recombination, transcription-coupled repair of oxidative DNA damage (specifically NER), and cell cycle checkpoints (115). Furthermore, BRCA1 deficient cells fail to appropriately check in S and G2 after DNA damage (As reviewed by (116)). BRCA-1 coimmunoprecipitates with a number of DNA repair proteins including: MSH2, MSH6, ATM, Rad51, and the Rad50-Mre11-

NSB protein complex, and it is known to localize to nuclear foci with these proteins after ionizing radiation and UV radiation (117).

Ataxia telangiectasia mutated (ATM) and

Ataxia telangiectasia mutated and Rad 3 related (ATR)

ATM and ATR are crucial in detecting the most lethal type of DNA damage, the double strand break, and they have distinct but overlapping substrate specificities including the abilities of both enzymes to target p53 (Ser-15) and BRCA1 (Ser-1423). They are both members of the phosphoinositide 3 – kinase like kinase (PIKK) family which includes ATM, ATR, and DNA-dependent protein kinase (DNA-Pk). ATM (350kD) phosphorylates numerous targets that mediate cell cycle checkpoints and DNA repair including Chk2, 53BP1, and H2AX (118-120). It is thought that large kinases are required to detect DNA damage so that they can provide a platform over which other detectors and repair proteins can assemble (102).

Chk1 and Chk2 protein kinases

Chk1 and Chk2 are ubiquitously expressed serine/threonine kinases and are critical for signaling DNA damage to cell cycle regulation proteins dependent on the ATM family of protein kinases (121-123). While the phosphorylation of its activation loop is not required for Chk1 activation, it is required for the activation of Chk2. Chk1 functions as an essential component of the G2/M checkpoint while Chk2 is required at G1/S for at least low dose ionizing radiation. Even

though the role of Chk1 in DNA damage signalling is not clear, Chk2 is thought to potentially act through BRCA1. Chk2 is a tumor suppressor and is important for DNA damage-induced apoptosis, while Chk1 does not have this property (68)

p53 binding protein (53BP1)

53BP1 was originally isolated as a p53 interacting protein using yeast two hybrid screens (124). It contains numerous (S/T)Q motifs and two C-terminal BRCT (BRCA1 carboxyl-terminal) repeats. 53BP1 proteins are phosphorylated in response to gamma IR, and IR causes 53BP1 proteins to rapidly relocalize to DNA repair foci. These foci also overlap with BRCA1 and gamma H2AX DNA damage induced foci. Gamma H2AX recruits 53BP1 to nuclear foci and physically interacts with 53BP1 (120, 125). Mice that are defective for 53BP1 are radioresistant, immune deficient, and predisposed to cancer. Also, a fragment of 53BP1 co-localizes with autophosphorylated DNA-PKcs at nuclear foci and can stimulate DNA end joining *in vitro* both suggesting that 53BP1 could play a role in NHEJ (as reviewed in (126)).

Histone 2AX (H2AX)

In addition, there is a method to indirectly monitor the presence of individual DSBs. Within a few moments after the induction of a DSB, hundreds to thousands of histone H2AX molecules are phosphorylated by DNA-PK in a chromatin domain several mega base pairs around the break site. Using an antibody specific for the phosphorylated form, γH2AX, these chromatin

modifications can be visualized within the cell nucleus by fluorescence microscopy. Currently, all evidence available points to a direct correlation between these modifications and the presence of DSBs (127). Recently, phosphorylation of H2AX was shown to be regulated by acetylation, and this supports the finding that histone acetylation critically functions in repairing DNA DSBs (128).

The role of these multiple DNA damage response and regulatory pathways in cells treated with GCV and UCN-01 is largely unknown, but will be further evaluated in this dissertation.

Goals of dissertation

Our **long-range-goal** is to improve HSVtk gene therapy on many fronts by enhancing or modulating the bystander effect (Cx-43, MRP-4), obtaining tumor specific gene expression (b-catenin responsive) and delivery of the enzyme with adenovirus vectors, improving the catalytic efficiency or substrate specificity of HSV-TK for GCV, and optimizing chemotherapy modalities (UCN-01 + GCV). All of these research arms for improving HSV-tk gene therapy are interrelated, and they have each generated useful data and tools for the specific angle of the project that is the subject of the dissertation.

The **objective** of these studies was to identify the molecular basis of the synergistic cell killing of the GCV and UCN-01 combinations by evaluating cell death and DNA damage response mechanisms. The **central hypothesis** for the our research was that the S-phase arrest and DNA damage pathway initiated

after GCV treatment sensitizes the cells to the treatment with UCN-01 because it prevents repair of GCV damage and causes further damage itself. A better understanding of the individual and synergistic mechanisms of the actions of GCV and UCN-01 could lead to the design of improved gene and chemotherapeutic combinations. Potentially, new molecular targets will be identified for further characterization and/or drug targeting.

Aim # 1:

Evaluate the role of the cell cycle, cell death mechanisms, and proteomic effects of cells treated with HSV-tk/GCV and UCN-01 drug combinations. HSV-TK expressing tumor cells were synchronized, drug treated, and evaluated by DAPI staining, western blotting for cell cycle proteins, DNA metabolic labeling, flow cytometry, caspase assays, and bromodeoxyuridine labeling. Surface Enhanced Laser Desorption Ionization Time of light mass spectroscopy and two dimensional gel electrophoresis were used as global proteomic approaches to study cancer cell hallmarks and proteome responses to GCV and UCN-01 treatment combinations.

Aim # 2:

Determine the signaling network and cause of DNA damage after treatment with GCV, UCN-01, and the combination. Immunofluorescence and western blotting of proteins involved in the DNA damage-signaling network, pulsed field

gel electrophoresis, and specific DNA repair inhibitors were used pinpoint the cause and execution of DNA damage and signaling.

Aim # 3:

Evaluate wild type and enhanced function HSV-tk variants in *in vitro* and *in vivo* TRAMP model combined with UCN-01. Similar methods used in Aim #1 were used to characterize the cell cycle and cell death mechanisms of HSV-tk variants. Transgenic adenocarcinoma murine prostate (TRAMP) cells were stably transfected with the TK variants and tested in an *in vivo* TRAMP model in addition to UCN-01 and GCV drug combinations. Animals will be injected with tumor cells and treated with the drugs after tumors are palpable. These initial animal studies will include tumor measurements and H&E staining of the excised tumors.

CHAPTER II

MATERIALS AND METHODS

Materials

UCN-01 was obtained from the Developmental Therapeutics Program, National Cancer Institute, National Institutes of Health. 10mM stocks were stored in DMSO at –20C and 30-1000nm were used in assays; Ganciclovir was obtained by prescription and stocks were made in water and concentration determined UV adsorbance. Concentrations used were between 0.1-100μm. Lactacystin was from Sigma (St. Louis, MO) and 10μM were used in assays; Caffeine was from Sigma (St. Louis, MO) and 1-6mM concentrations were used in assay; NU7026(2-(morpholin-4-yl)-benzo[h]chromen-4-one),a DNA-Pk specific inhibitor, was from Calbiochem(San Diego, CA) and 8.9 mM stocks were made in DMSO and stored at –20°C;10-100 μm was used in assays; Methoxyamine was from Sigma (St. Louis, MO) and 1.2 M stocks were made in water and stored at –20°C; concentrations between 3-20 mM were used. Nitrocellulose blotting membranes were from Schleicher and Schuell (Keene, NH); MTT (3-(4,5-dimethylthiazol-2-yl)-2,5-diphenyltetrazolium bromide) was from Sigma (St. Louis, MO); BrDU metabolic labeling kit was from BD Biosciences (San Diego, CA); Caspase Activation Kit was from Clontech (San Diego, CA); ApopTag™ apoptosis kit wasfr om Serologicals Corporation (Norcross, GA).

Antibodies for western blots and immunofluorescence microscopy

Primary Antibodies:

Cyclin B and cyclin A were from Pharmagen (Hauppauge, NY); Cdk1 and cdk1-p were from Cell Signalling (Beverly, MA); Bcl-X_L was from Transduction Laboratories, Inc. (Lexington, KY); Cdc25C, Chk1, and Chk2 were from Santa Cruz Biotechnology (Santa Cruz, CA); Phospho-Chk1 (Ser345) and Phospho-Chk2 were from Cell Signalling Technology (Beverly, MA); γH2AX (phosphorylated Histone 2AX) was from Trevigen (Gaithersburg, MD); BRCA and 53BP1 were from Bethyl Laboratories (Montgomery,TX)

Secondary Antibodies:

HRP-conjugated goat-anti-rabbit and goat-anti-mouse secondary antibodies were from Bio-Rad (Hercules, CA). Alexa Fluor 488nm and 546nm goat anti-mouse and anit-rabbit IgGs were from Molecular Probes/Invitrogen (Eugene, OR)

Cell Lines

HSV-TK Expressing Cell Lines

The three HSV-TK-expressing human colon tumor cell lines and one HSV-tk- expressing human breast cancer cell line (SW620.TK, HT-29.TK, HCT-116.TK, and MCF-7.tk) were maintained in RPMI 1640 supplemented with 10% FBS. Each HSV-TK expressing cell line was previously generated following transfection and G418 selection with a bicistronic HSV-TK/neo Moloney Murine Leukemia Virus-derived plasmid, pLTKEN, as previously described (23). Each

cell line was characterized for sensitivity to GCV cell killing and HSV-TK expression (23).

Normal Colon Cell Lines

CSC-1 and NCM 460 cells were obtained from InCell™ Corporation (San Antonio, TX) and maintained in InCell™ M3:10 media.

Cell Viability Assays

The cell line of interest was seeded in 96 well plates in 0.1 ml media (7,000 cells/well). After 48 hrs, MTT (3-(4,5-dimethylthiazol-2-yl)-2,5-diphenyltetrazolium bromide) (50 µg/well) was added for 1.5 hours, followed by DMSO (dimethyl sulfoxide) solubilization of the cells and absorbance readings at 540 nm (129). Data were recorded in Excel and graphed relative to percent of untreated control values.

Clonal Dilutions

Cells ($1X10^5$) were seeded in 24 well plates, and after 24 hours, different drug treatments were added. After another 24 hours, the media was removed, and the cells were rinsed and treated with trypsin. After addition of 1 ml fresh medium, each of the wells was then sequentially diluted from 1:10 to 1:10,000 in 1ml of medium in a separate 24-well plate. After 7 days, surviving cell colonies were fixed in 100% methanol, stained with 0.1% methylene blue and counted.

Clonal Survival Assays

2000-3000 cells were plated/ well in 24-well plates. Different drug treatments were added 24 hours later. After 7 days, surviving cell colonies were fixed in 100% methanol, stained with 0.1% methylene blue and counted.

Cell synchronization

HSV-TK expressing cells were synchronized by the double thymidine block method (130). Initially, 10^5 cells were plated in a 60mm plate. The following day, 2 mM thymidine was added to each well for 16 hours. After extensive rinsing of the cells, fresh media (without thymidine) was added to each well for 9 hours, followed by subsequent addition of 2 mM thymidine for an additional 16 hours. Following this second thymidine block and rinsing, cells were incubated in media plus or minus the chemical or drug of interest.

Radiation exposure

Double thymidine blocked SW620.tk cells ($2.4X10^6$) were resuspended in 6 mls of media in 15ml conical tubes and were exposed to 4 Gy or 12 Gy of radiation via a Cesium-137 source in a lead chamber apparatus. After radiation, cells ($0.4X10^6$) were seeded in 6-well plates. Cells were treated with either radiation only or an addition of UCN-01. Control cells were taken from the cell suspension prior to radiation.

Cell cycle analysis

For cell cycle analysis, cells were fixed in 70% ethanol, stained with propidium iodide and analyzed by flow cytometry on a FACSCalibur instrument (Becton Dickinson, Mountain View, CA) as previously described (23).

Western Blot Analysis

Prior to loading onto the SDS-PAGE gel, 1ul was used in a Bradford assay (BioRad) to determine protein concentration. Pelleted cells were resuspended in 75ul of dH20 and then 25ul of sample loading buffer (4M Urea, 20mM DTT, 100mM Tris pH 8.0, 4%SDS and Bromophenol Blue) were added immediately after samples were resuspended in the water. Samples were boiled for 5 minutes prior to loading. Usually about 80-120ug of protein were added per well. Equal loading was measured by protein loaded, gel staining, and β-actin western blots. 10% SDS-PAGE gels were used for western blots of proteins between 30 and 80kd. Gels were run overnight at 8mA per gel. Proteins were transferred to nitrocellulose (Schicher and Schuell) at 100V for 1 hour at room temperature. Michelle Wezeman was responsible for cdc25C, cyclin B and Cdk1/Cdk1-P in the SW620.tk cell line westerns shown in Figure 5.

Metabolic Labeling with Bromodeoxyuridine (BrDU)

SW620.tk or SW620 parent cells ($2.7X10^5$) were plated in 60mm plates with 0 or 10μM BrdU, and the next day 2mM thymidine was added. After 16 hours, the thymidine was rinsed from the plates 2 times, and media and BrDU

were added for 9 hours outgrowth followed by the second addition of 2mM thymidine for the plates not pulsed. 16 hours later, the plates were rinsed 2 times and the preincubation BrDU was removed and the media and drugs were added to the plates. BrDU was only added to the plates without the preincubation for a 2-hour pulse before their harvest. HSVtk variants cells lines were not synchronized, and were only pulsed with BrDU.

10^6 cells were harvested for flow preparation and resuspended in the BD Cytofix/Cytooperm buffer and incubated for 15-30 mins at room temperature. Cells were washed with 1ml of the BD/Perm/Wash buffer and centrifuged at 200-300g for 5 minutes. Cells were then resuspended in BD cytoperm plus buffer and incubated for 10 min on ice and washed as mentioned above. Cells were re-fixed with Cytofix/Cytooperm buffer and washed. Then the pellet was resuspended with 100ul of DNAse (30ug per sample) and cells were incubated at 37C for 1 hour. Cells were washed and then stained with 20µl of 7-AAD solution. Also, 1 ml of staining buffer was added to each tube to further resuspend the cells. Cells were analyzed by flow cytometry. Analysis assistance was provided by Dr. Richard Britten and Ellen Jing in the flow cytometry facility.

Caspase-3/DEVDase Assays

SW620.TK cells were double thymidine synchronized, then released into media alone or media containing 10 µM GCV, 0.3 µM UCN-01 or 10 µM GCV/0.3 µM UCN-01. At different time points cells were removed and assayed for caspase 3-like activity using a Clontech colorimetric kit with DEVD-pNA cleavage

from protein extracts derived from 2 X 10^6 cells. Each condition was done in triplicate. DEVDase activities were quantitated at 405 nm. Dr. Richard Drake carried out these experiments.

DAPI-staining

SW620.TK cells were plated in 8 well chamber slides (2 X 10^5/well), double-thymidine blocked, and released with media or the indicated GCV and UCN-01 combinations for 24 hrs. The cells were fixed in methanol and stained with 1μg/ml DAPI, and visualized with a Zeiss fluorescent microscope on 40*X* magnification. The areas of at least 10 random nuclei per slide were quantitated using Metamorph imaging software.

Cellular Apoptosis Detection

The ApopTag™ apoptosis kit was used to detect the amount of apoptosis of HSVtk variants treated and untreated with GCV. 200,000 cells were seeded on glass slides and were incubated in 100 mm dishes. Cells were double thymidine blocked prior to 20μM GCV addition for 24 hours. Cells were fixed in 1% paraformaldehyde and permeabolized in 1% Triton X100, and were prepared according to manufacturer's protocol. A detailed explanation of the use of this protocol is provided in section C. After the entire protocol was completed, cover slips were mounted onto glass slides with Vectashield™ mounting medium and allowed to air-dry overnight before viewing and quantitation of the number of apoptotic cells per field at a 25X magnification.

Metabolic labeling assays

Cells were plated (5 $X10^5$/well) in triplicate in a 6-well plate. The following day, cells were incubated for 18 hours in 1.5 ml of media containing 1 μCi [^{3}H]GCV (17.4 Ci/mmol) (Moravek) and 1 μM unlabeled GCV alone, or in combination with 0.3 μM UCN-01. Nucleotides were extracted with 70% methanol, and the supernatants were separated on PEI-cellulose thin layer chromatography plates with 1M LiCl as previously described (23). The methanol insoluble pellet was extensively washed with phosphate buffered saline, then resuspended in minimal 0.1 ml water, and quantitated by scintillation counting as an indicator of DNA incorporation (23). Dr. Richard Drake carried out these experiments and was authorized by the Radiation Department of Occupational Health and Safety at the University of Arkansas for Medical Sciences.

Immunofluorescence

80,000 cells were seeded onto each well of a 2-well Permanox slide. These cells will be then double thymidine blocked and released into media alone, 10μm GCV, 0.3 μM UCN-01, or 10μM GCV/0.3 μM UCN-01 for 12 hours. Cells were first washed with PBS two times and then were fixed with 2% paraformaldehyde at room temperature for 12 minutes; washed three times with PBS and then permeabolized with 0.5% Triton X-100 for 5 minutes at room temperature. Then, cells were washed four times with PBS and incubated with the appropriate antibody in 3% bovine serum albumin (Sigma) overnight at 4°C in a humidified chamber. The next day, the primary antibody was removed and the

cells were washed with 1%PBS-Tween 3 times. The secondary antibody was diluted in 3% BSA and incubated in the wells for 1 hour at room temperature in a humidified chamber in the dark. Cells were then washed 2 times with 3% BSA and 2 times with PBS. Cover slips were mounted with Vectashield™ mounting medium and were allowed to dry for 1 hour in the dark. Images were captured using a Zeiss confocal microscope.

Pulsed Field Gel Electrophoresis

For each drug treatment and time point, cells were spun down at 200g for 5 minutes and resuspended in ice-cold PBS. This procedure was repeated 3 times. The final cell suspension should be approximately 3X 10^6 cells/ml; 300µl of this suspension was mixed with 300µl molten 1% InCert agarose (FMC, Rockland, ME, USA; 1% in solution with PBS) in a 15 ml conical tube. The cell-agarose mixture was pipetted into a plug former on ice and refrigerated for 15 minutes. The formation of agarose plugs of whole cells for DNA analysis prevents shearing of the DNA prior to electrophoresis. Plugs were then removed from the formers, and incubated in ESP solution (0.5M EDTA, 1% w.v. sarcosyl, and 1mg/ml proteinase K; pH 9) for 2 hours at 4°C and at 49°C for 20 hours. Then, the plugs were washed in TE buffer (10mM Tris-HCL 1mM EDTA, pH 7.5) three times, each for one hour. The DNA in the plugs was separated by Pulsed Field Gel Electrophoresis in a 12.5 X 14 X 0.5 cm electrophoresis grade gel (0.5% solution in 0.5X TBE buffer plus Ethidium Bromide). Plugs containing the DNA from ~9 X 10^4 cells (~5 µg) were loaded into each well and sealed with

0.5% agarose. The gel was run for 24-48 hours on a CHEF-DR II (BioRad, Richmond, CA) operating at 40 V (~1.21 V cm^{-1}) with a switch time of 4500 seconds. The 0.5X TBE buffer was re-circulated by a temperature-regulating unit maintained at 16°C (131).

For the alkaline elution studies, plugs were incubated in alkaline buffer (50mM NaOH; 1mM EDTA (pH 12.5) adapted from (132)) for 2 hours prior to loading in to the gel with gel electrophoresis parameters the same as for neutral elution as described above. Images were captured using a Kodak gel imaging system. All plugs were run on another agarose gel using a standard electrophoresis unit at 1 hour for 45 volts to detect DNA laddering indicative of apoptosis that may be responsible for PFGE elution.

Surface enhanced Laser Desorption Ionization Time of Flight (SELDI-TOF) Mass Spectroscopy

Cell lysates for SELDI-TOF

SW620.tk cells ($5X10^6$) were synchronized and treated with media, 10μM GCV, 0.3μM UCN-01 or 10μMGCV/0.3μM UCN-01. Cell lysis buffer (20mM Hepes pH 7.5 and 1% Triton X 100 1μl aprotinin) was added to pelleted cells and then cells were sonicated for 1 minute and spun at 4°C for 10 minutes at 14,000 rpm, and then the supernatant was placed into fresh tubes.

Nuclear Lysates

SW620.tk cells (2 X106) were plated in T-75 tissue culture flasks, synchronized, and drug treated as previously described. After 24 hours, the cells were harvested. The nuclear fractions from the cells were separated from the cytosol and membranes and enriched by differential centrifugation using NE-PER reagents from Pierce (Rockford, IL).

Protein Chip Preparation and Protein Sample loading

Strong Anion Exchange (SAX) Protein Chips were prepared by adding 20mM Tris pH 7.5 with 0.1% Triton-X to each well, shaking for 5 minutes at room temperature, and discarding of the buffer. (repeated once). Dilutions (1:25 or 1:50) of the samples were made in the Protein Chip buffer prior to placing the samples on the chips. After the bioprocessor was assembled, 200ul of the appropriate Protein chip buffer was added to the sample wells and placed on shaker for 5 minutes. This was done two times. 100µl of the diluted sample were added to the chips and the processor was shaken overnight to allow specific binding. The liquid was discarded after the overnight incubation and therefore anything unbound was removed. 200µl of the appropriate Protein Chip buffer was applied to the chips and removed after 5 minutes of shaking. (repeated once) Chips were then rinsed with HPLC grade water twice and were air-dried at least 2 hours. Sinapinic Acid (0.5 mg SPA), the energy adsorbing molecule, was resuspended in 100µl 1% trifluoroacetic acid and 100µl of acetonitrile. SPA (0.5µl) was added to each spot on the protein chip twice.

Spectra

A surface-enhanced laser desorption/inoization (SELDI) PBS-II mass reader from Ciphergen Biosystems was used to generate the protein spectra, mass ranged from 0-20000 daltons. The protein masses were calibrated externally using purified peptide standards. Cell lysates were read using the lowmass method: Machine settings: Detector voltage 1850-1900 volts; high mass to 200000 daltons; optimized from 3000 daltons to 50000 daltons; starting laser intensity at 220; starting detector sensitivity to 7; focus lag time at 900 ns; SELDI acquisition parameters set to 23, delta to 4, transients per to 12 ending position 83. The spectra were analyzed with the Ciphergen ProteinChip® software (version 3.1) and normalized using total ion current. Peaks were identified using auto identify from 2000 daltons to 100000 daltons.

Two Dimensional gel electrophoresis (2D gel electrophoresis)

Cell lysates

Initially, $1X10^6$ HSV-tk expressing cells were plated in $100mm^2$ plates and treated with GCV, UCN-01, or the combination. After 24 hours treatment, the cells were harvested and counted. 100µl of BioRad Rehydration/sample buffer was added for every 100,000 cells, and typically 0.5 X 10^6 to 1X 10^6 cells for each condition were harvested. Equal amounts of protein from the cell lysates were diluted again in rehydration/sample buffer for a total of 200µl including 5 µl of an 2D gel-electrophoresis standard (BioRad). Since the reagents in the rehydration/sample buffer interfere with standard protein assays, we used the

RC-DC protein assay kit from BioRad to determine protein concentrations from the cell lysis step. Typically 20µg to 200µg proteins were loaded on the IPG strips. The samples were allowed to hydrate using either the pH 3-10 or pH 5-8 IPG strips for 11-16 hours, and then the strips were placed in the isoelectric focusing unit.

Nuclear extracts

Cells were plated and synchronized in 100mm^2 plates and treated with GCV, UCN-01, or the combination for 24 hours. Cells were then scraped into ice cold PBS and spun down at 1000 rpm for 5 minutes. 5X10^6 cells were pelleted and resuspended in 200µl ice-cold buffer 1 (10mM HEPES (pH 7.9) 10mM KCl, 0.1 mM EDTA 0.1 mM EGTA 1mM DTT and protease cocktail inhibitor from Invitrogen). Cells were chilled on ice for 15 minutes, and then they were lysed with 0.6% Nonidet p-40 derivative followed by mixing by inversion several times. Nuclei were pelleted at 200g for 5 minutes at 4°C. The supernatant was decanted and the pellet was resuspended in ice-cold buffer 2 (20mM HEPES (pH 7.9) 0.4 NaCl, 1 mM EDTA 1mM EGTA 10% v/v glycerol, 1mM DTT and Protease Cocktail from Invitrogen). Nuclei were resuspended gently and lysed by shaking for 30 minutes at 4°C. The lysates were then centrifuged at 12000g for 10 minutes at 4°C, and were stored in dilute protease cocktail and snap frozen on dry ice (133). 20µg of nuclear extract was diluted in rehydration/sample buffer for focusing.

Isoelectric Focusing

A Protean IEF Cell (BioRad) was used for the first dimension isoelectric focusing of IPG loaded strips. A standard focusing program began at 250 volts for the first 15 minutes, the next 2.5 hours the voltage was set to reach 8000 volts. The 8000 volts was maintained until a total of 35,000 volt hours occurred.

Gel electrophoresis

Following first dimension isoelectric focusing, the IPG strip was equilibrated in Buffer 1 (6M urea, 0.375 M Tris, pH 8.8, 2% SDS, 20% glycerol, and 2% w/v DTT) for 15 minutes in a plastic tray in an orbital shaker and then for another 15 minutes in buffer 2 (6M urea, 0.375 M Tris, pH 8.8, 2% SDS, 20% glycerol, and 2.5 % w/v iodoacetamide). The strips were then loaded on an 8-16% gradient Criterion precast gels and placed in a Criterion cell (BioRad). Two gels at a time were run in the cell for 1 hour at 200V to completion.

Protein Gel Staining

A SilverQuest™ (Invitrogen) silver staining kit was used according to manufacturer's basic protocol. Gels were stored in water indefinitely.

2D Spot Identification by LC-MS/MS

In-gel Trypsin Digest

Gel slices were cut into 1-2 mm cubes, destained with the SilverQuest™ destaining kit (Invitrogen) as per manufacturers instructions and incubated in

100% acetonitrile for 45 minutes. The material was dried in a speed-vacuum and rehydrated in a 12.5 ng/μL modified sequencing grade trypsin solution and incubated in an ice bath for approximately 45 minutes. The excess trypsin solution was then removed and replaced with 40-50 μL of 50 mM ammonium bicarbonate, pH 8.0. The digest was allowed to proceed overnight, and peptides were extracted 3 times with 50% acetonitrile, 5% formic acid, dried in a speed-vacuum, and stored at -20°C until sequencing analysis.

LC-MS/MS Analysis

Digests were resuspended in 20 μL Buffer A (5% Acetonitrile, 0.1% Formic Acid, 0.005% heptafluorobutyric acid (HFBA)) and 3 – 6 μL were loaded onto a 12-cm X 0.075 mm fused silica capillary column packed with 5 μM diameter C-18 beads (The Nest Group, Southboro, MA) using a N2 pressure vessel at 1100 psi. Peptides were eluted by applying a 55 minute, 0 – 80% linear gradient of Buffer B (95% Acetonitrile, 0.1% Formic Acid, 0.005% HFBA) at a flow rate of 130 μL/min with a pre-column flow splitter resulting in a final flow rate of ~200 nL/min directly into the source. The LCQ-DecaXP (Thermofinnigan) was run in automatic collection mode with an instrument method composed of a single segment and 4 data-dependent scan events with a full MS scan followed by 3 MS/MS scans of the highest intensity ions. Normalized collision energy was set at 30, activation Q was 0.250 with a minimum full scan signal intensity at 5 X 10^5 and a minimum MS2 intensity at 1 X 10^4. Dynamic exclusion was turned on utilizing a three-minute repeat count of 2 with the mass width set at 1.50 Da.

Sequence analysis was performed with Sequest™ using an indexed human subset database of the non-redundant protein database from NCBI. Processing of the samples through the LC-MS/MS identified the most abundant 200-300 peptides in the sample. All sequence determination was performed by Michael Ward at the Eastern Virginia Medical School Proteomics Facility.

Transgenic adenocarcinoma murine prostate (TRAMP) model

In vitro

The TRAMP-C1P3 cells were kindly provided by Drs. Kenneth Somers and Richard Ciavarra (134). Stably expressing HSV-TK and active site variants TRAMP-C1P3 lines (TRAMP-TK, GK1 and GK2) were generated and characterized for sensitivity to GCV and UCN-01. These cell lines were generated and characterized with the assistance of Adrienne Granger and Dr. Drake following transfection and G418 selection with a bicistronic HSV-TK/neo Moloney Murine Leukemia Virus-derived plasmid, pLTKEN, as previously described (23). Cells were maintained in Dulbecco's Modified Eagle Medium 1X high glucose with L-glutamine and without sodium pyruvate (Gibco), 5% Nu-Serum IV (Collaborative Biomedical Products), 5% FBS from Hyclone, 5μg/ul insulin (Sigma), 25ug/ml penicillin-streptomycin (Gibco), and .001μM dihydroxytestosterone.

In vivo

HSV-tk variants: C57/BL6 mice were injected subcutaneously with $5X10^6$ cells comprised of 90% parent TRAMP-C1P3 and either 10% TRAMP-TK (wt)(n=18), 10% TRAMP-GK1 (n=18), 10% TRAMP-GK2 (n=6). After 20 days, mice were randomized within their respective groups and half were treated with GCV (7 or 70 mg/kg, i.p. once daily) for 5 days. Tumor volumes were monitored by calipers starting at day 22.

For initial evaluation of UCN-01 and GCV treatments, twenty C57/BL6 mice were each injected with 5×10^6 cells comprised of 90% parent TRAMP-C1P3 and 10% TRAMP-TK cells in the chest wall (ectopic model). This ratio was used to better reflect the clinical aspects of HSV-TK/GCV therapy, and to ensure that the injected cells would form tumors, in case G418 selection of the TRAMP-TK modified their *in vivo* properties. Tumors were allowed to grow for 22 days, prior to randomization into four groups of 5 mice each. Five mice each were injected i.p. with either 70 mg/kg GCV once daily for five days (days 22-26), 2 mg/kg UCN-01 for 5 days, or a combination of both (70 mg/kg GCV and 2 mg/kg UCN-01) for 5 days. Tissue sections from a subset of these treated mice were saved, but have not yet been profiled for tumor infiltrating cells and cytokines to evaluate an immune response.

This *in vivo* experiment was a collaborative effort including Dr. Richard Drake and Saurabh Gupta for mouse handling and injections, and Dr. Ciavarra overall assistance and consultation. If any animal began to show signs of pain or distress (loss of body condition, inability to ambulate, loss of appetite, etc.) or if a

tumor volume exceeded 10% body weight, the animal was euthanized. Data were analyzed using a 2-way ANOVA analysis using Prism GraphPad Software (San Diego, CA). Repeated measures analysis of variance was used to test for significant differences among the treatment effects and indicated whether there were significant differences ($p =< 0.05$). A minimum of five mice were randomly assigned to each treatment group. All procedures were approved by the EVMS IACUC and were in compliance with the NIH guide for the Care and Use of Laboratory Animals.

CHAPTER III

AIM # 1: EVALUATE THE ROLE OF THE CELL CYCLE, CELL DEATH MECHANISMS, AND PROTEOMIC EFFECTS OF CELLS TREATED WITH HSV-TK/GCV AND UCN-01 DRUG COMBINATIONS

In previous studies, MTT and clonogenic survival assays showed the combination of UCN-01 and HSV-TK/GCV had an apparent synergistic killing effect on HSV-TK expressing colon and breast cancer cell lines (60). UCN-01 has been paired with other DNA-damaging agents including nucleoside analogs, and a similar synergy has been observed (85, 95) and as summarized in Table 3 in the Introduction. By comparing the response of HSV-TK expressing tumor cells to GCV and UCN-01 singly and in combination, the mechanistic basis for how these drugs effect cell cycle and DNA damage response proteins inhibited by UCN-01 upstream of the DNA damaging events caused by GCV was evaluated. The mechanism of both drugs and the combination remains largely unknown. UCN-01 is a potent Chk1 inhibitor has this led us to our first studies that have implicated the cell cycle proteins as the main targets for our mechanism. Our first question was how the cell cycle is involved in the mechanism of cell death and if that cell death involved classical apoptosis.

Synchronization and cell cycle analysis

Previous data generated in the Drake laboratory have indicated that cdc25C protein levels decrease after treatment of cells with UCN-01 and the combination with GCV, and subsequently, studies of the cell cycle effects of these drugs were pursued. To better address these effects, SW620.TK and HCT-116.TK cells were synchronized at the G_1/S boundary using a double-thymidine block procedure prior to UCN-01 and GCV treatments. As described in *Materials and Methods*, this procedure routinely resulted in synchronization of at least 95% of the treated cell populations. Following the second thymidine block, cells were released into media alone, or media containing 10 μM GCV, 0.3 μM UCN-01 or 10 μM GCV/0.3 μM UCN-01. At different time points, cells were analyzed for cell cycle progression using propidium iodide staining of DNA, BrDU labeling, or multiple Western blot analyses.

Propidium iodide staining and flow cytometry

As presented in Figure 1, SW620.TK cells released into media alone following double-thymidine treatment progressed through one cell cycle as a synchronized population. By the end of 24 hrs and completion of the synchronized cycle, the cells returned to a normal unsynchronized growth pattern. Cells released into 10 μM GCV alone never progressed past late S-phase/early G2 phase. Cells released into 0.3 μM UCN-01 appeared to progress normally through the cell cycle, but at a slightly altered rate relative to control cells. There also appeared to be a greater accumulation of cells into G1

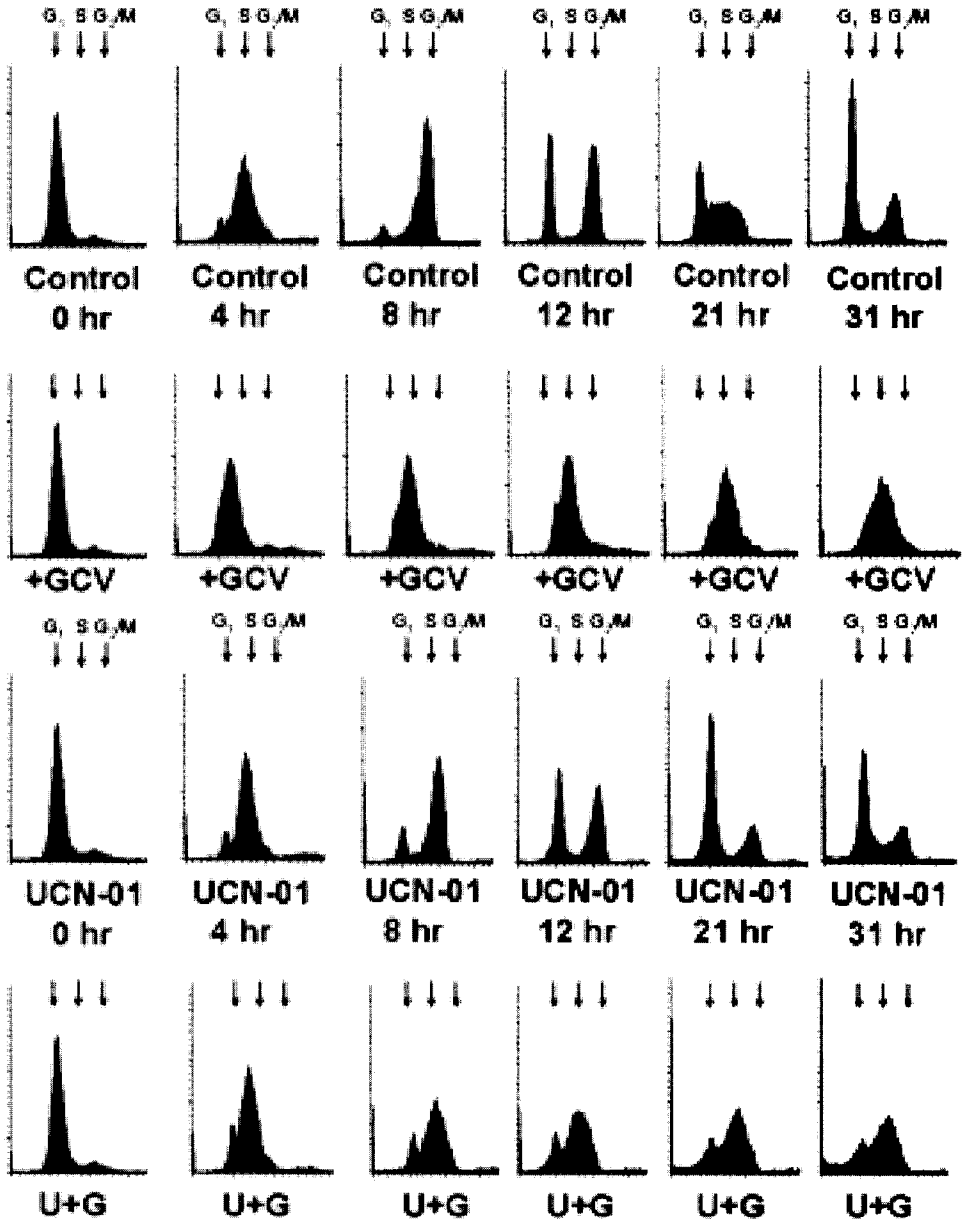

Fig. 1. Double Thymidine Block Cell Synchronization – Flow Cytometry Evaluation of GCV and UCN-01 Effects. SW620.TK cells were treated with 2 mM thymidine for 16 hrs, followed by growth in fresh media for 9 hrs, then another 2 mM thymidine dose for 16 hrs (46). Cells were released into media, 10 μM GCV, 0.3 μM UCN-01 or 10 μM GCV/0.3 μM UCN-01. At different time points, cells were removed and fixed in 70% ethanol. Cell pellets were resuspended in propidium iodide and DNA content was measured using a FACScalibur flow cytometer (Becton Dickinson).

following mitosis, consistent with results described in previous UCN-01 studies (67, 135, 136). Cells treated simultaneously with the same UCN-01 and GCV concentrations remained largely in S-phase, but with an apparent broader spectrum of cells in S-phase and early G2. However, like with GCV treatment alone, no cells apparently progressed through to mitosis.

Bromodeoxyuridine Metabolic labeling coupled with flow cytometry

It is difficult to interpret rate and cell cycle accumulation versus arrest using PI staining only; therefore, we used bromodeoxyuridine (BrDU) labeling coupled with 7-AAD (7-aminoactinomycin D) DNA staining to track cell cycle progression. Cells were synchronized as stated above, however they were pulsed for 2 hours with 10μM BrDU before harvesting at each indicated time point. Our system was unique in that the cells we were testing were already stably transfected with HSV-tk, and BrDU is a substrate for this enzyme. In fact, a 5-bromo derivative, 5-bromovinyldeoxyuridine (BrVUrd), is one of the most potent and selective inhibitors of HSV-1 viral replication because it is one of the best substrates identified for HSV-tk (137). Therefore, we restricted the cells to the pulsed time to address our cell cycle question because any long-term incubation with BrDU in the HSV-tk expressing cell could affect cell viability and cell cycle response.

Synchronized SW620.tk cells treated with media only (control) actively took up BrDU and were progressing into G_2 at the 6-hour time point (Figure 2), and at the 12-hour time point, control cells had lower levels of BrDU because they had

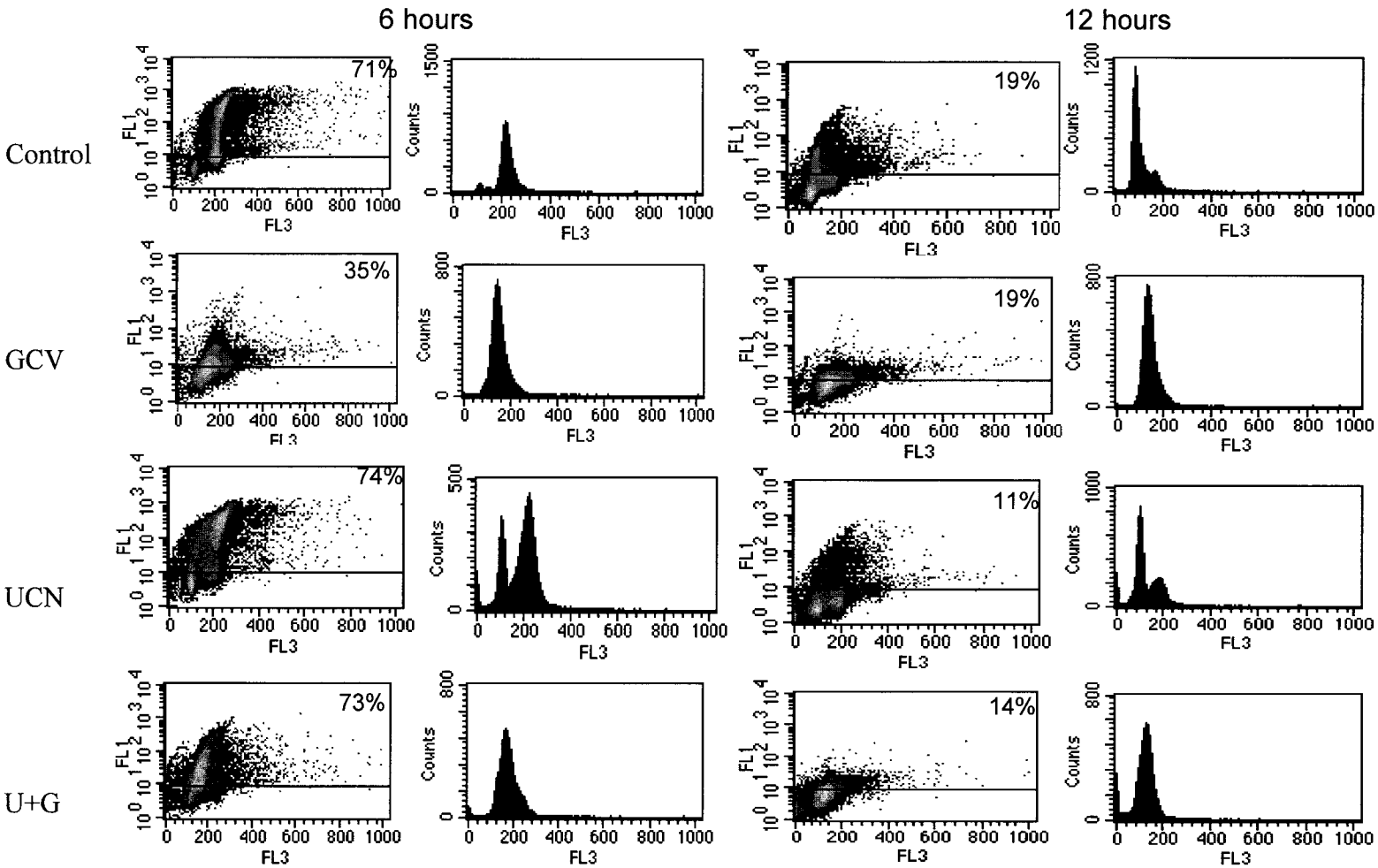

Fig. 2. Synchronized SW620.tk cells and Bromodeoxyuridine labeling. Cells were incubated in media, 10μM GCV, 0.3μM UCN-01 or U+G and were pulsed with 10μM BrDU 2 hours prior to harvest and flow cytometry preparation.

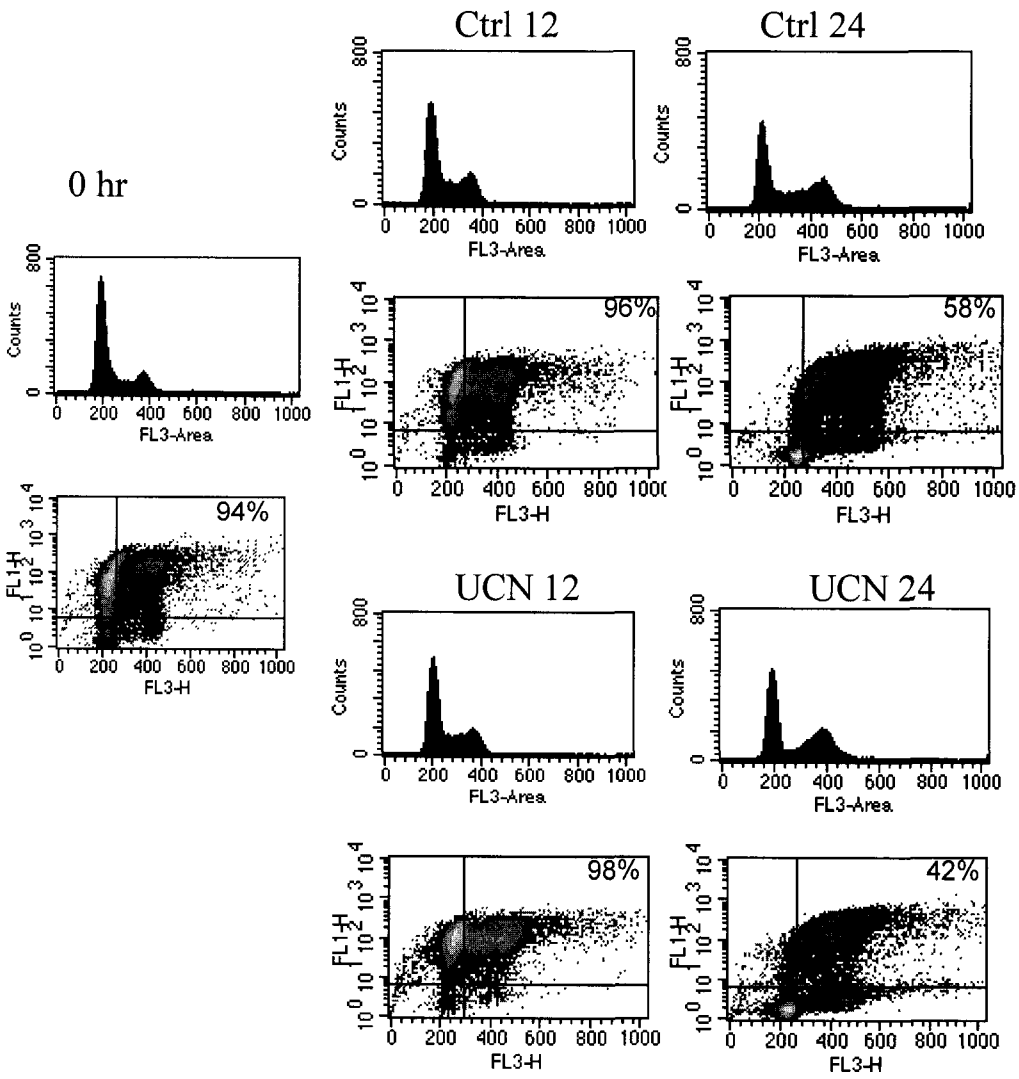

Fig. 3. 36 hour Bromodeoxyuridine labeling of SW620 cells. Cells were incubated with 10 μM BrDU for 36 hours prior to drug or media addition at time 0. Fl1= BrDU and Fl3- 7-AAD. Percent BrDU positive cells is indicated in the upper right hand corner of each densitometry plot.

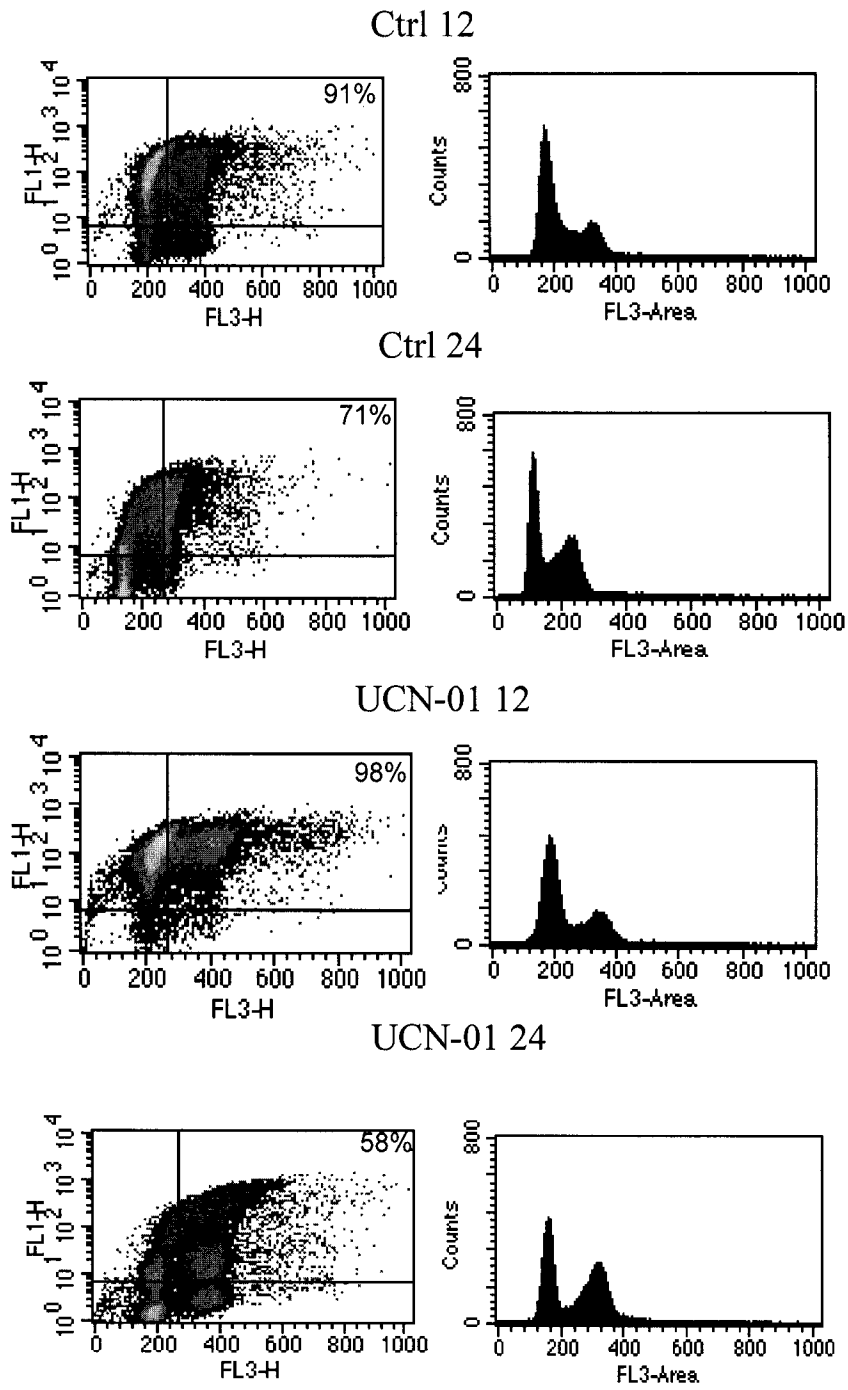

Fig. 4. 2 hour pulse Bromodeoxyuridine Labeling. Medium or UCN-01 were added for 12 or 24 hours, and 10μM BrDU was added for 2 hours prior to harvesting the cells. Cells were harvested and processed for flow cytometry. FI1= BrDU and FI3- 7-AAD. Percent BrDU positive cells is indicated in the upper right hand corner of each densitometry plot.

most of the population was in G_1 (Figure 2). In contrast, GCV treated cells appeared to already have lower incorporation of BrDU by 6 hours, indicative of an S-phase arrest. By 12 hours GCV treated cells were still in S-phase with even less BrDU incorporation. At 6 hours, cells began to accumulate in S-phase after the combination of UCN-01 and GCV; however, BrDU incorporation levels remained higher than in cells treated with GCV only. Although all levels of BrDU incorporation were fairly low at 12 hours, it is believed that the lower levels in control and UCN-01 are due to the population of cells in G1, and the lower levels in GCV and U+G are due to cells in an S-phase arrest. If the GCV treated cells were accumulating in S-phase as opposed to arresting, a DNA profile in S-phase with high levels of BrDU incorporation similar to the 6 hour time point of U+G would be expected.

UCN-01 results were more difficult to interpret because by 6 hours, it appeared that most of the population of cells were in G_1 and G_2/M phases of the cell cycle compared to the synchronous control population in G_2/M (Figure 2). In order to determine if these UCN-01 treated cell were cycling more rapidly or were having difficulty exiting G_2, SW620 parent cells (no HSV-tk) were chosen for tracking BrDU incorporation after pre-incubation followed by UCN-01 treatment. Two separate but parallel experiments were conducted in the SW620 cells, one set with a 2 hour pulse of BrDU prior to harvesting the cells and the other with a 36 hour pre-incubation that was removed when the treatment conditions were added to the cells. In Figure 3, nearly all of the control and UCN-01 treated cells had incorporated BrDU as expected during the 36 hour pre-incubation and were

transiting from G_1 at the 0 hr time point into G_2/M by the 12 hour time point. By 24 hours, the decrease in BrDU cells is expected as control and UCN-01 cells divide and return to G_1. However, there appears to be a sharp decrease in S-phase cells and almost twenty percent less BrDU positive cells. Pulse data in Figure 4 confirm these findings. By 24 hours with UCN-01, there are not as many BrDU positive cells compared to control and a sharp decrease in cells in s-phase.

Western blots of cell cycle proteins

The SW620.TK cells were synchronized, treated with UCN-01 and GCV and then harvested at several time points. The effects of these treatments on protein levels of cdc25C, cdk1, phospho-cdk1, Cyclin B, Cyclin A and Bcl-X_L evaluated by western blots. As shown in Figure 5, cdc25C levels varied between steady and possibly accumulating with cell cycle phase in the control cells and in the S-phase arrested GCV treated cells, but progressively decreased dramatically after 8 hrs following UCN-01 or UCN-01/GCV treatments. A similar loss of protein in response to UCN-01 and UCN-01/GCV after 8 hrs was observed for cyclin B (Figure 5), and after 4 hrs for cyclin A (Figure 5). For cdk1, a phospho-tyrosine specific antibody (for Tyr-15) and polyclonal antibody were used. In the UCN-01 treated cells, a total loss of the Tyr-15 phosphorylated form of cdk1 occurred after 8 hours (Figure 5). In the UCN-01/GCV treated cells, a persistent loss of Tyr-15 phosphorylation occurred between 8 hrs and 31 hrs (Figure 5). Levels of cdk1 protein remained largely unchanged in all of the treatments (Figure 5).

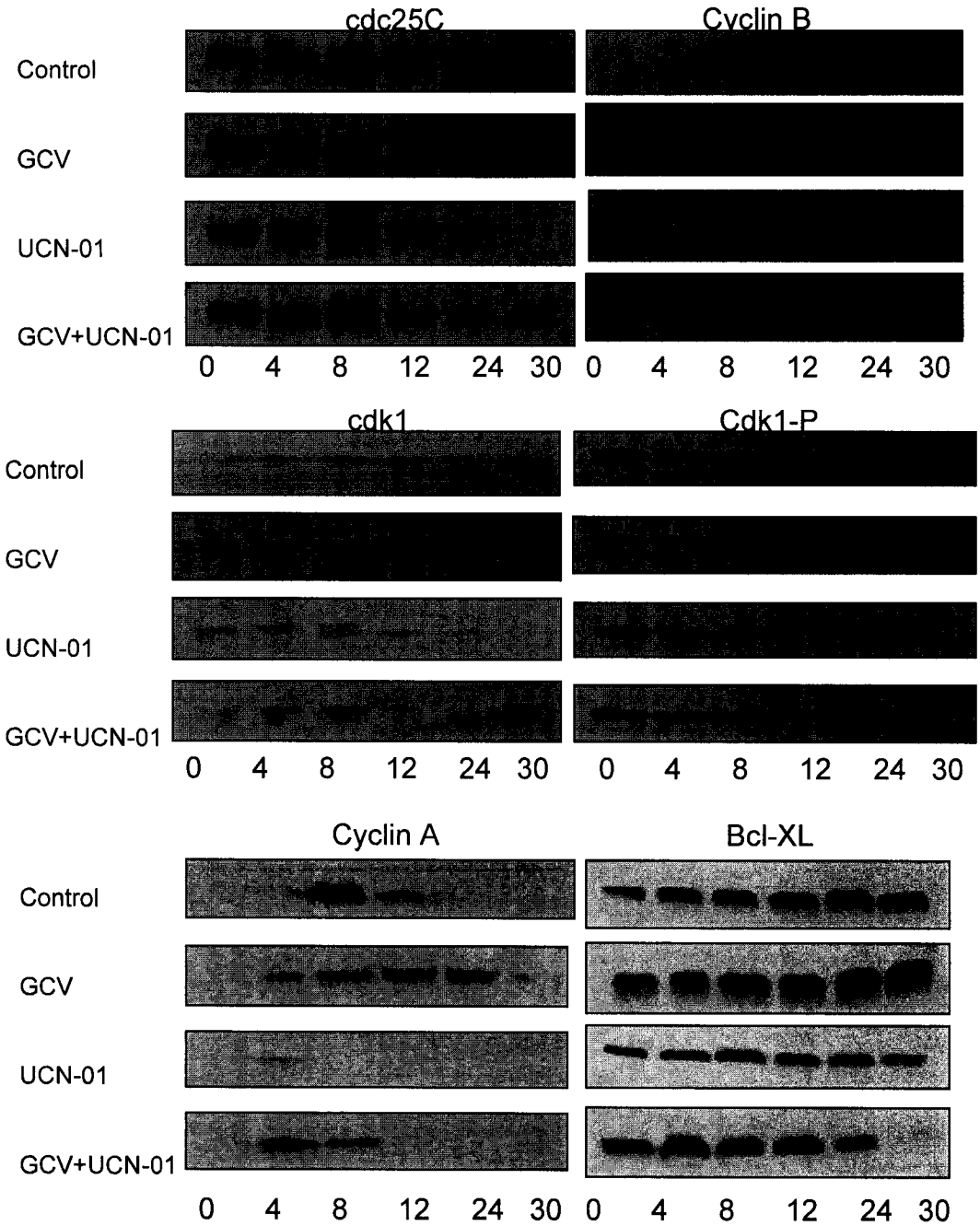

Fig. 5. Western Blot Determinations of cdc25C, cyclin B, cyclin A, Cdk1/cdk1-P, and Bcl-xl in SW620.TK Cells Treated with GCV and UCN-01. SW620.TK cells were double thymidine synchronized, then released into media, 10 μM GCV, 0.3 μM UCN-01 or 10 μM GCV/0.3 μM UCN-01. At different time points cells were removed and processed for Western blot analysis.

Lastly, the levels of Bcl-X_L were evaluated (Figure 5). Only in the later time points of the UCN-01/GCV combination was there a dramatic reduction present in the levels of Bcl-X_L. A similar effect on Bcl-XL levels in response to this combination was previously reported in HCT116.tk cells (60). For GCV treatments alone, the levels of each protein evaluated were stabilized or slightly increased (Figure 5). Similar cell cycle responses and Western blot profiles were obtained in double-thymidine blocked HCT-116.TK, MDA-435.TK, and DU145.tk cell lines treated with the GCV and UCN-01 combinations (data not shown).

Cell death assays

The induction of apoptosis in the SW620.TK cells following double thymidine block and treatment with the same GCV and UCN-01 combinations was evaluated by caspase 3-DEVDase assays and nuclear morphology staining with DAPI. Within 6 hrs, UCN-01 and UCN-01/GCV led to activation of caspase 3, while GCV caused a steady increase in caspase 3-DEVDase activity over treatment time (Figure 6). The decrease in UCN-01/GCV caspase activities are reflective of cell viabilities at the later time points. In Figure 7, DAPI-staining indicated nuclear morphologies indicative of apoptosis, especially in the UCN-01/GCV treated cells. GCV alone causes a noticeable S-phase swelling of nuclei, indicative of S-phase arrest as previously reported (8). To comparatively assess the effects on nuclear morphology, quantitation of relative nuclear sizes of the cells after different treatments were determined over time, as presented in Figure 8. Clearly, there are pronounced differences between the nuclear sizes of cells

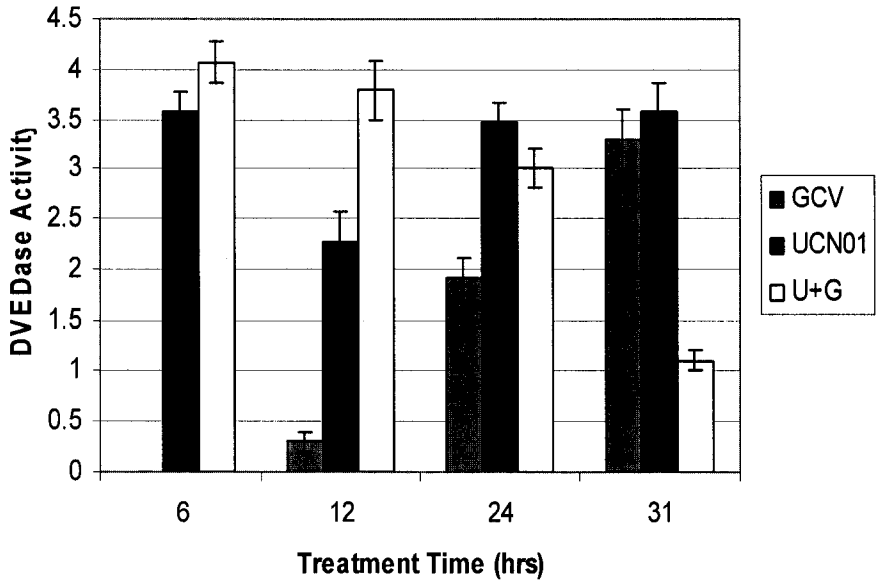

Fig. 6. Caspase 3 Assays SW620.TK Cells Treated with GCV and UCN-01. SW620.TK cells were double thymidine synchronized, then released into media, 10 μM GCV, 0.3 μM UCN-01 or 10 μM GCV/0.3 μM UCN-01. At different time points, in triplicate, cells were removed and assayed for Caspase 3 activity using a Clontech colorimetric kit with DEVD-pNA cleavage from protein extracts derived from 2 X 10^6 cells. DEVDase activities were quantitated at 405 nm.

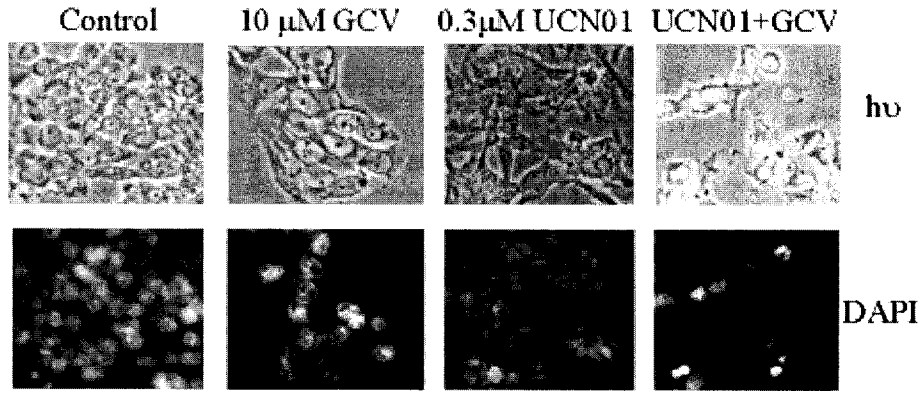

Fig. 7. DAPI-Staining of SW620.TK Cells treated with GCV and UCN-01. SW620.TK cells were plated in 8 well chamber slides (2 X 10^5/well), double-thymidine blocked, and released with media for the indicated GCV and UCN-01 combinations for 24 hrs. The cells were fixed in methanol and stained with 1μg/ml DAPI; cells were visualized with a Zeiss flourescent microscope on 40*X* magnification.

treated with GCV that increased with treatment times, and cells treated with UCN-01 or the combination of the two drugs.

Metabolic labeling

It has been previously described that UCN-01 treatment leads to decreased expression of thymidylate synthase (138). Because it is also known that inhibition of thymidylate synthase increases the effectiveness of GCV phosphorylation in HSV-TK expressing cells due to loss of competing intracellular thymidine nucleotides (139), the effect of UCN-01 on metabolism of [^{3}H]GCV was evaluated in thymidine-blocked SW620.TK cells. Following 18 hrs treatment with [^{3}H]GCV (1 μM) alone, or with 0.3 μM UCN-01, methanol soluble nucleotides and GCV-incorporated DNA fractions were isolated and quantified for levels of [^{3}H]GCV. Phosphorylated [^{3}H]GCV metabolites were separated from [^{3}H]GCV using thin layer chromatography plates. As shown in Figure 9, a greater than 4-fold increase in soluble GCV-DP/TP metabolites and a 2-fold increase in GCV-incorporated DNA were present in the UCN-01 treated cells. This effect of UCN-01 on increasing the intracellular levels of GCV metabolites may represent the pharmacologic basis for the contribution of GCV to the increased rate of tumor cell killing following UCN-01 and GCV treatment combinations. We have also hypothesized that the combination allows GCV incorporation in the DNA to go unrepaired due to the known inhibition of NER (Nucleotide excision repair) proteins by UCN-01 (79) plus the damage it is causing itself.

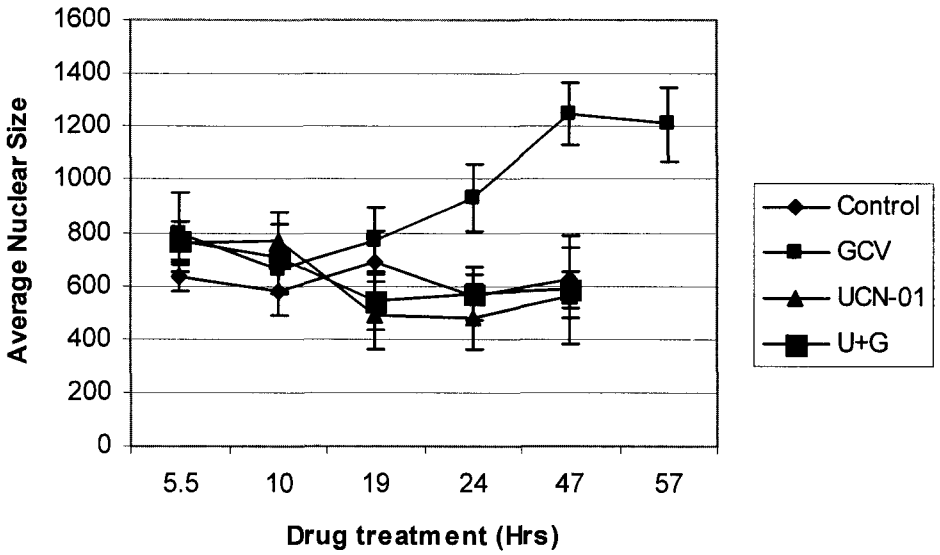

Fig. 8. Average nuclear size post treatment. SW620.TK cells grown in chamber slides were double thymidine synchronized, then released into media, 10 μM GCV, 0.3 μM UCN-01 or 10 μM GCV/0.3 μM UCN-01. At different time points, the cells were fixed in methanol and stained with 1μg/ml DAPI, and visualized with a Zeiss flourescent microscope on 40*X* magnification. The areas of at least 10 random nuclei per slide were quantitated using Metamorph imaging software.

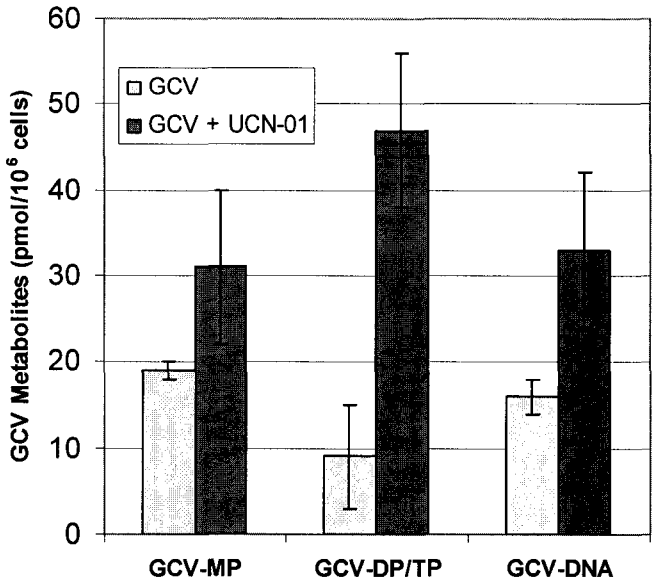

Fig. 9. Metabolic Labeling with [^{3}H]Ganciclovir. SW620.TK cells were plated (5 X10^5/well) in triplicate in a 6-well plate, then incubated for 18 hours in 1.5 ml of media containing 1 μCi [^{3}H]GCV/1 μM GCV alone (light bars), or in combination with 0.3 μM UCN-01 (dark bars). Nucleotides were extracted with 70% methanol, and the supernatants were separated on PEI-cellulose thin layer chromatography plates with 1M LiCl as previously described (8). The values for GCV-monophosphate (GCV-MP) and the combined diphospate/triphosphate levels (GCV-DP/TP) are presented. The methanol insoluble pellet was extensively washed and quantitated as an indicator of DNA incorporation by scintillation counting (8).

The effects of proteosome inhibition on the UCN-01 mechanism

We hypothesized that the ability of UCN-01 to kill the cells so effectively could be linked to its ability to target the essential mitotic proteins for degradation. Therefore, we treated the SW620.tk cells with the proteosome inhibitor lactacystin followed by GCV, UCN-01, and the combination. Cells were harvested at different time points and analyzed by flow cytometry. Lactacystin by itself appeared to "arrest" the cell in G_2, and UCN-01 plus lactacystin showed subtle signs of abrogating that arrest (Figure 10) as a small peak in G_1 appeared at 24 hours with cells treated with lactacystin and UCN-01. Interestingly, U+G combined with lactacystin appeared to be arrested in S-phase from 4-12 hours, but by 24 hours, the majority of the cell population appeared to be in G2. These data are particularly difficult to interpret since initial combinations of UCN-01 with lactacystin in our cell systems have resulted in rapid and enhanced cytoxicities, making it difficult to interpret the role of the proteasome in the process.

Order of addition

Cell viability assays were used to determine the efficacy of changing the order of addition with the combination of GCV and UCN-01. For these experiments, one drug was added singly for 12 hours then the second drug was added. GCV added first showed significantly enhanced cell killing at as low as 25nM UCN-01 added 12 hours later. This level of killing was equivalent to the two drugs added simultaneously (Figure 11). UCN-01 added first then the addition of GCV 12 hours later was never as toxic as the GCV first or the

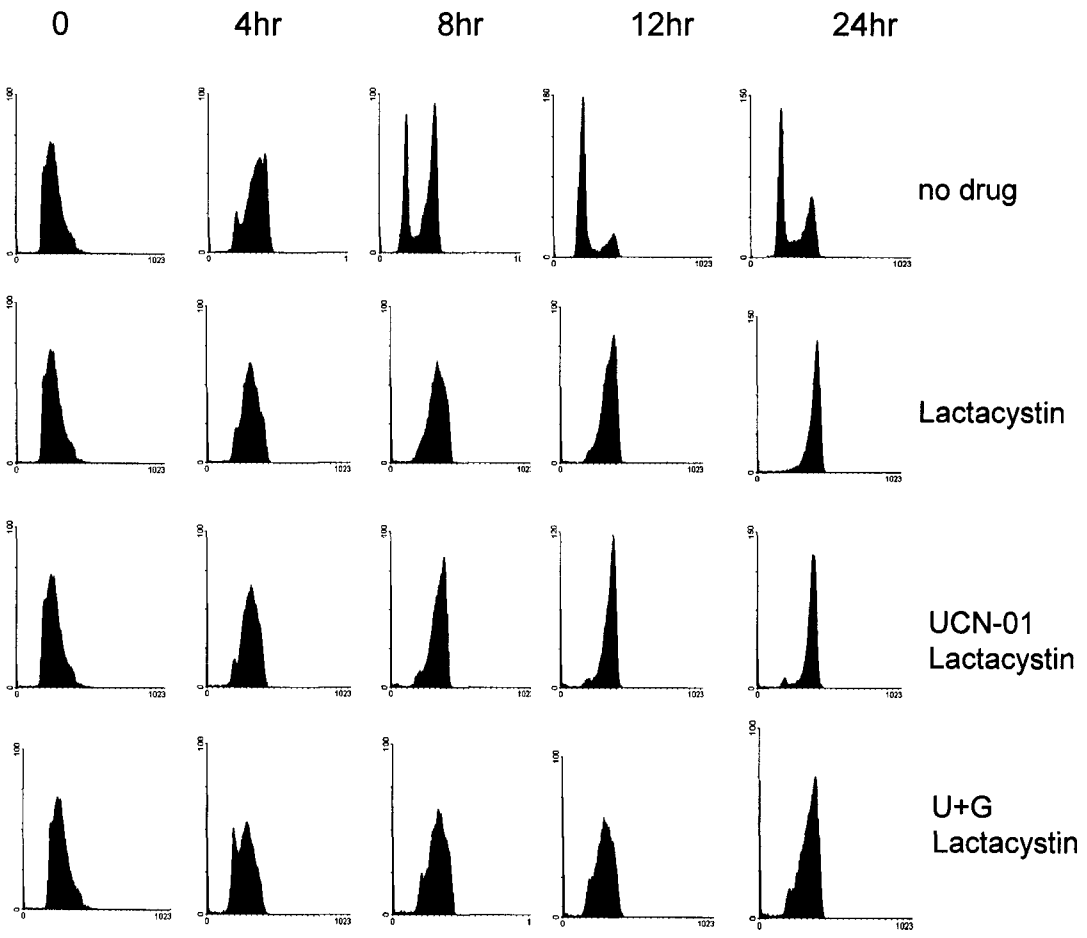

Fig. 10. Flow cytometry in Synchronized SW620.tks treated with Lactacytstin. Following double-thymidine block, SW620.tk cells were released into media, 10 μM GCV, 0.3 μM UCN-01 or 10 μM GCV/0.3 μM UCN-01 as before, but also in the prescence of 10 μM lactacystin. At different time points, cell were removed and fixed in 70% ethanol. Cell pellets were resuspended in propidium iodide and DNA content was measured using a FACScalibure flow cytometer (Becton Dickinson)

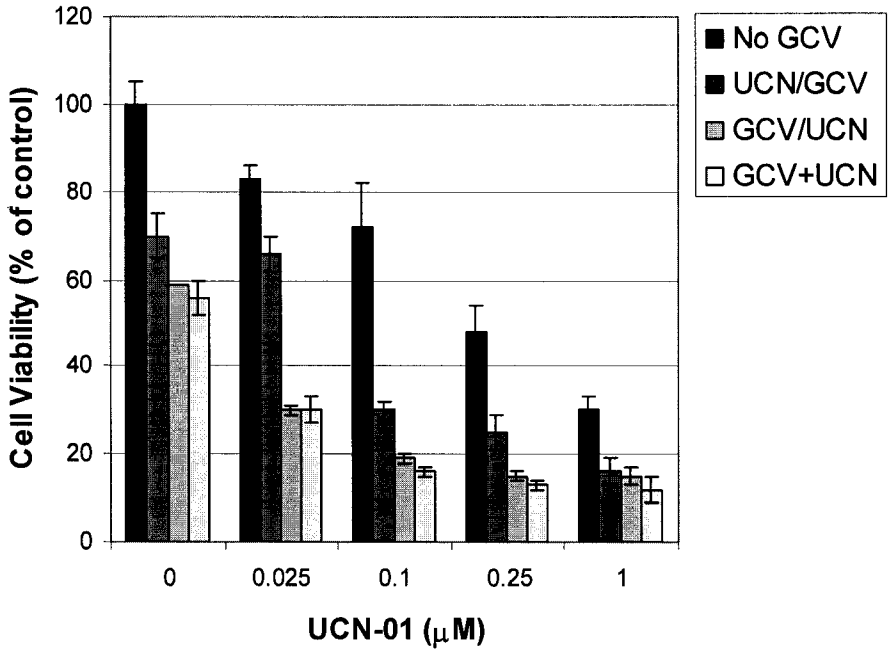

Fig. 11. Cell Viabilities: UCN-01 and GCV Order of Addition. UCN-01 drug doses or GCV (at 10 μM) were added singly 12 hours apart. After 48 hours, MTT was added to determine cell viabilities. The 0 μM UCN-01 lanes represent the GCV alone samples. The first bar series represent UCN-01 tested singly.

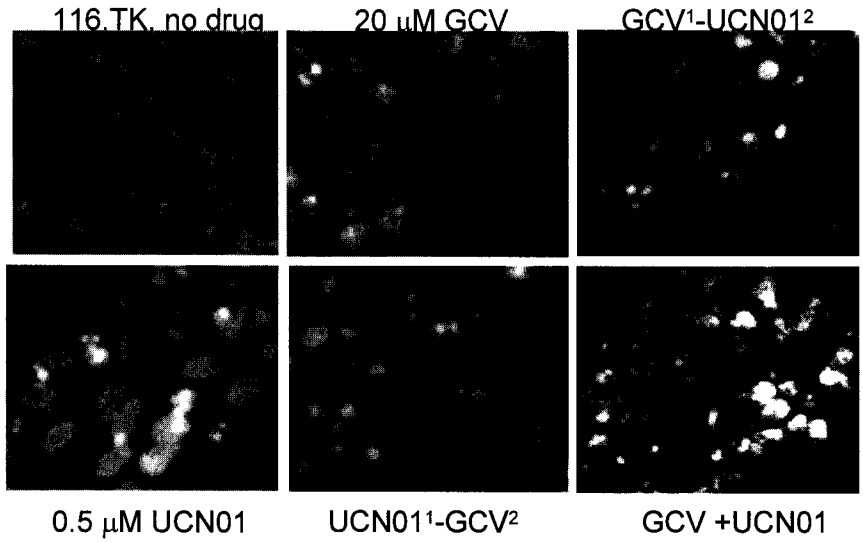

Fig. 12. Order of addition DAPI-Staining of SW620.TK Cells treated with GCV and UCN-01. HCT116.TK cells were plated in 8 well chamber slides (2 X 10^5/well), double-thymidine blocked, and released with media for the indicated GCV and UCN-01 combinations for 24 hrs. The cells were fixed in methanol and stained with 1μg/ml DAPI; cells were visualized with a Zeiss flourescent microscope on 40*X* magnification.

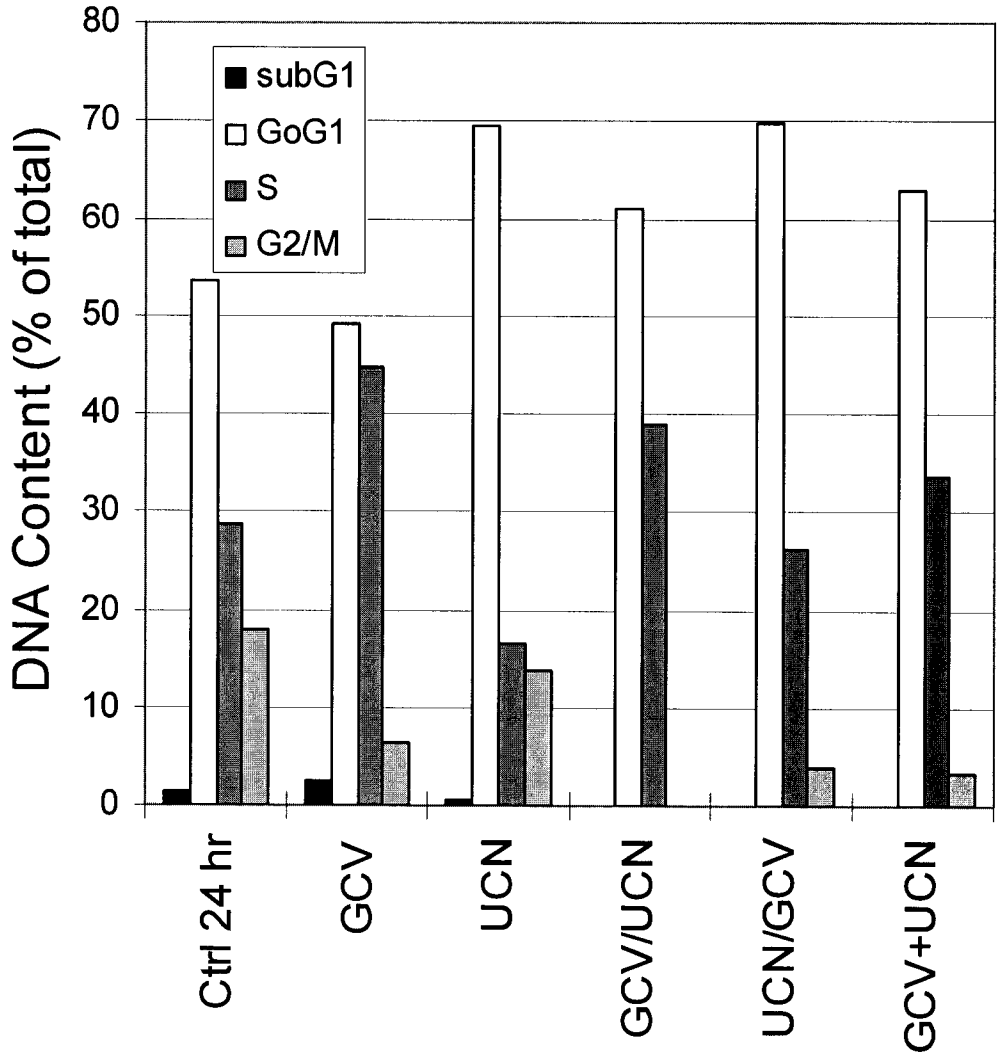

Fig. 13. Cell cycle Evaluation of Order of Addition Effects. SW620.tk cells were treated with 2mM thymidine for 16 hours followed by growth in fresh media, then another 2mM thymidine for 16 hours. Cells were released into media, 10 μM GCV, 0.3 μM UCN-01, U+G, GCV for the first 12 hours then UCN-01, or UCN-01 for the first 12 hours then GCV. At 24 hours, cells were removed and fixed in 70% ethanol.

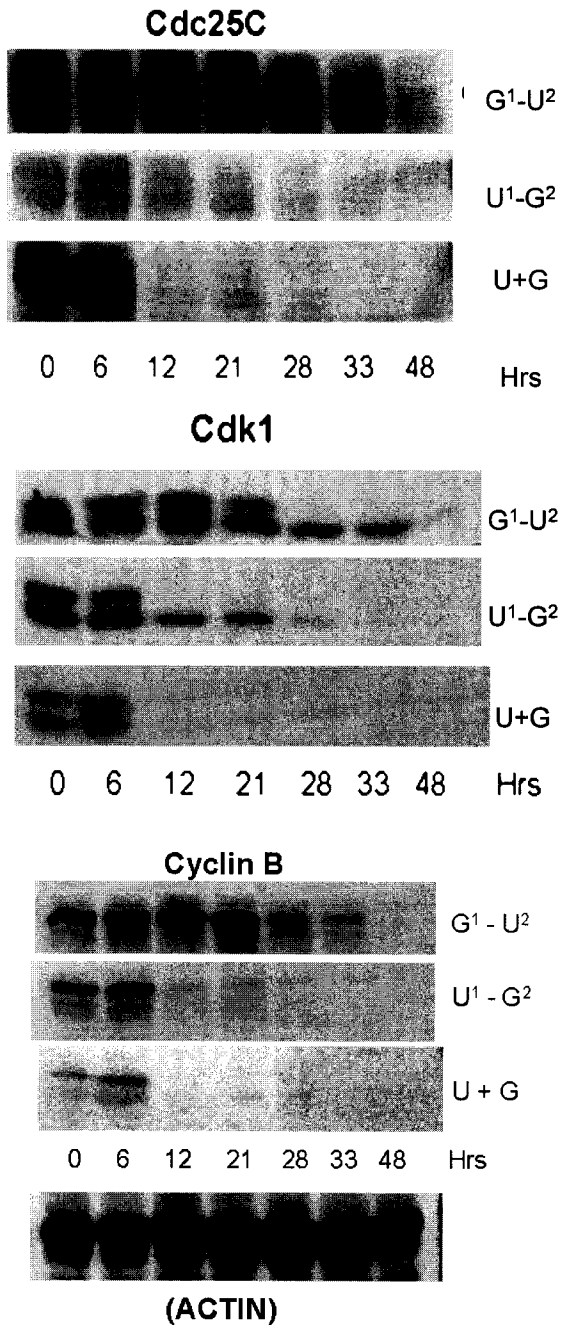

Fig. 14. Order of Addition: Western blots of mitotic proteins. SW620.tk cells were treated with 2mM thymidine for 16 hours followed by growth in fresh media, then another 2mM thymidine for 16 hours. Cells were released into media, 10 μM GCV, 0.3 μM UCN-01, U+G, GCV for the first 12 hours then UCN-01, or UCN-01 for the first 12 hours then GCV. At different time points, cells were removed and processed for western blot analysis.

combination, and these data also coincided with DAPI staining results. The different combinations of UCN-01+GCV consistently generated DAPI stained foci indicative of apoptosis, as shown in Figure 12.

Double thymidine synchronized cell cycle studies revealed that cells treated with GCV at any point had more cells in S-phase than compared to UCN-01 treatment alone, and this appears to prevail in UCN-01/GCV treated cells. (Figure 13) In Figure 14, western blots revealed that the addition of UCN-01, whether it was first or 12 hours later, appeared to dominate the effects on cdc25C, cyclin B, and CDK1 by promoting their disappearance.

Global proteomic approaches

SELDI-TOF MS

In 2001, our laboratory was connected to a state of the art proteomics facility allowing access to global proteomics tools. Surface Enhanced Laser Desorption Ionization Time of Flight (SELDI-TOF) Mass spectroscopy was one such method, and it was pioneered in 1993 by Hutchens and Yip (140) and commercialized by Ciphergen Biosystems. This process involves adding samples to aluminum ProteinChips® with different chromatographic surfaces. These chips allow for specific, selective binding of proteins in a sample to a particular surface chemistry while washing away any non-specific interactions (as reviewed by (141)). SELDI seemed beneficial in our quest to determine a complex signaling pathway after treatment with GCV, UCN-01, and UCN-01+GCV; therefore, we applied this method to analyze cell lysates and nuclear

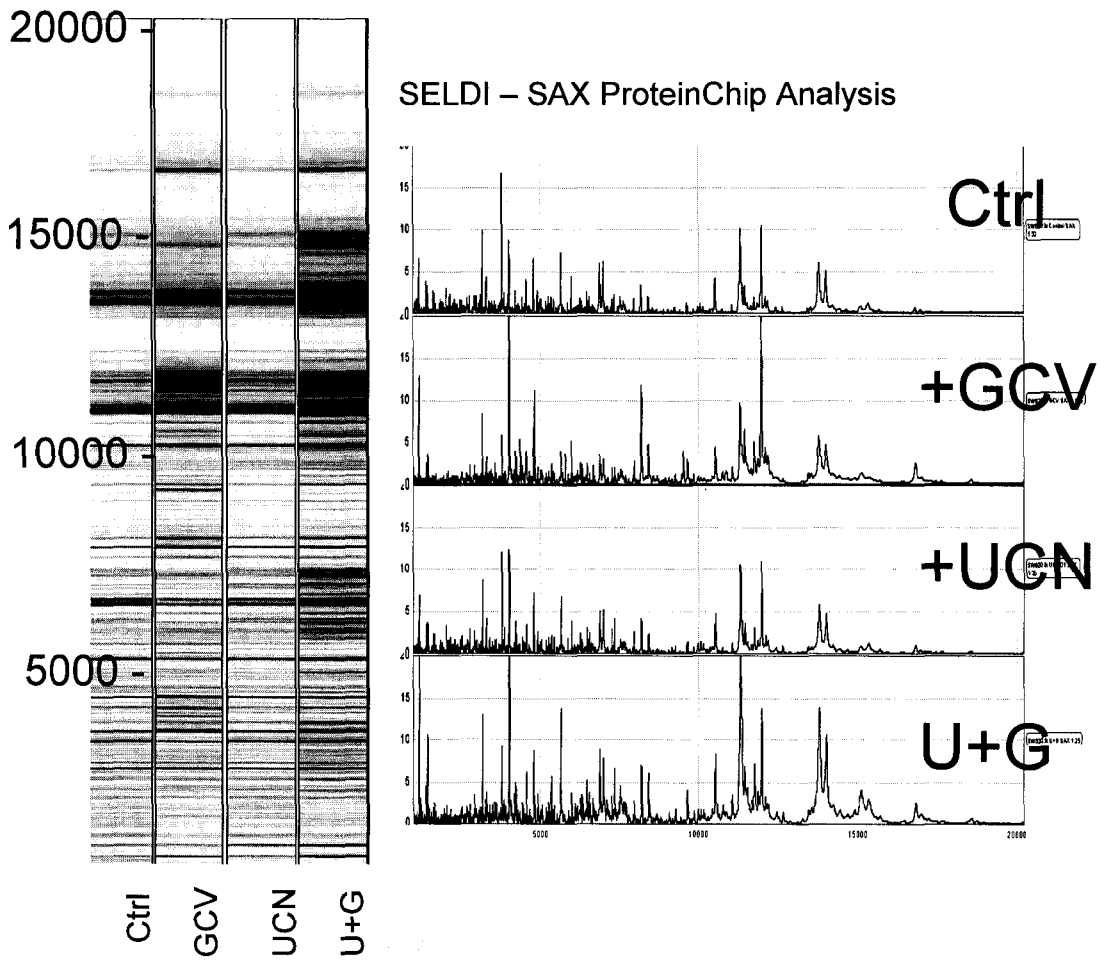

Fig. 15. SELDI-tof Profiling of SW620.tk cells treated with UCN-01 and GCV. SW620.tk cells ($5X10^6$) were treated with media, 10 μM GCV, 0.3 μM UCN-01 or 10μM GCV/0.3μM UCN-01 for 24 hours. Total cell lysates were prepared in Tris/1% TX-100 lysis bufer plus sonication. Supernatant was applied to a strong cation surface ProteinChip from Ciphergen Biosystems. A surface-enhanced laser desorption/ionization (SELDI) PBS-II mass reader (Ciphergen Biosystems) was used to generate the indicated protein spectra, mass ranges from 0-20000 daltons.

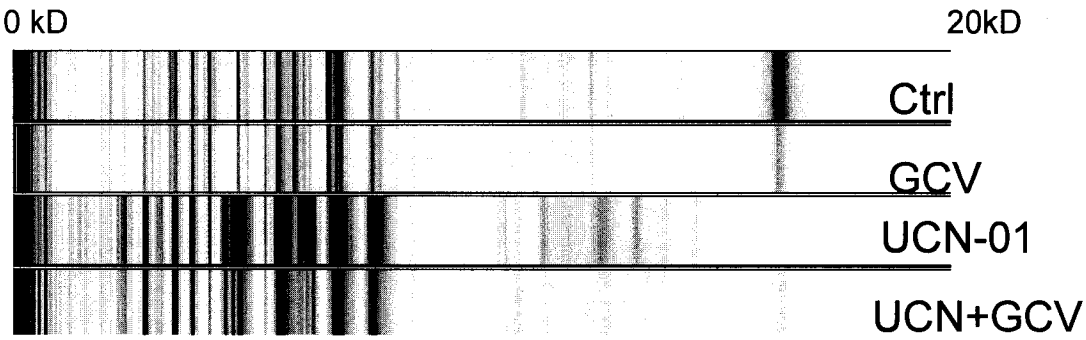

Fig. 16. SELDI-tof MS Analysis of Nuclei from drug treated SW620.tk cells. 2 $X10^6$ cells were plated in T-75 tissue culture flasks, synchronized, and drug treated as previously described. After 24 hours, the cells were harvested. The nuclear fractions from the cells were separated from the cytosol and membranes, and enriched by differential centrifugation using NE-PER reagents from Pierce. The nuclei were diluted and loaded onto the prepared ProteinChips. (Strong Anion Exchange (SAX) in this figure) After the chips dried, the energy adsorbing molecule, Sinapinic Acid (SPA) was added to each spot. The coated chips were placed in the mass spectometer. Data was collectedat a low laser energy to obtain sharp peaks in the low mass range. The data was recorded by Ciphergen Biosystems analysis software.

lysates of cells treated with GCV, UCN-01, and U+G. Several attempts were made to optimize the system, and as shown in Figures 15 and 16, Strong Anion Exchange (SAX) chips produced excellent spectra with low background for comparison with both cell lysates and nuclear lysates. As expected, the quality spectra produced several drug specific peaks. However, identification of these drug-specific peaks was not possible with SELDI methods, and remains to be followed up on with the newer instrumentation now available in the Center for Biomedical Proteomics.

Two-Dimensional Gel Electrophoresis (2D gels)

Another powerful tool for our proteome comparisons was two-dimensional gel electrophoresis. This is an attractive technology for its abilities for comparisons of many proteins at once between samples and further identification of spots of interest via spot extraction, trypsin digest, and MS analysis. The sample rehydration/lysis buffer provided by BioRad was used to lyse the cells at 100,000 cells per 100ul ratio, and then the RC/DC protein concentration determination kit (BioRad) was used to determine protein concentration. Optimization of this approach yielded excellent spot formation by loading 20-60 µg of protein. Figure 17 shows very distinct and well-resolved protein separation between drug treatments. Spots of interest were identified and excised from the gels. Prohibitin was identified in all drug treatments and was not visible in the control gel, and peroxiredoxin (aka Natural Killer enhancing factor) was identified in Control and GCV gels, but was not visible in the UCN-01 or U+G gels. NM23

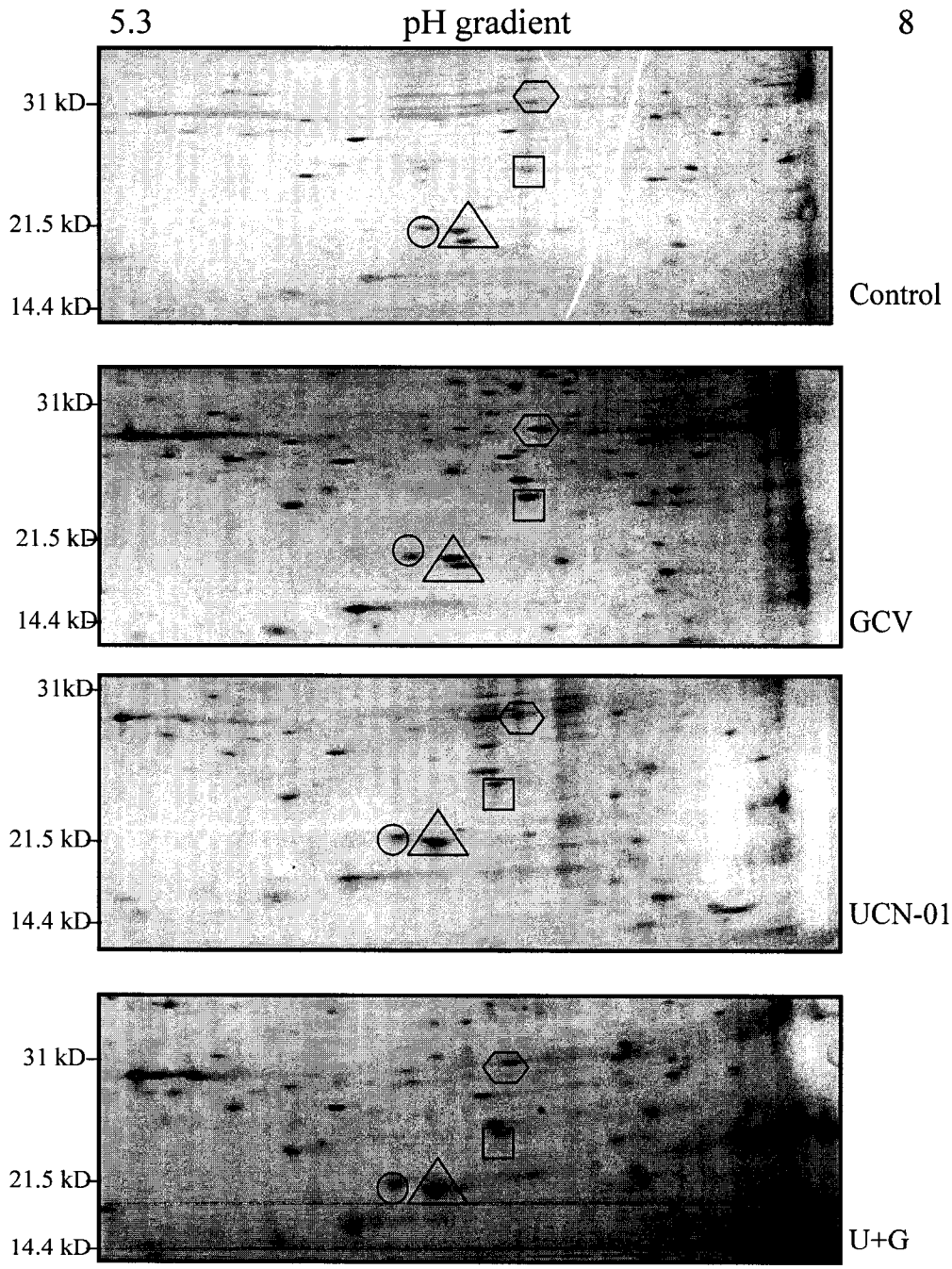

Fig. 17. 2D Gel electrophoresis of control and drug treated SW620.tk cells. SW620.tk cells were plated and drug treated for 24 hours. 20µg of cell lysates were loaded onto pH 5-8 IPG strips and focused 35000 volt hours. Strips were subsequently run on 8-16 % gradient gels, and then the gels were silver stained. Spots of interest: Square= Peroxiredoxin; circle= NM23; hexagon= prohibitin; triangle= spots in the queue.

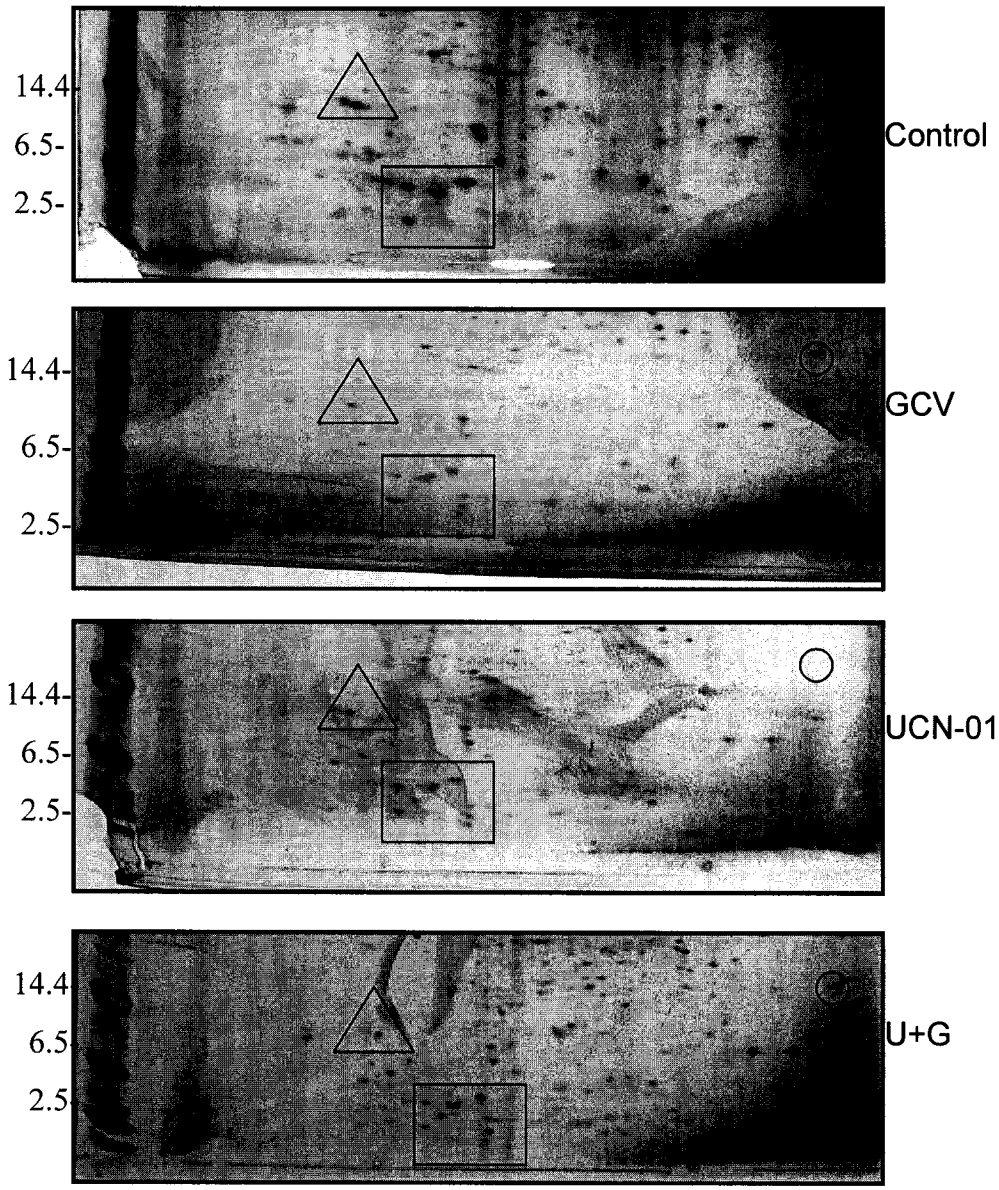

Fig. 18: 2D Gel Electrophoresis of control and drug treated SW620.tk nuclear lysates. Nuclear lysates were prepared as described in Materials and Methods. 20µg of protein from the nuclear lysates were added onto pH 3-10 IPG strips and focused for 35000 volt hours. Strips were subsequently run on 8-16% gradient gels, and then gels were silver stained. Spots or areas of interest have been marked on the gels. No protein identifications are available yet.

was identified in all the samples. (see Figure17 for labeled locations of these spots)

Since many of our target proteins reside in the nucleus, we prepared nuclear lysates of SW620.tk cells after drug treatments. It was thought that this additional purification step prior to loading the sample onto the IPG strip would allow for examination of the cellular compartment of interest and reduction of the number of proteins to examine. Nuclear lysates were run on 2D gels, and the protein spots resolved well. Currently, we do not have the identity of any differential spots, but excised spots are in the queue for identification as indicated on the gels in Figure 18.

Discussion

Using a combination of cell cycle analyses, western blots and apoptosis assays in synchronized cell cultures, the single and combination effects of UCN-01 and GCV on the cell cycle were evident. One of the most significant results in respect to GCV mechanism was the profound S-phase arrest in the synchronized cells, even in the presence of UCN-01. GCV alone led to an S-phase specific cell cycle arrest and steady levels of all six proteins examined by Western blot. Apoptosis of the GCV-treated cells was S-phase specific, and caspase 3 activation increased steadily from 6-31 hours. Under the conditions tested in the synchronized SW620.TK cells, UCN-01 led to a time dependent disppearance of cyclin B, cyclin A and cdc25C proteins, and loss of phosphorylation of Tyr15 on Cdk-1. Caspase 3 was maximally activated within 6 hrs of UCN-01 treatment.

UCN-01 plus GCV did not alter the cell cycle arrest in S-phase, but it did accelerate induction of apoptosis. The S-phase specific death is similar to that reported with gemcitabine and UCN-01 combinations (85). The UCN-01/GCV combination caused the same effects on the cyclins and cdc25C as with UCN-01 alone, but at a slower rate. A more pronounced decrease in Bcl-X_L levels was evident within 24 hrs. The nuclear morphology of the combination treated cells reflected that of UCN-01 treatment, in contrast to the S-phase induced swollen nuclei morphology of GCV alone. The dose of 300 nM UCN-01 is a median one, and we have observed empirically that the cellular effects described are consistent in the 50-500 nM ranges, but diminish below 30 nM doses (data not shown).

The key observation in the initial experiments was the drug induced decrease in cdc25C protein levels (Figure 5). Before determining that the GCV and UCN-01 combinations in synchronized cells was an S-phase specific response, we had hypothesized that UCN-01 inhibition of Chk1, and therefore continued activation of cdc25C, would result in activated cdk1/cyclinB complexes, abrogation of a G2-block, and entrance of the cell into the mitotic phase as has been reported for UCN-01 in combination with camptothecin (88), cisplatin (86), or mitomycin C (89).

Our lab has shown previously that the absence of cdc25C after 24 hours of UCN-01 treatments contrasted that of the effect of 100 nM taxol. As we had previously reported, taxol and GCV combinations in the SW620.TK cells leads to non-additive interactions and increased cell viability in the time frame of the

experiments(60). It is known that one of the primary effects of taxol is to cause a G_2/M phase arrest due to stabilization of the microtubule spindle fibers (142, 143), although this effect is variable depending on the taxol concentrations utilized. High doses of taxol (0.2-30 μM) are required to induce maximal microtubule effects and induction of apoptosis, while low range doses (1-100 nM) can have multiple cell cycle and apoptotic effects depending on cell tumor type and dose duration (142). These results are consistent with the S-phase arrest caused by GCV, which likely prevented the arrested cells from interacting with taxol during its most effective phase of the cell cycle, G_2/M.

Because many studies have shown that UCN-01 plus a DNA damaging agent results in better cell killing than either drug alone (64, 67), the UCN-01 plus GCV data further reinforce the mechanistic observations that GCV incorporation into DNA is a primary pharmacological activator of cellular responses. This effect is consistent with the reported inhibitory functions of UCN-01: the AKT survival pathway (78), DNA excision repair (79), and Chk1 (73). Other effects that we have identified indicative of the UCN-01 and GCV combinations besides our original observations of increased apoptosis (60) included a heightened degradation of Bcl-X_L (Figure 5), acceleration of the GCV-induced S-phase apoptotic cell death (Figure 2), and increased incorporation of GCV into DNA in the presence of UCN-01 (Figure 8). The combination of GCV and UCN-01 caused enough of a DNA damage response that there is no mitotic progression, apparently due to the UCN-01 induced degradation of regulatory proteins like cyclin B and cdc25C. This ultimately led to increased rates of apoptosis, as

indicated by the DAPI staining and caspase activity assays (Figures 6-8). Furthermore, UCN-01 promotes increased incorporation of GCV into the DNA (Figure 9), probably by two mechanisms. Because GCV alone leads to an S-phase arrest, the addition of UCN-01 may inhibit part of those repair mechanisms or checkpoints induced by GCV, and thus allow further incorporation of GCV-TP into nascent DNA strands. Also, since UCN-01 has been reported to suppress the transcription of thymidylate synthase (138), the result is less intracellular thymidine nucleotides present that could compete with GCV for phosphorylation by HSV-TK. It has been well documented in combination therapies of HSV-TK/GCV with cytidine deaminase/5FC (139, 144), or hydroxyurea (58), GCV metabolism is enhanced when thymidine nucleotide pools are depleted. The multiple inhibitory functions of UCN-01 thus contribute to this increased GCV incorporation, thus contributing to the acceleration of apoptotic cell death seen with the GCV and UCN-01 treatments.

From the perspective that GCV treatment leads to DNA damage, and that UCN-01 treatment leads to the potential degradation of cdc25C, what then is the mechanism by which cdc25C is being targeted for degradation? For another cdc25 family member, degradation of cdc25A by the ubiquitin-proteasome pathway is well documented (145-149). However, reports of similar degradations of cdc25C in response to DNA damage or drug treatments are less well defined, and only recently being described (150-153). In one study (153), arsenite treatment was shown to induce cdc25C degradation through the ubiquitin-proteasome pathway. There is also evidence linking cdc25C degradation to p53

status of the cell. HCT116 p53 +/+ cells infected with adeno-associated virus (AAV) showed degradation of cdc25C following a G_2 cell cycle arrest response. In contrast, AAV induced apoptosis in HCT116 p53 -/- cells, but cdc25C levels remained steady (152). However, we have not seen major differences in the levels of cdc25C degradation following UCN-01 treatments in relation to p53 status of the HSV-TK cell lines tested, including HCT116 (p53+/+) and SW620 (p53 -/-). Clearly, more studies evaluating the mechanism of cdc25C degradation and its regulation in response to UCN-01 and UCN-01/GCV treatments are warranted. For example, how the degradation of cdc25C is linked to other DNA damage response regulators like Chk1 and Chk2, both known to be inhibited by UCN-01 and use cdc25C as substrates, remains to be delineated.

At the time when the SELDI-TOF spectra were obtained, algorithms used to classify and determine "peaks" were still being developed and had only really been successful on serum analysis using a "quality control" or pool of sera to provide a signature spectra for experiment to experiment comparisons. Since completing our SELDI experiments, equipment for sample preparation has evolved quickly. ProteinsChips® and samples can now be completely prepared in an automated fashion with a robot, and this boosts reproducibility allowing us to derive conclusions from experiment to experiment more confidently. Interestingly, once peaks of interest have been identified from the spectra, the chemistries of the chip surface can be used for subsequent purification and identification of the peaks (as reviewed by (141)).

In the 2D gel experiments, making comparisons completely by eye proved extremely daunting, however, computer software is now available to assist in identification of proteins of interest. We have obtained BioRad imaging software called PD Quest set to help analyze the gels. Since gel to gel differences, sample preparation and sample origin can all cause differential spots, it will be imperative to set up multiple replicates for each condition so the software have multiple gels of each condition to set up representative templates of each gel. Comprehensive proteomic studies using 2D gel technology have been suggested in *Chapter VI: Conclusions*.

Use of the two-drug combination has also identified a putative molecular pathway whereby the DNA-damage resulting from GCV incorporation translates into arrest of cells in S-phase. Further delineation of the components of this pathway and specific target proteins involved in the surveillance, signaling, and repair of DNA damage are the focus of *Chapter IV* of this dissertation.

CHAPTER IV

AIM #2: DNA DAMAGE AND REPAIR: IMPLICATIONS FOR MECHANISM AND EFFICACY OF HSV-TK/GCV AND UCN-01 TREATMENT SCHEMES

The main focus of investigation into the mechanism of UCN-01 by our lab and others has been related to the cell cycle, yet newer studies have shown that the inhibitory effect of UCN-01 is not always related to cycle progression. In section A, we revealed that UCN-01 can abrogate survival in GCV treated TK expressing cells that are arrested in S-phase without cell cycle progression. This still had not answered the questions about how UCN-01 was acting used singly and with HSV-tk/GCV treatments. Based on our observations, we began to consider the different actions of UCN-01 as an agent that disrupts the equilibrium between activation and inhibition of DNA repair processes. We began our studies with a global approaches using powerful tools such as SELDI-TOF mass spectroscopy and confocal microscopy, however, our concluding studies focused specifically on a potentially new DNA damage mechanism of UCN-01.

Evaluation of abrogation of G_2/M arrest

Since caffeine is a known Chk1, ATM/ATR inhibitor it was tested in combination with GCV to compare with the enhanced killing when cells are treated with UCN-01. Figure 19 shows GCV plus caffeine did not produce enhanced cell killing. Furthermore, we did establish that UCN-01 was able to

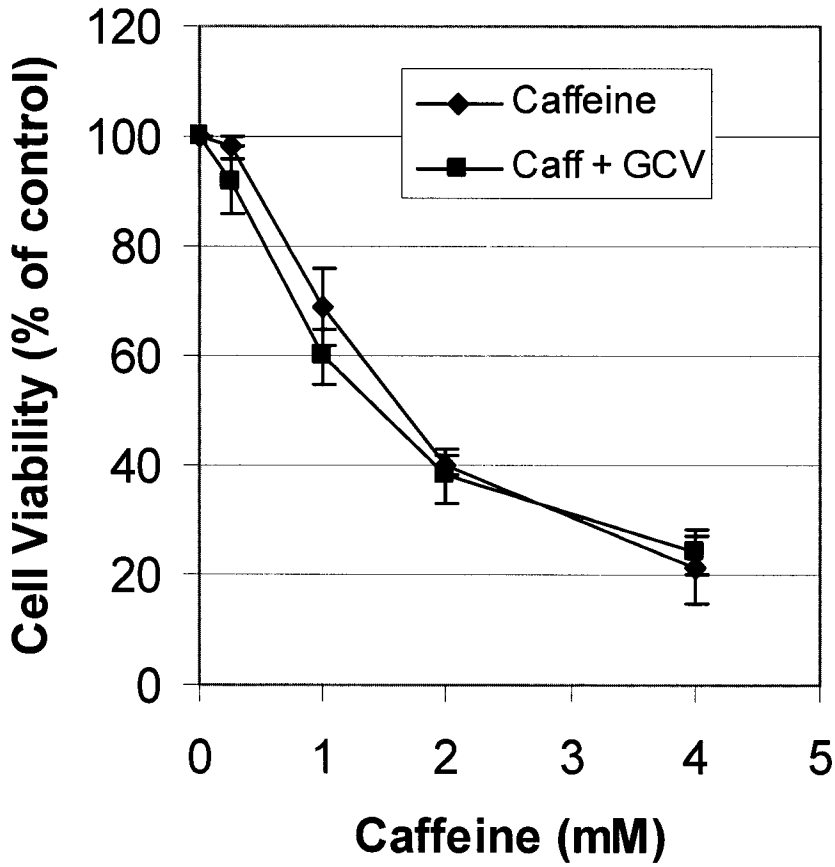

Fig. 19. Cell Viabilities of Cells after Caffeine and GCV treatment. SW620.tk cells were treated with increasing concentrations of caffeine only or plus 10μM GCV. MTT was added 48 hours later to determine cell viability.

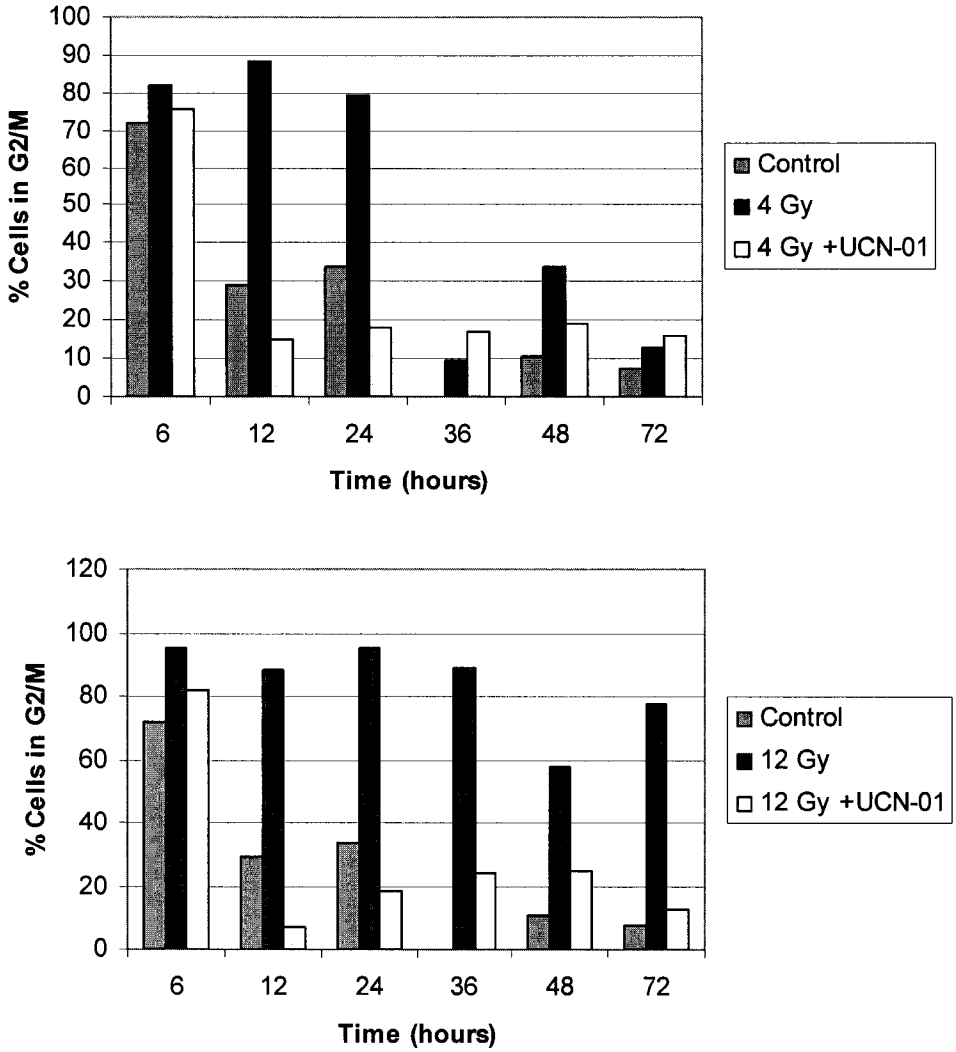

Fig. 20. Cell cycle analysis of SW620.tk cells treated with radiation and UCN-01. Cells were synchronized and treated with media only, 4 or 12 Gy radiation alone or combined with 0.3μM UCN-01. Cells were harvested at the indicated time points and resuspended in 70% ethanol.

abrogate G_2/M arrest in SW620.tk cells induced after irradiated the cells with 4 or 12 Gy radiation as shown in Figure 20 revealing that the signaling cascade functions to arrest cells after radiation, and after UCN-01 is added, that arrest is abolished. Our system can function in the classical definition of UCN-01 to abrogate G_2/M arrest, but our findings with GCV and UCN-01 treatments still coincide with the S-phase specific cell death when combining Gemcitabine and UCN-01 (85). These findings prompted our laboratory to seek global proteomics changes in order to identify new leads for understanding the mechanisms behind UCN-01 and GCV treatments.

DNA damage signaling

Immunocytochemistry

Since DNA damage surveillance proteins have been shown to form foci and punctate spots upon DNA damage (115, 120),we have screened many DNA damage response proteins using immunofluorescence as summarized in Table 5. The most distinct drug dependent localization or pattern shifts were observed with 53BP1 and Chk1/Chk1-P (Figure 21). The immunofluorescence results of 53BP1, Chk1-P, following UCN-01 treatment is consistent with a DNA damage response (Figure 21A and 21D) and levels of Chk1 did not change (Figure 21C); however, it is unknown if UCN-01 is directly responsible for this damage. The phosphorylation of Chk1 via ATM/ATR would be expected after DNA damage, as seen following UCN-01 treatment (compare Figure 21C and 21D). The absence of the Chk1-P signal in the U+G treated cells could be due to the time point

Table 5 *Confocal Microscopy of proteins involved in a DNA damage response*

Protein	Hours treated/unsynchronized or synchronized	Differences between drug treatments	Description or hallmarks
53BP1	24/unsynch 12/Synch	Yes	UCN-01, nuclear and very punctate
BRCA-P	12/synch	Subtle	UCN-01, nuclear punctate
BRCA	12/synch	No	Nuclear
Chk1-P	12/synch	Yes	GCV and UCN-01 bright nuclear staining
Chk1	12/synch	No	Nuclear
Chk2	12/synch	Subtle	Follows nuclear organization changes; muliple round bodies in U+G
Chk2-P	12/synch	No	No detection at all; no detection in westerns
Cdc25C	12/synch 24/synch	No	Cytosolic
Cdc25A	12/synch	Subtle	Nuclear disorganization in UCN-01 and U+G

Table 6 *Summary of Cell lines used for PFGE*

Cell Line	Description	p53 status	Mismatch repair status
HT-29	Colon Cancer	Mutant	Proficient
MCF-7	Breast Cancer	Wild Type	Proficient
CSC-1	Normal colon	Wild type	Proficient
NCM460	Normal colon	Wild type	Proficient

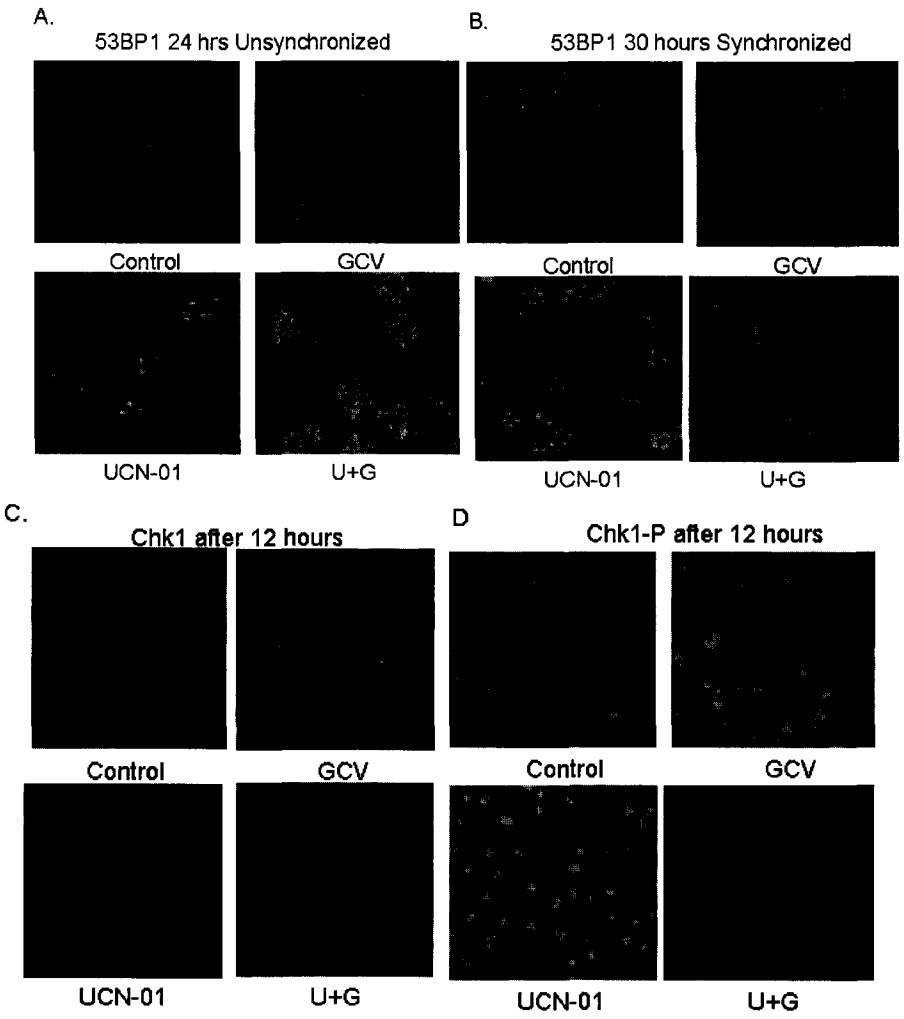

Fig. 21. Confocal Microscopy of 53BP1, Chk1, and Chk1-P in Treated SW620.tk cells. 80,000 cells were seeded onto each well of a 2-well Permanox slide. These cells were double thymidine blocked then released in to media, 10μm GCV, 0.3 μM UCN-01, or 10μM GCV/0.3 μM UCN-01 for 12 hours. The 24- hour panel was not synchronized, just released into treatments. Cells were fixed and permeabolized with 2% paraformaldehyde and 0.5% triton X-100 and incubated with the indicated primary antibody. A) and B) 53BP1 was from Bethyl Laboratories, C) Chk1 was from Santa Cruz and D) Chk-P was from Cell Signalling Technologies. The secondary antibody was an anti-rabbit IgG conjugated to AlexaFluor 488nm (Molecular Probes) Images were captured using a Zeiss Confocal Microscope. All images are maximum projections of a z series.

analyzed. This phosphorylation could have already occurred, consistent with the increased apoptotic responses from this drug combination, or this drug combination could circumvent Chk1 completely.

Determination of DNA Double Strand Break Formation

γH2AX westerns

Next, phosphorylation of histone H2AX as a marker of double stranded DNA breaks was evaluated to examine whether UCN-01 causes damage to the DNA itself. Up to this point, we had only seen several components of the DNA damage signaling activated, and therefore we decided to look specifically for the kind of DNA damage that was occurring. Western blots for the phosphorylated form of histone H2AX, γH2AX, showed induction of the phosphorylation after 30 hours of GCV treatment, 8 hours for UCN-01 and 8 hours for U+G. (Figure 22) For reference, one DSB induces the phosphorylation of 0.03% of the total cellular H2AX, which corresponds to 2 Mbp of chromatin (154).

Pulsed Field Gel Electrophoresis for the detection of DSBs

In light of 53BP1 immunofluorescence and γH2AX western blots, we pursued a method to detect double strand breaks after UCN-01 treatment in TK expressing cells. We employed the method of pulsed field gel electrophoresis under the supervision of Dr. Richard Britten, Ph.D. at Eastern Virginia Medical School Department of Radiation Oncology. Mega base pair length (Mbp) DNA fragments can be separated by size by using pulsed electric fields with

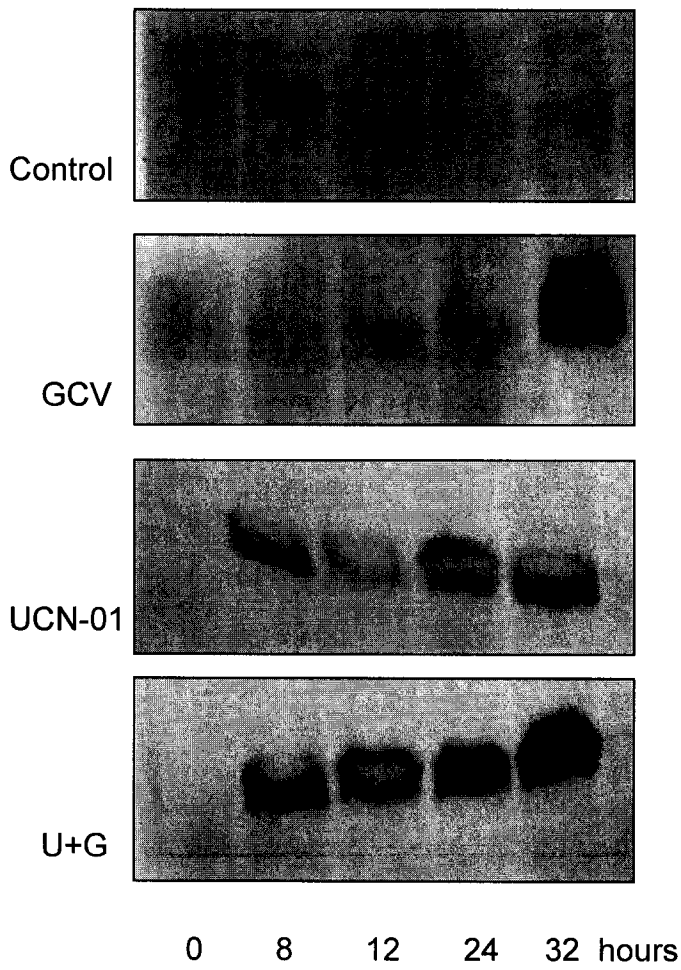

Fig. 22. Western Blot Determinations of γH2AX levels in SW620.tk Cells Treated with GCV and UCN-01. SW620.tk cells were double thymidine synchronized, then released into media, 10uM GCV, 0.3 μM UCN-01, or 10μM GCV/0.3μM UCN-01, or 10 μM GCV/0.3 μM UCN-01. At different time points, cells were removed and processed for Western Blot analysis. Anti-γH2AX antibody was obtained from Trevigen.

periodically changing direction. By changing pulse duration, field strength or even agarose concentration, the PFGE protocol can be optimized for separation of different sized fragments (155). Only DNA fragments smaller than 10 mbp can be investigated by PFGE and many breaks have to occur per cell (113).

Unsynchronized SW620.tk cells were drug treated with 10μM GCV, 0.3μM UCN-01, and U+G for 8 and 24 hours, and were harvested and immediately prepared into agarose plugs. The placement of whole cells into the agarose was to ensure that there would not be any shearing of the DNA prior to PFGE. Initial experiments with drug treated SW620.tk cells showed subtle DNA elution out of SW620.tk cells treated with UCN-01 and U+G (data not shown), indicative of double strand breaks. We then also tested several other cell lines to determine if elution would be detectable in other cell lines tested with UCN-01. Those cells and their descriptions are summarized in Table 6. In all cell lines tested, compared to control, UCN-01 induced significant double strand breaks as detectable by PFGE (Figure 23).

Since HT29.tk cells revealed increased elution after UCN-01 treatment compared to SW620.tk cells, they were used to further evaluate DSB formation after UCN-01 and GCV treatments. Unsynchronized HT29.tk cells were treated with media, GCV, UCN-01, and U+G for 8 hours and 24 hours prior to harvesting the cells for PFGE. There were no easily detectable DSBs by 8 hours in control and GCV treated cells; however, there was faint elution out of the UCN-01 and U+G plugs (Figure 24). By 24 hours, significant elution was visible in UCN-01 and U+G treatment lanes (Figure 24).

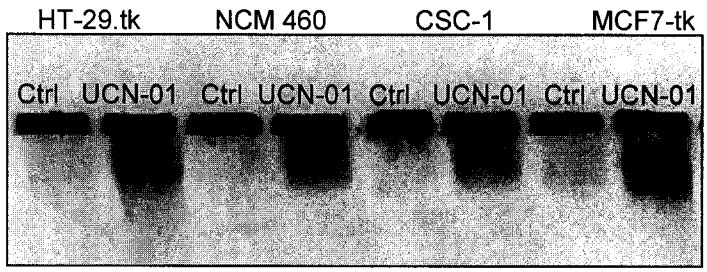

Fig. 23. Pulsed Field Gel Electrophoresis of Multiple Cell lines treated with UCN-01. Cell lines were plated in 100mm^2 plates and treated with 0.3 μM UCN-01 for 24hours. Cells were harvested and processed into plugs. Plugs were run on PFGE for 24 hours using the electrophoresis conditions described in *Materials and Methods*.

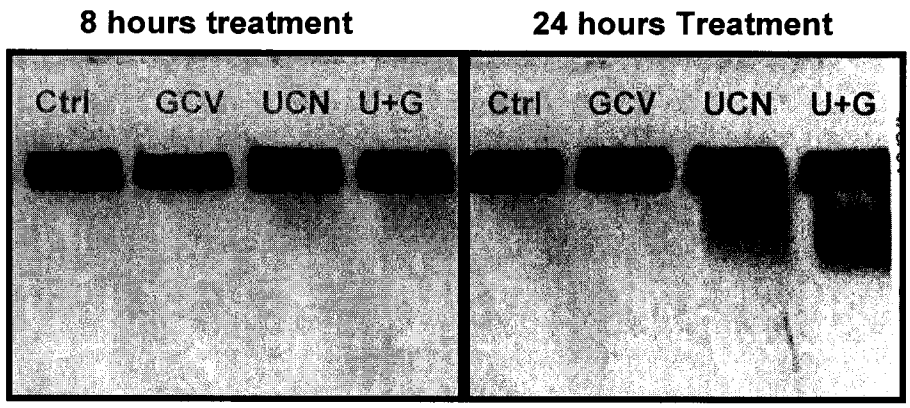

Fig. 24. Pulsed Field Gel Electrophoresis of HT29.tk cells treated with GCV, UCN-01, and the combination. Unsynchronized HT29.tk cells were treated with 10 μM GCV, 0.3 μM UCN-01, and U+G for either 8 or 24 hours prior to plug formation. PFGE was run for 24 hours prior to imaging with ethidium bromide.

Mechanism of Double Strand Break Induction by UCN-01

Inhibition of endogenous double strand breaks

Although the previous data indicates that the addition of UCN-01 can cause double strand breaks in most cell lines tested, the origin of these double strand breaks still had not been determined. We next asked the following question: Does UCN-01 inhibit the repair of endogenous double strand breaks?

A newly designed and tested **DNA-Pk selective inhibitor NU7026 (2-(morpholin-4-yl)-benzo[h]chromen-4-one)** from Calbiochem was chosen because it has 60-fold greater potency against DNA-Pk compared with Phosphoinositol 3-Kinase(PI3K) and is inactive against both ATM and ATR (156). We hypothesized that if UCN-01 was causing double strand breaks by inhibiting the main repair pathway for endogenous double strand breaks, then we would detect this on PFGE, and the levels of elution would be comparable to UCN-01 elution.

Figure 25 reveals that endogenous levels of double strand breaks (those after NU7026 treatment) do not compare in size or intensity to those of UCN-01 induction; however, the combination of UCN-01 and NU7026 suggests that UCN-01 could be co-dependent on active DNA-Pk for DNA signaling and further damage because it appears that the elution is less intense. The breaks however appear to the same size as indicated by the arrow in Figure 25. However, clonal survival assays did not suggest that active DNA-PK was required for UCN-01 toxicity because the cells were not significantly rescued with the UCN-01 and NU7026 combination compared to UCN-01 alone (Figure 26). A lower dose of

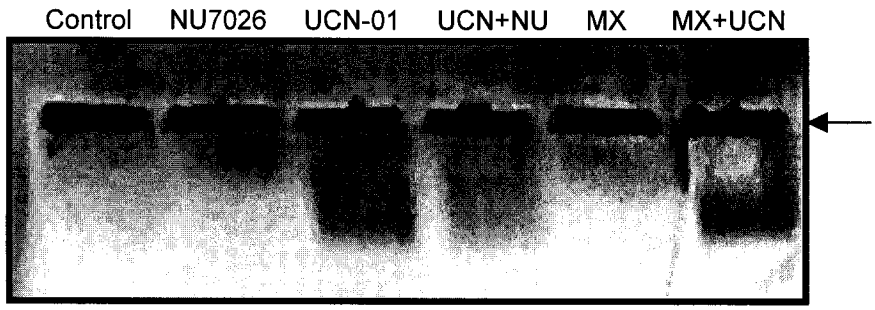

Fig. 25. Pulse Field Gel Electrophoresis of HT29.tk cells treated with media, NU7026, UCN-01, U+N, or MX+UCN-01. HT29.tk cells were treated for 24 hours with media, 250nM UCN-01, 15μM NU7026, 6mM Methoxyamine or the indicated combination. Cells were processed into agarose plugs, and plugs were were run in PFGE for 30 hours and stained with EtBr.

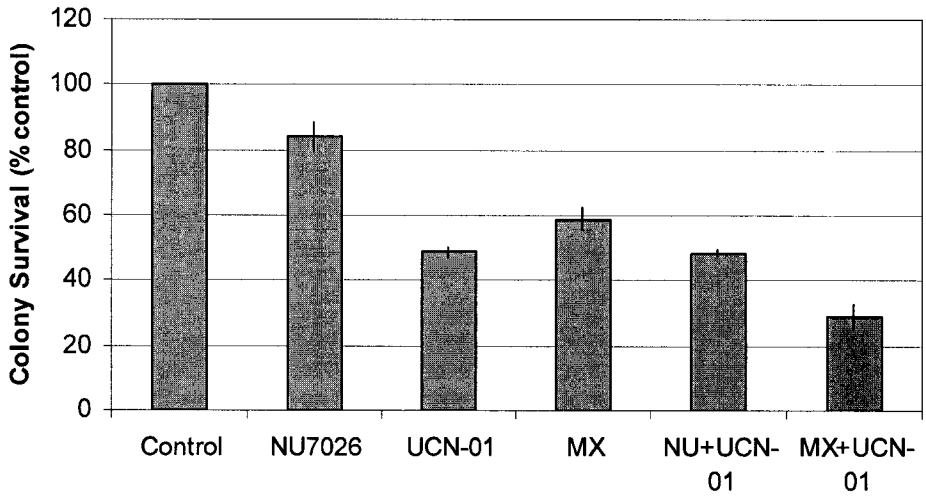

Fig. 26. Clonal Survival Assay of HT29.tk cells treated with methoxyamine, NU7026, and UCN-01. 2000 cells were plated per well in a 24 well plate. The next day 15 μM NU7026, 37nM UCN-01, 6mM Methoxyamine or the combination with UCN-01 were added, and colonies were stained and counted 6 days later. Data are representative of three separate experiments with each condition performed in triplicate.

UCN-01 (37nm) was used in the clonal survival assays because higher concentrations were too toxic for any colonies to form. In order to determine if there was any synergy or antagonistic effects with UCN-01, the colony numbers had to be high enough to detect these types of interactions with NU7026 and methoxyamine.

Inhibition of Base Excision Repair

Another possible explanation of double strand break induction after UCN-01 treatment is unrelated to the inhibition of endogenous double strand breaks. We developed a more interesting but complex theory involving base excision repair (BER). We asked the following question: Does UCN-01 inhibit base excision repair (BER) therefore causing double strand breaks? In Figure 25, the BER inhibitor methoxyamine alone did not generate detectable DSBs compared to UCN-01, but the combination of MX and UCN-01 revealed a key effect: UCN-01 treated cells resulted in similar migration no matter what treatment, as long as UCN-01 was present. In MX + UCN-01 treatments, most of the intermediate sizes of double strand breaks were gone, and only one size appeared to migrate.

DNA Single strand breaks: Alkaline elution of agarose plugs

We also wanted to look for DNA single strand breaks after our drug treatments, and we adapted an alkaline method for our cells already in agarose plugs. To our knowledge, alkaline elution has never been performed in a PFGE system. Single strand breaks have alkaline labile sites that convert to double

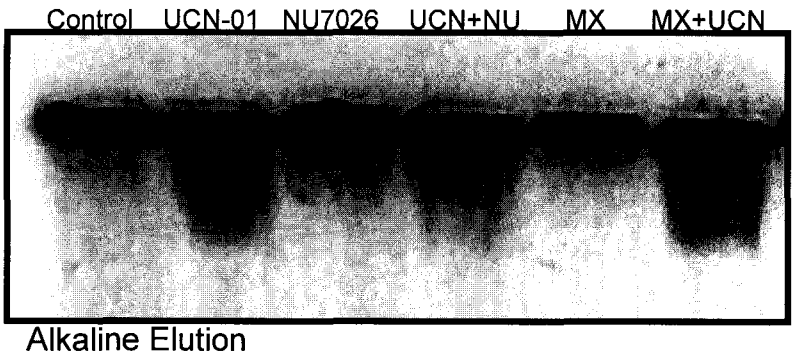

Fig. 27. Alkaline elution Pulse Field Gel Electrophoresis of HT29.tk cells treated with media, NU7026, UCN-01, U+N, or MX+UCN-01. HT29.tk cells were treated for 24 hours with media, 250 nM UCN-01, 15μM NU7026, 6mM Methoxyamine or the indicated combination. Cells were processed into agarose plugs, and plugs were were run in PFGE for 30 hours and stained with EtBr. Alkaline elution was performed by incubating the plugs in alkaline buffer for 2 hours prior to electrophoresis in a 0.5% alkaline buffer gel in 0.5X TBE buffer.

strand breaks after alkaline exposure. Plugs were incubated in alkaline buffer for 2 hours prior to loading into an alkaline agarose gel. PFGE was then performed under standard conditions as outlined in *Materials and Methods* in Chapter II. Figure 27 shows no elution or single strand breaks in either control, NU7026, or MX treated cells. Inhibition of BER did not reveal single strand breaks from cells, but our data suggests that all cells treated with UCN-01 generated single strand breaks. We believe that this data suggests that UCN-01 is not inhibiting repair of DNA single strand or double strand breaks and the damage it is causing is due to its specific interaction with the DNA itself.

Discussion

Confocal microscopy was a successful approach for evaluation of many proteins involved in the DNA damage signaling pathways induced after drug treatments. As we titrate drug concentrations and test multiple cell lines, we will investigate H2AX and 53BP1 foci formation as a measure of DSB induction. This will be compared to PFGE results of the same cells and treatments. The data showing the phosphorylation of H2AX within 8 hours of treatment with UCN-01 are important because UCN-01 as a single agent has never been reported to be capable of inducing DNA double strand breaks. Furthermore, phosphorylation of H2AX appears to play a critical role in the recruitment of repair or damage signaling sites of DNA damage (120, 125, 157-159). Therefore, detection of this phosphorylation fits well with our immunofluorescent data shown foci formation with 53BP1. The indication of double stranded breaks at 30 hours of GCV

treatment is more consistent with an observed apoptotic response to GCV (23, 60). The shorter time frame for UCN-01 could also be related to an apoptotic response; however, it could equally be possible that this is a result of UCN-01 induced double strand breaks.

We considered using cells lines deficient in DNA-PK such as the glioblastoma cell line MO59J, however it has been shown that they also contain reduced levels of ATM compared to MO59K cells that have DNA-Pk (160). The advantage to using these selective chemical inhibitors is that they can be used in our HSV-Thymidine Kinase stably transfected cell lines because future studies will include the complete characterization of these inhibitors combined with GCV treatment. Inhibition of endogenous DSB repair by treatment with NU7026 did not produce similar PFGE results to UCN-01 treated cells. However, we are interested in future experiements with this combination, because order of addition may change the levels of DSBs since UCN-01 could be causing replication stress itself, therefore adding a DSB repair inhibitor after UCN-01 would seal the fate of the cell.

Base excision repair employs DNA lesion-specific glycosylases to recognize and bind to the damaged sites, and remove the base. After removal of the problem (methylated) base by a purine glycosylase, which creates the abasic or apurinic-apyrimidinic (AP) site, the phosphodiester bond is immediately hydroylzed by AP endonuclease (APE), initiating the repair of the AP site (104, 161). **Methoxyamine** specifically binds to the AP site and reduces the APE cleavage of the backbone by more than 300-fold compared with the cleavage of

normal AP sites (162). We hypothesize that UCN-01 causes damage directly to the DNA in a systematic manner, and these aberrations could be normally repaired by BER. Fragments of different sizes elute after UCN-01 treatment, and no smaller fragments result because BER is successful at repairing some of the lesions. With BER inhibited, UCN-01's systematic adduct/breakage is apparent. The nature of this interaction with the DNA has never before been documented, and will be need to be further studied as discussed in *Chapter VI*. In addition, concentrations should be tested for their impact on elution of DNA from treated cells, and addition of MX and NU could be altered to zero in on the signaling mechanism for repair of UCN-01 induced lesions.

We are also intrigued in the sub-additive cell killing seen with the combination of MX and UCN-01. Methoxyamine has been shown to significantly enhance the antitumor effects of the methylating agent temozolomide (TMZ) in both MMR proficient and MMR deficient human colon cancer xenografts (163). Interestingly, Tominic *et al.* obtained data using MX indicating that protection of HSV-tk transfected CHO cells treated with GCV was provided by DNA polymerase beta dependent single nucleotide and long patch BER (33). Overcoming this protection with MX is something we will pursue in multiple TK expressing cells lines in combination with UCN-01 and GCV.

We had mentioned that HT29.tk cells were selected for pulsed field DNA elution studies because we were able to detect greater amounts of elution compared to SW620 cells. As we have been investigating the DNA damage repair inhibitory compounds by MTT and clonal survival assays, an interesting

theme had emerged. The HT29s appear to be more sensitive to UCN-01, correlating to higher amount of DNA eluting on the PFGE. This has been documented before when Canman *et al.* report showed that increased sensitivity to flurodeoxyuridine correlated with HT29 elution on PFGE compared to SW620 cells(164). Further studies will need to be done comparing the more sensitive HT29 cells to less sensitive cell lines like SW620.

In summary, it is very possible that the therapeutic utility of UCN-01 comes from its effects on several targets as opposed to just one. There is mounting evidence that UCN-01 may be interacting with the DNA, but its existence and precise contributions of this binding to the overall cellular cytotoxicity remain to be fully explored.

CHAPTER V

AIM # 3:

IN VITRO AND *IN VIVO* EVALUATION OF HSV-TK VARIANTS AND EFFICACY OF GCV AND UCN-01 *IN VIVO*

Another way to improve the overall efficacy of the HSV-tk/GCV system would be to utilize HSV-tks that were more specific for phosphorylation of GCV relative to thymidine, thus replacing the multi-substrate functions of HSV-tk. The study of these GCV-kinases (GK) fits well within our overall aim to improve HSV-tk/GCV gene therapy using several interrelated approaches. Several metabolic mutants were created in our laboratory using advanced modeling programs and characterized for GCV metabolism (52) and several interesting candidates emerged to test those effects *in vitro* and *in vivo*: GK1, GK2, and GK3. In that study, Mercer *et al.* described the kinetic properties of several site-specific mutants of HSV-tk (52). A summary of those properties is provided in Table 7.

A previous study by Drake *et al.* had already established differential GCV-mediated cell killing by mutants of HSV-tk (23), and those studies confirmed the findings by several others that GCV treatment of HSV-tk expressing cells could induce S and G2/M phase cell cycle arrests in HSV-tk expressing glioma and melanoma cell lines (19, 21, 34, 165).

Chapter V reveals the outcome of the variants characterized in a similar manner to wild type TK as described in Chapter III and their efficacy *in vivo.* We

Table 7 *Enzymatic Characteristics of HSV-tk variants*

HSV-tk	Thymidine Km (μM)	Thymidine Kcat/Km	Ganciclovir Km (μM)	Ganciclovir Kcat/Km
Wild type	0.9	$6.7X10^4$	69	$6.8 X 10^3$
Q7530 (GK1)	53	$1.1X10^3$	40	$3.2X10^2$
N7530 (GK2)	90	18	71	84
N30-3 (GK3)	ND	ND	ND	ND

Table 8 *IC_{50} for GCV treatment in multiple cell ines using MTT assay*

Cell Line	IC_{50}
DU145-tk	0.1
TRAMP-tk (wt)	0.3
TRAMP-GK1	0.3
TRAMP-GK2	10
TRAMP-GK3	N.D.
HCT116-tk (wt)	0.1

Table 9 *Summary of GCV effects in HCT116 tk variants*

Cell line	GCV metabolism	% BrDU incorp.after GCV	Caspase-3 activity	Number of Apoptotic cells	Animal Model results
WT	High	Lower	High	Medium	Apoptotic
GK1	High	Lower	High	High	Apoptotic
GK2	Low	Lower	Low	High	Apoptotic and Necrotic
GK3	Very low	Same as control	Very low	Very low	Not determined

concluded our studies looking at wild type TK in combination with UCN-01 and GCV in the TRAMP tumor model.

Flow cytometric analysis of HSV-tk variants treated with GCV

Propidium Iodide Staining

As shown in Figure 28, double thymidine treated synchronized, untreated HSV-tk expressing wild type HCT-116 cells, proceeded through a full synchronous cycle with the majority of the cells returning to G1 within 12-24 hours. Following the addition of 10 μM GCV, these wild type TK expressing cells accumulated in S-phase from 4-8 hours, then slowly progressed to the S/G_2 boundary at 12 hours. In contrast, the GK1 expressing cells immediately arrested in S-phase following GCV addition, and did not progress with time. GK2 expressing cells treated with GCV did not accumulate in S-phase, but in G_1 and G_2, while GK3 cells appeared to pause in S-phase but returned to cycling as normally as the untreated controls. These cell cycle results prompted us to test BrDU labeling in these variants after treatment with GCV.

Bromodeoxyuridine Metabolic Labeling

As stated in Chapter III, BrDU labeling was used with the caveat that BrDU is a substrate for HSV-tk; therefore, the cells were only pulsed for 2 hours during the evaluation of the HSV-TK/GK variant and GCV treatment. Figures 29 and 30 show densitometry plots of BrDU and 7-AAD. The percent of cells that were positive for BrDU is shown in the upper right corner of each graph, and this

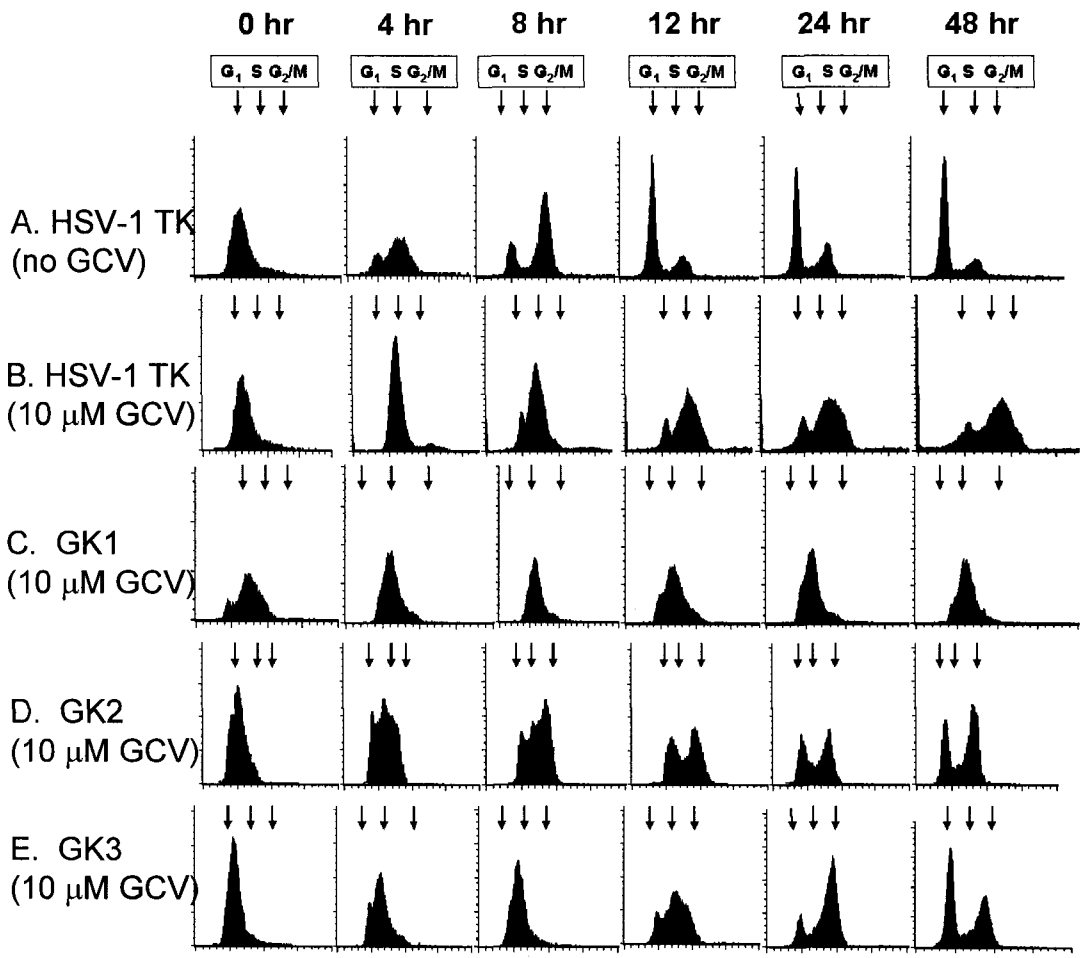

Fig. 28. Double Thymidine Block Cell Synchronization and Flow Cytometry of GCV treated HSV-1 TK and GK expressing cells. HSV-1 TK, GK1, GK2 and GK3 expressing cells were synchronized by double thymidine treatment, and released into fresh media alone or containing 10 μM GCV for 4-48 hours as described in *Materials and Methods*. At the indicated times, cells were fixed in 70% ethanol, stained with propidium iodide and analyzed by flow cytometry on a FACSCalibur instrument (Becton Dickinson, Mountain View, CA) as previously described (7). Presented are representative flow profiles of each time point for the GCV treated samples.

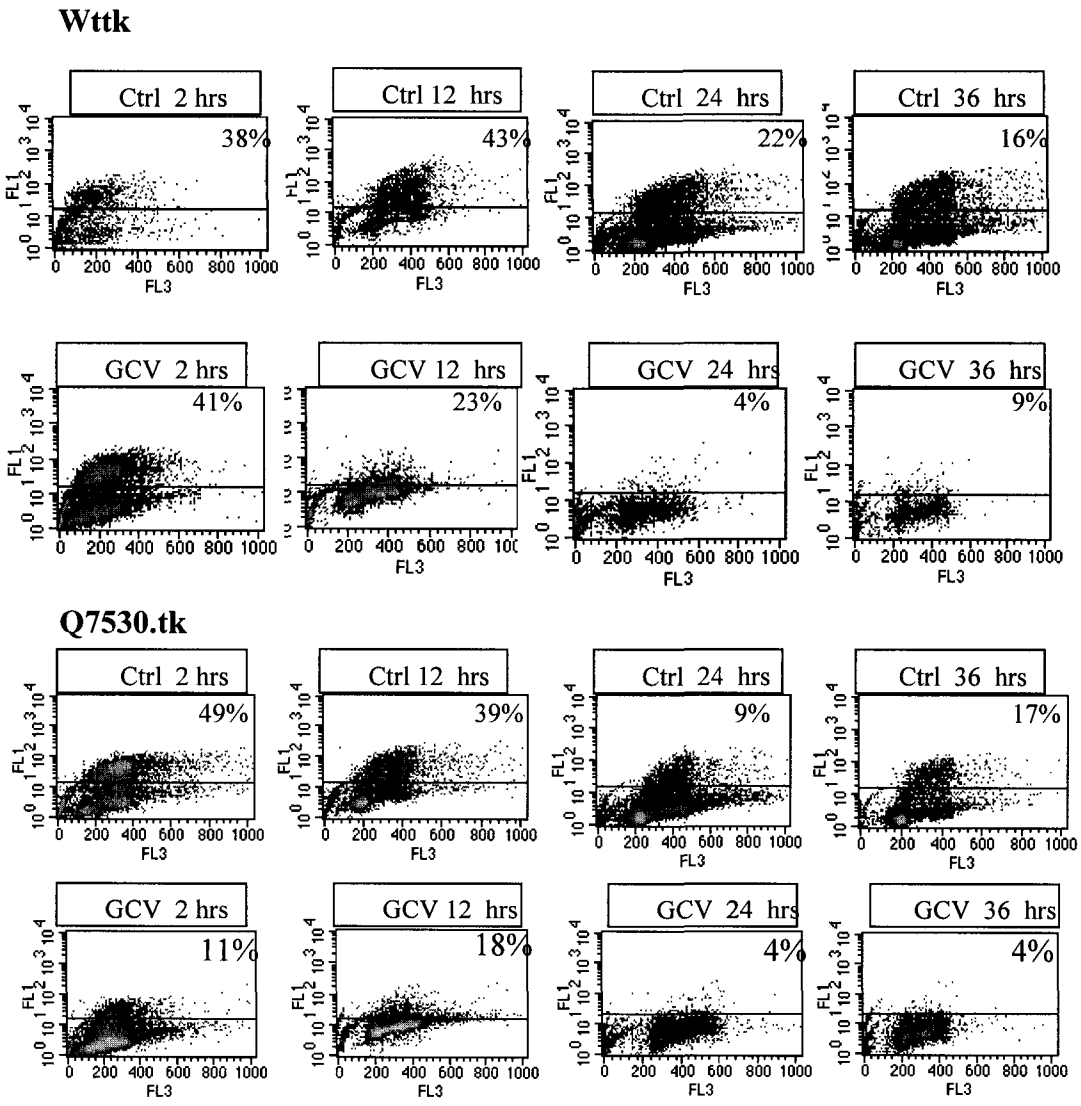

Fig. 29. 2 hour pulse labeling with 10 μM BrDU of Wttk and Q7530.tk expressing cells treated with media or 10 μM GCV. HSV-tk expressing cells (150,000) were plated in 60mm² dishes. Cells were pulsed 2 hours prior to the 2, 12, 24, or 36 hour time points before getting harvested for flow after drug treatment at the indicated time points. Fl1= BrDU and Fl3=7-AAD. The percent of BrDU positive cells is indicated in the upper right corner.

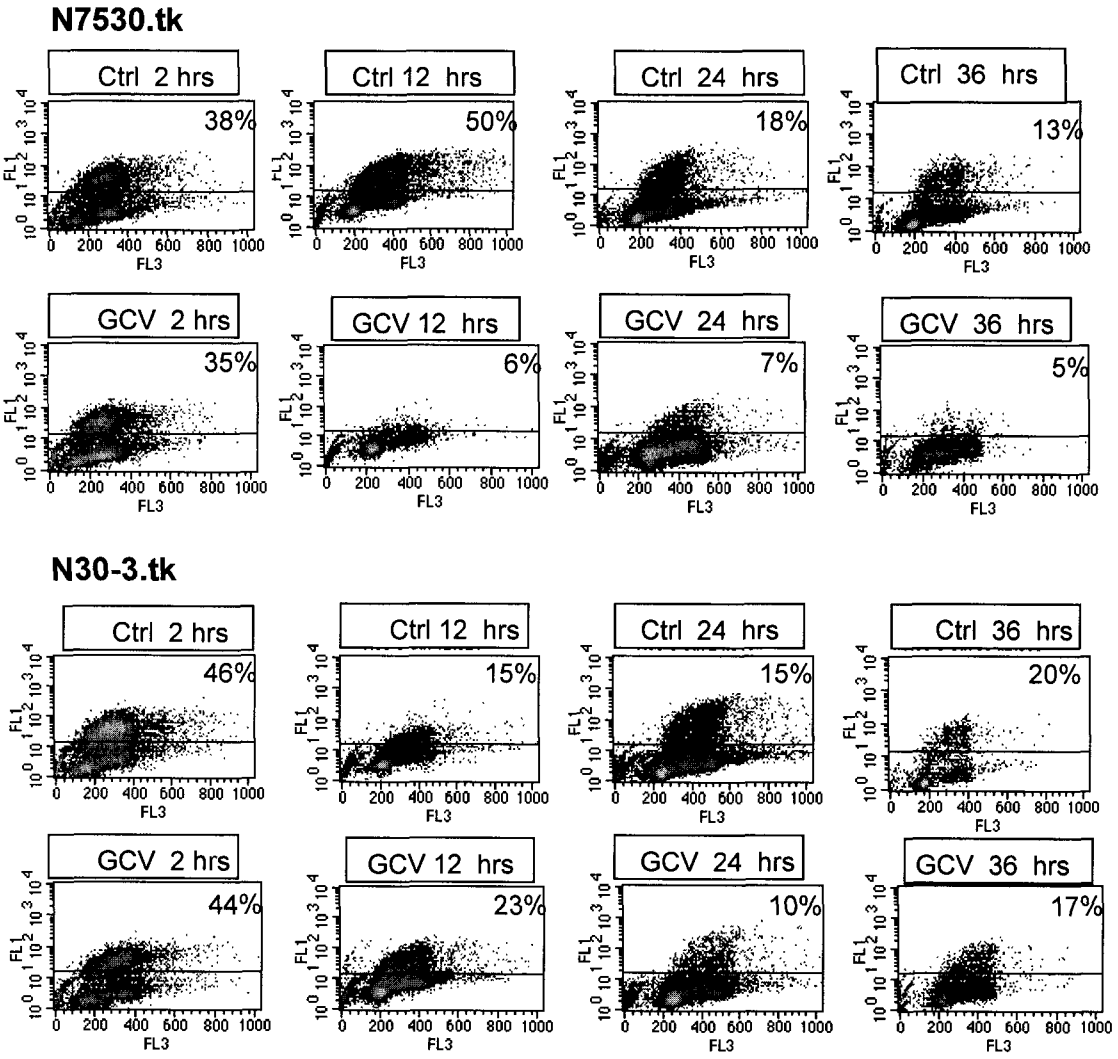

Fig.30. 2 hour pulse labeling with 10 μM BrDU of N7530.tk and N30-3 HSVtk variants treated with media or 10 μM GCV. HSV-tk expressing cells (150,000) were plated in 60mm^2 dishes. Cells were pulsed 2 hours prior to the 2, 12, 24, or 36 hour time points before getting harvested for flow after drug treatment at the indicated time points. FI1= BrDU and FI3=7-AAD. The percent of BrDU positive cells is indicated in the upper right corner.

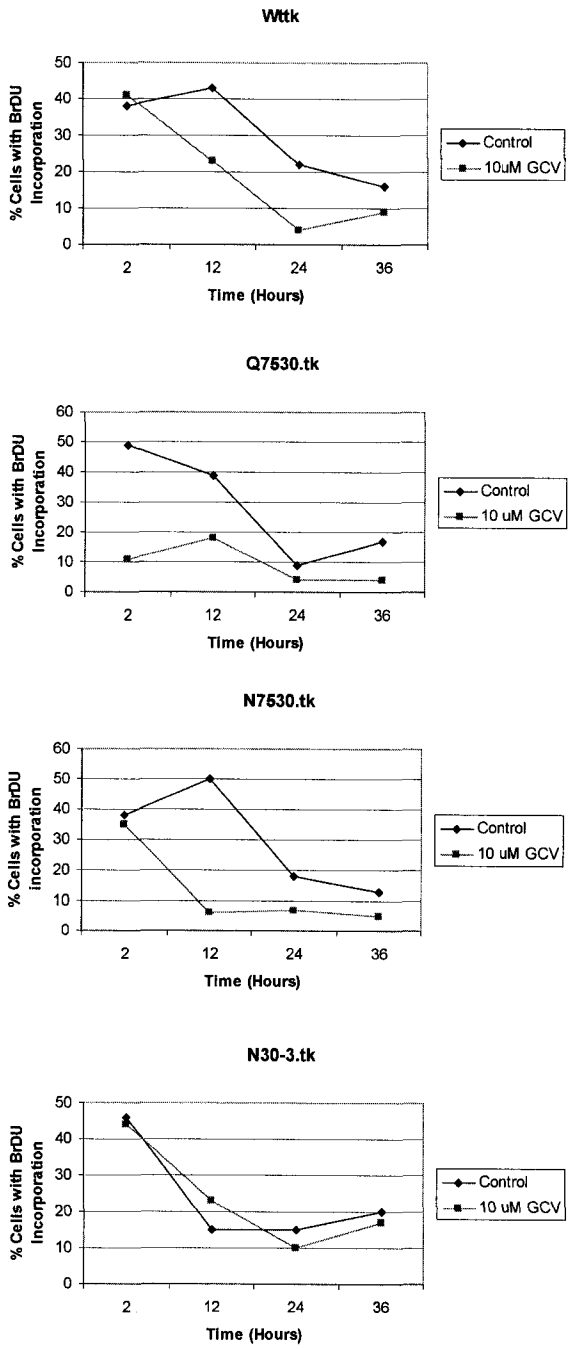

Fig. 31. Summary of BrDU incorporation in untreated and 10μM GCV treated HSV-tk variant cell lines. Percent BrDU incorporation is represented graphically from Figures 29-30 for comparison.

incorporation is also summarized in the line graphs in Figure 31. Wild-type TK, GK1, and GK2 expressing cells treated with GCV had decreased levels of BrDU incorporation compared with control. In contrast for the GK3 expressing cells, levels of BrDU incorporation remained very similar in control and GCV treated cells. This correlates well with what we described in Figure 28 with the cell cycle analysis, and the decrease in BrDU uptake in GCV treated WT and GK1 cells indicates an S-phase arrest, as opposed to accumulation in S-phase.

^{3}[H]GCV Metabolic labeling

It is thought that higher levels of GCV metabolism and incorporation correlate positively to apoptosis after GCV treatment (166), therefore the metabolism of GCV was compared across the HSV-tk variants. As shown in Figure 32, WT and GK1 expressing cells both had high levels of GCV phosphate forms correlating with increased DNA incorporation. The GK2 and GK3 expressing cells had significantly reduced levels of GCV metabolites and incorporation into the DNA, but GK2 expressing cells still higher metabolism than GK3 expressing cells. Furthermore, cytotoxicity assays revealed that killing of cells expressing HSV-TK and variants after GCV treatment (52) also correlates with the levels of GCV incorporation shown in Figure 32.

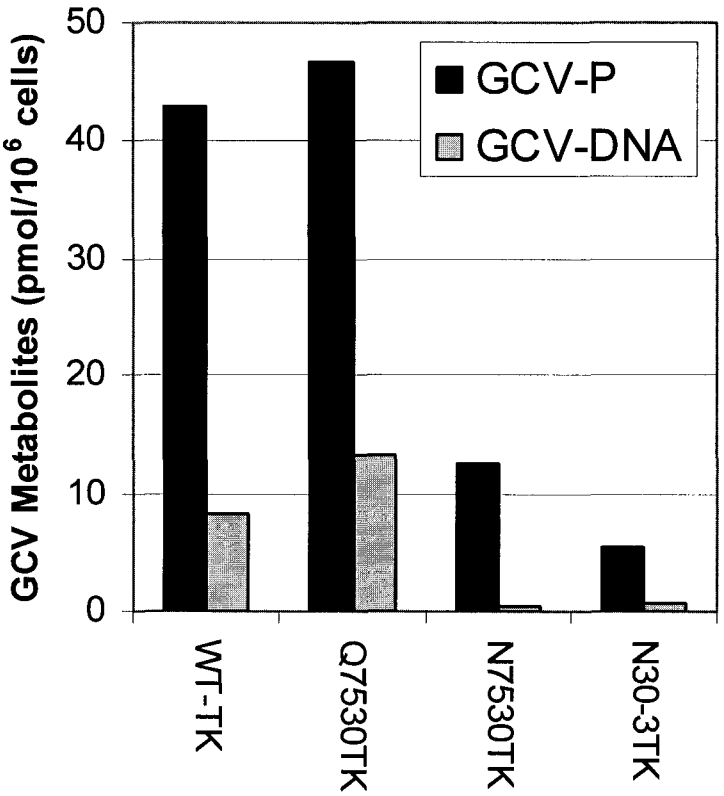

Fig. 32. [^{3}H]GCV Metabolic Labeling of HSV-1 TK and GK expressing HCT-116 cell lines. HSV-1 TK, GK1, GK2, and GK3 expressing HCT-116 cells were incubated for 18 hours with 1 μM [^{3}H]GCV (in triplicate). [^{3}H]GCV metabolites were extracted with 70% methanol, and further separated on PEI-cellulose thin layer chromatography plates with 1M LiCl as described in *Materials and Methods*. Values from the GCV mono-, di- and triphosphate metabolites were pooled (dark bars). The methanol insoluble pellet was extensively washed, resuspended and quantitated by scintillation counting, and used as an indicator of DNA incorporation (gray bars).

Characterization of Cell Death after GCV treatment

DAPI staining and Measurement of Caspase Activity

WT and GK2 expressing cells had the most classical indicators of apoptosis as revealed by DAPI staining and caspase-like activity. Both variants had more than double the caspase like activity compared to GK2 and GK3 expressing cells (Figure 35). In Figure 33, DAPI staining revealed the relative levels of swelling that we have seen as hallmarks of GCV treatment. Figure 34 summarizes the average nuclear size of the nuclei presented in Figure 33. Nuclei from GK3 expressing cells were the most similar to the HCT-116 parent cell line. The same nuclei sizes at 10 μM GCV were detected in WT, GK1, and GK2 expressing cells; however, the nuclear size in the GK2 cells was smaller at the 1 μM GCV dose.

ApopTag™ (Intergen) Kit for apoptosis detection

DNA fragmentation induced by apoptosis can be measured by enzymatic labeling of the free 3'-OH termini with modified nucleotides. The ApopTag™ method allows medium throughput analysis of many samples providing fluorescent or colorimetric data for quantitation. The nucleotides contained in the reaction buffer are enzymatically added to the DNA by terminal deoxynucleotidyl transferase (TdT). TdT catalyzes a template-independent addition of nucleotide triphosphates to the 3'-OH ends of double stranded or single stranded DNA. The incorporated nucleotides form an oligomer composed of digoxigenin nucleotide and unlabeled nucleotide in a random sequence. The bound anti-dioxigenin

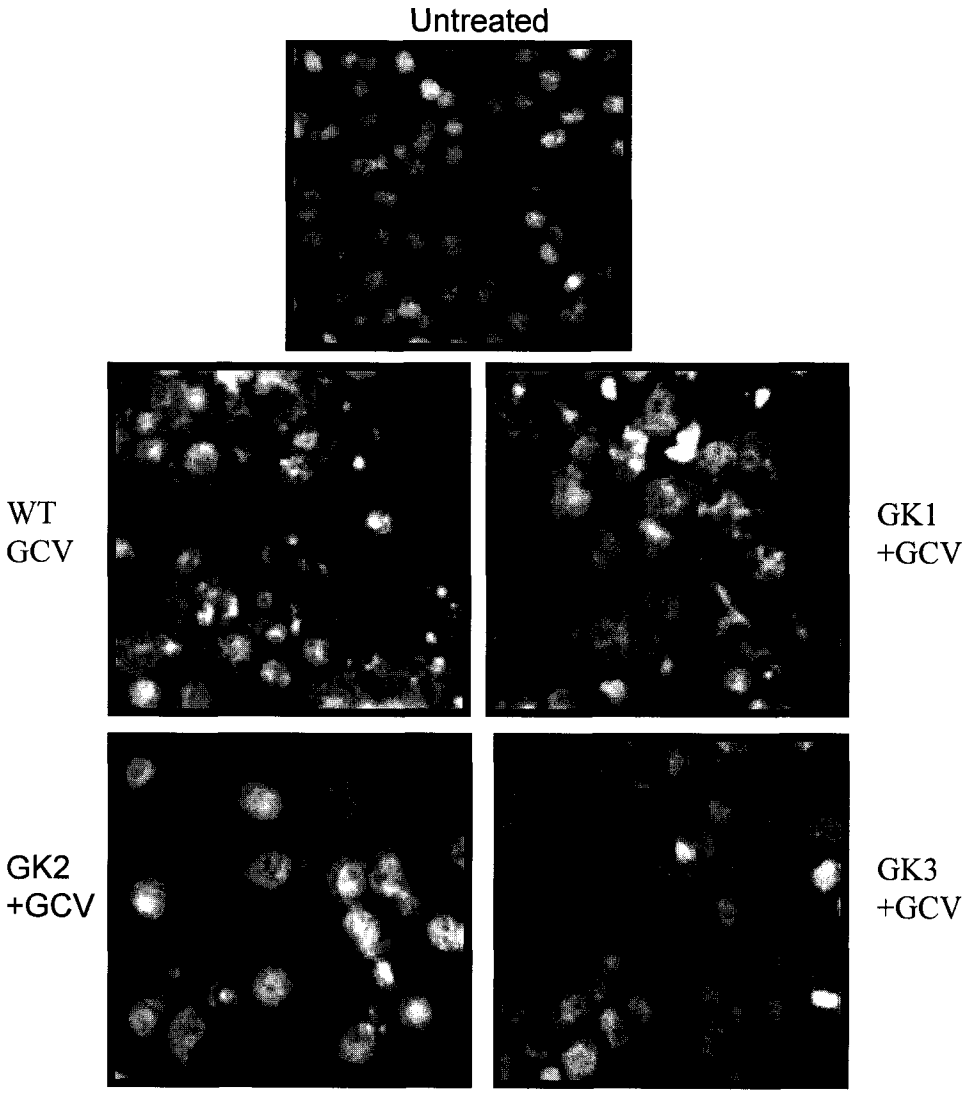

Fig. 33. DAPI staining of GCV treated HSV-1 TK and GK expressing cells. Parental and HSV1 TK, GK1, GK2 and GK3 expressing HCT-116 cells were plated in 8-well chamber slides and treated with GCV (0, 0.1, 1, 10 μM) in triplicate for 72 hours. Cells were stained with 1 μg/ml DAPI in 100% methanol at 37°C for 10 minutes (Drake 1999 ref). The cells were visualized with a Zeiss fluorescent microscope with a DAPI (460 nm) specific filter at a magnification of 40X. Representative fields of DAPI-stained nuclei from parental HCT-116 (+ 10 μM GCV), HSV-1 TK (+ 1 μM GCV), GK1 (+ 1 μM GCV), GK2 (+ 1 μM GCV) and GK3 (+ 10 μM GCV) cells are shown.

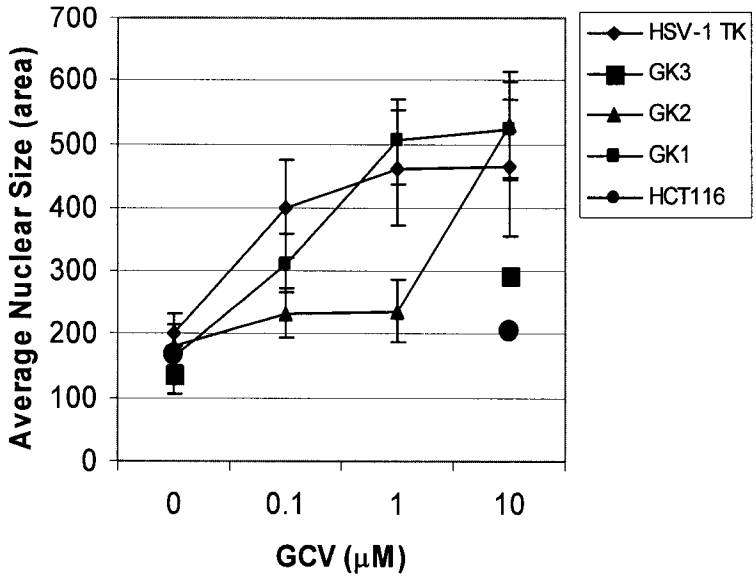

Fig. 34. Average Nuclear Size of HSV-tk variants treated with GCV. The areas of at least 10 stained nuclei were determined using Metamorph imaging software and plotted versus GCV dose: HSV-1 TK (diamond), GK1 (small square) and GK2 (triangle); for HCT-116 (large circle) and GK3 (large square), only the 0 and 10 μM GCV points are shown.

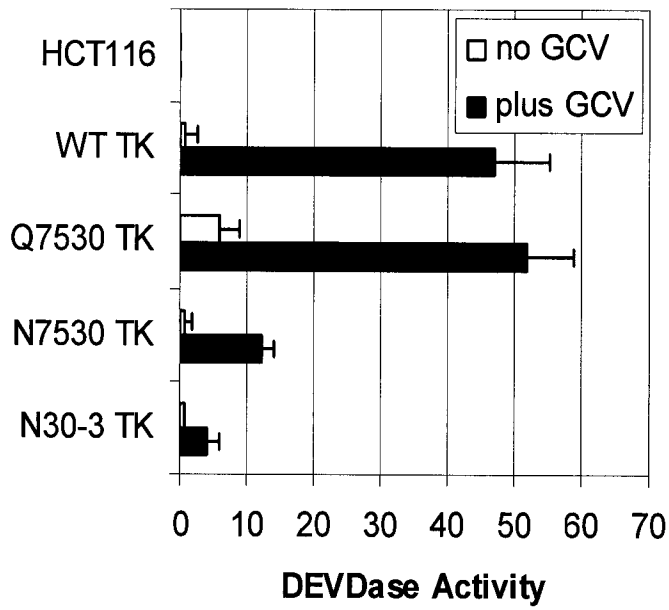

Fig. 35. Caspase 3 Assays HCT116 and HCT116-tk variants Treated with GCV. Cells were double thymidine synchronized, then released into media, 10 mM GCV. In triplicate, cells were removed and assayed for Caspase 3 activity using a Clontech colorimetric kit with DEVD-pNA cleavage from protein extracts derived from 2 X 10^6 cells. DEVDase activities were quantitated at 405 nm.

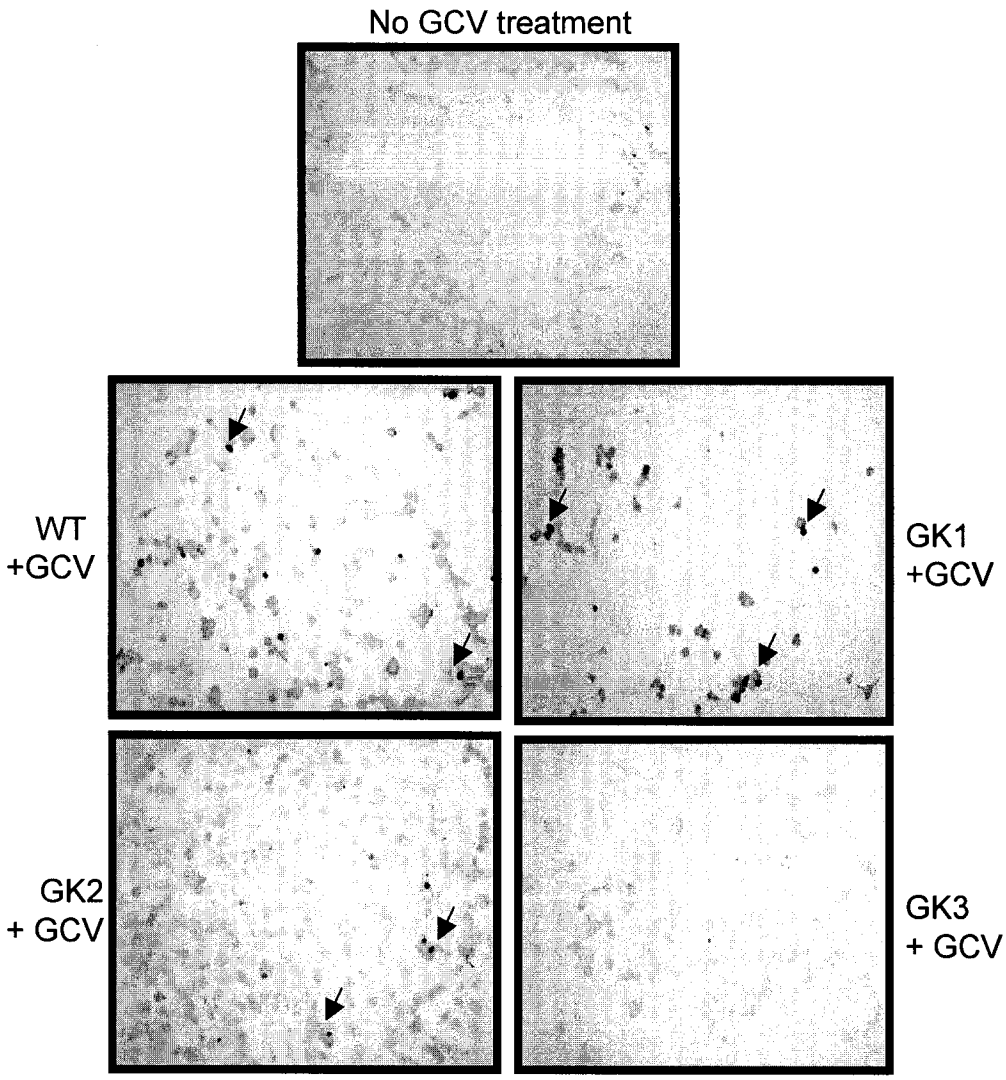

Fig. 36. Measurement of DNA fragmentation in HSV-TK variants treated with GCV. HSV-tk expressing cells were seeded on coverslips and treated with 10 μM GCV. ApopTag kit was used for DNA fragmentation detection. Arrows indicate examples of positively stained cells which are very dark in contrast to the negative cells.

peroxidase antibody conjugate enzymatically generates a permanent, intense, localized staining from chromogenic substrates providing sensitive detection in immunocytochemistry. Cells were prepared as described in *Materials and Methods*, and the average number of apoptotic cells per field at 25X magnification were visualized and counted with a light microscope. Number of apoptotic cells GCV/Ctrl treatment for each TK expressing cell line: WT: 20/2 GK1: 38/2 GK2: 35/1 GK3: 13/3. A visual representation of ApopTag results is presented in Figure 36. Cells positive for apoptosis stained very dark in contrast to background. We expect to fully screen these cells with treatment of a range of GCV concentrations, and since this method is easily adaptable for analysis with flow cytometry, it has been considered for future experiments to help generate quantitative data.

The characterization of cell death and GCV metabolism have revealed a positive correlation with increased GCV and increased DNA fragmentation associated with apoptosis. The next section describes our results testing the HSV-tk variants in the *in vivo* TRAMP model.

In vivo TRAMP Model

HSV-TK Variants

HSV-tk active site variants have been tested recently *in vivo*, and they proved to be effective at reducing tumor burden (51). However, this model was based in SCID mice, therefore the role of the immune system could not be evaluated. Fortuitously, when we moved to EVMS, we formed a collaboration

with Dr. Ciavarra's laboratory, which provided access to an excellent animal model, the transgenic adenocarcinoma mouse prostate (TRAMP). Greenberg *et al.* developed the original TRAMP model in which the rat probasin promoter drives the expression of SV40 large T-antigen that is restricted to the epithelial cells of the prostate gland in C57Bl/6 mice (167). A derivative of this model was then developed using cell lines derived from the in vivo TRAMP tumors (TRAMP-C1, C2, C3) (168), and since these cell lines no longer express T-antigen at the RNA or protein level (168), and they can be used to evaluate immunotherapeutic response to treatments. We obtained a derivative of these cells lines, termed TRAMP-C1P3, that had been serially passaged three times in mouse prostate gland of C57/Bl6 mice and clonally re-isolated developed by Drs. Kenneth Somers and Richard Ciavarra at Eastern Virginia Medical School.

In order to begin our animal model, HSV-tk expressing TRAMP-C1P3 cells were established by transfection with wild type HSV-TK, GK1, GK2, and GK3 plasmids as described in *Materials and Methods*. The IC_{50} for GCV for all TRAMP.tk cell lines was determined and appeared comparable with a human prostate cell line (DU145.TK) and the colon cell line HCT116.TK used in many of our studies. Those concentrations are presented in Table 8.

A TRAMP-GK3 clone that robustly expressed GK3 was never successfully isolated and characterized. It is important to note that all TK variants were tested in combination with UCN-01, and MTT assays revealed that the TK variant did not impact the enhanced killing effect of UCN-01 with GCV (data not shown). This was important to verify since the overall goal of our laboratory is to combine

the multiple approaches in the animal model to investigate efficacy. These utants were subsequently tested in the TRAMP animal model with GCV only as described in the next section.

C57/BL6 mice were injected with $5X10^6$ cells comprised of 90% parent TRAMP-C1P3 and either 10% TRAMP-TK (wt)(n=18), 10% TRAMP-GK1 (n=18), 10% TRAMP-GK2 (n=6). After 20 days, mice were randomized within their respective groups and half were treated with GCV (7 or 70 mg/kg, i.p. once daily) for 5 days, and beginning on day 22, tumor volumes were monitored by measurement with calipers. On each graph in Figure 37, days 21-25 represent the 5 days of prodrug treatment. The WT-TK and GK1 tumors were equally responsive to the 70mg/kg doses. What is not evident with GK1 is that half of the tumor volumes were less than 1000 mm^3 at day 40, while other tumors grew out in the same cohort. There was an apparently greater tumor reduction with 7mg/kg GCV in TRAMP-GK1 mice than with WT, consistent with GK1 being more efficient at metabolizing GCV, at lease at low doses. Interestingly, TRAMP GK2 (N7530) tumors responded the best to 70mg/kg GCV that was either equal or superior to WT or GK1.

At approximately day 38-40 at treatment termination, tumor samples from the responding mice were fixed in formalin for H&E staining. Figure 38 shows images from the H&E stains, taken near the border between the more active tumor cells near the surface versus the less dense core regions. Each section was observed by a pathologist, Dr. Jose Diaz (Dept. of Anatomy and Pathology,

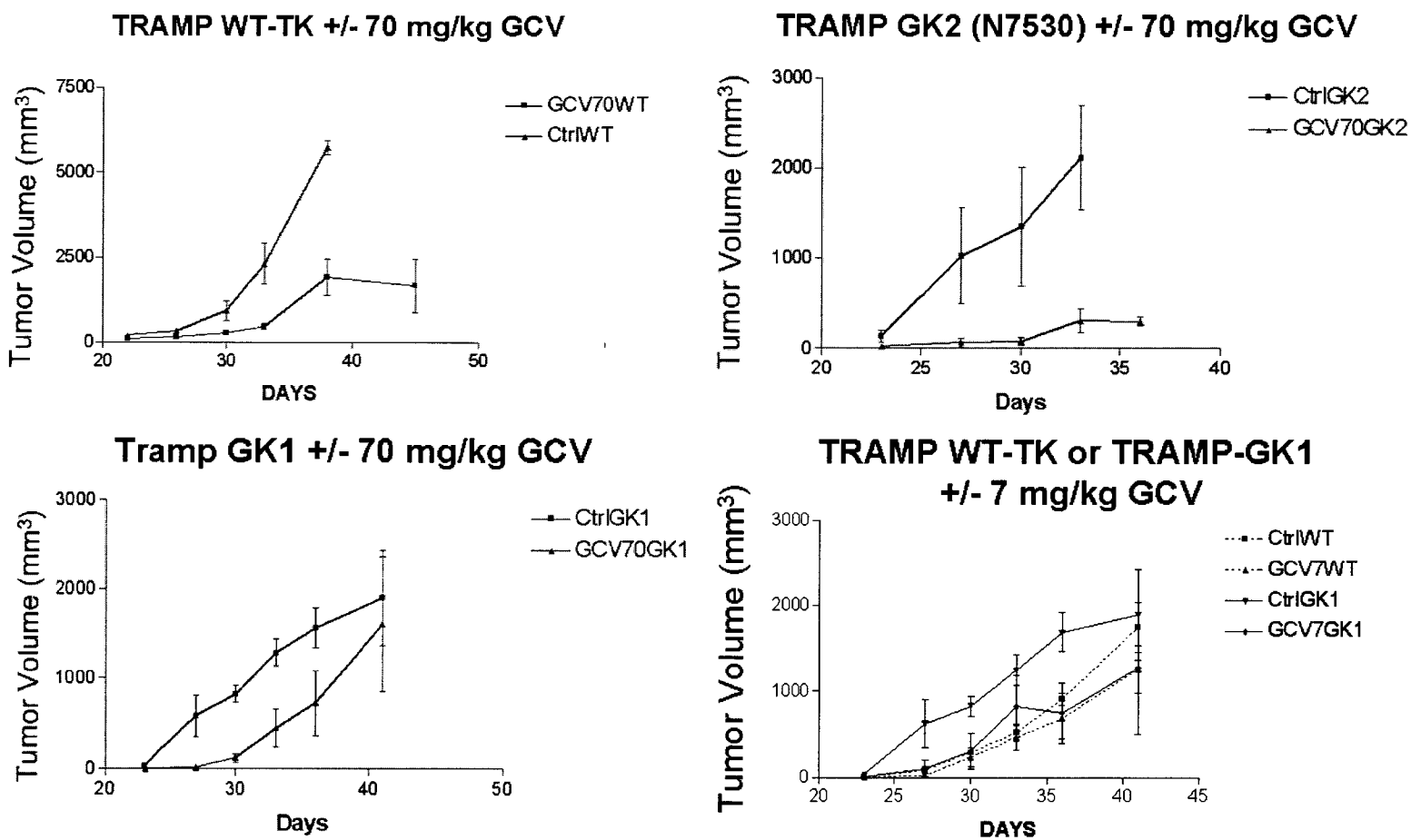

Fig. 37. *In vivo* TRAMP model evaluation of HSVtk and variants after treatment with GCV. C57/BL6 mice were injected with $5X10^6$ cells comprised of 90% parent TRAMP-C1P3 and either 10% TRAMP-TK (wt)(n=18), 10% TRAMP-GK1 (n=18), 10% TRAMP-GK2 (n=6), or 10% TRAMP-GK3 cells (n=6). After 20 days, mice were randomized within their respective groups and half were treated with GCV (7 or 70 mg/kg, i.p. once daily) for 5 days.

EVMS), and arrows in the figure indicate evidence of apoptosis. It was obvious in looking at the entire group of tumor slices that relative to untreated tumor samples, GCV treatment led to less dense tumor cores with evidence of pockets of apoptotic cell death and large regions of necrotic cells. The tissues from WT and GK1 tumors treated with GCV looked very similar in this regard. However, there was a striking increase in interior hemorrhagic necrosis in GCV treated GK2 tumors as evidenced by the presence of pools of red blood cells and increased number of necrotic cell remnants mixed with apoptotic cells. Future immune cell infiltration studies are suggested in *Chapter VI: Conclusions.*

In vivo assessment of GCV, UCN-01, and U+G

McMasters *et al.* discovered the enhanced cell killing with the combination of GCV and UCN-01 (60) , and Chapters III and IV were dedicated to determining the underlying molecular mechanism of their action. This final section tests their efficacy *in vivo.* As determined by MTT assay in TRAMP cells, the IC_{50} for GCV was found to be 0.1 μM, and for UCN-01, 0.03 μM. The combination of GCV and UCN-01 was additive in cell killing in TRAMP.TK cells *in vitro.* (Data not shown)

Twenty C57/BL6 mice were injected ectopically (into the chest wall) with $5X10^6$ cells comprised of 90% parent TRAMP-C1P3 and 10% TRAMP-Tk cells. Tumors were allowed to grow for 22 days, and then mice were randomized into 4 groups of 5 mice each. Group 1: 70mg/kg GCV once daily for five days (day 22-26). Group 2: 2mg/kg UCN-01 for 5 days. Group 3: Combination of 70mg/kg GCV once daily for five days and 2mg/kg UCN-01 for 5 days. Group 4: Control,

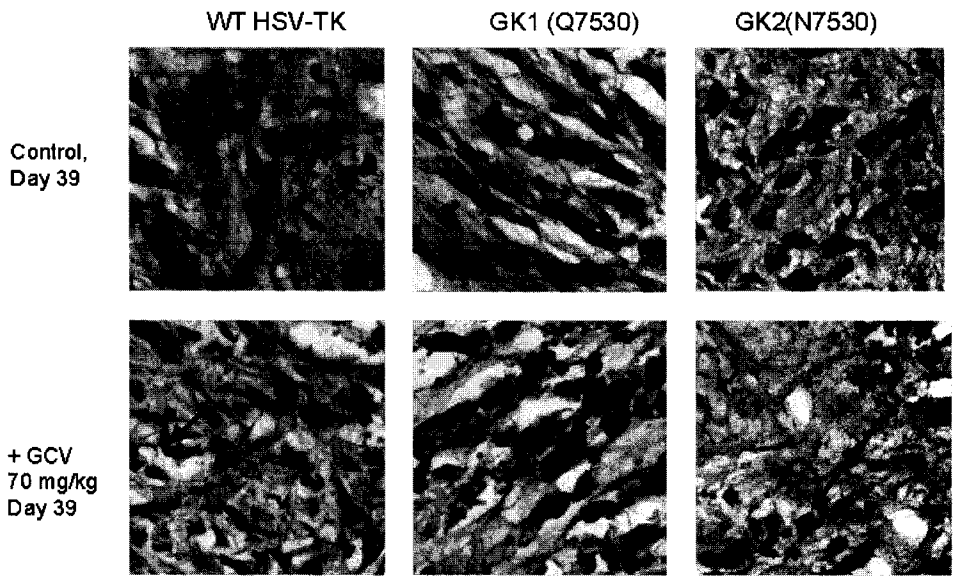

Fig. 38. H&E Stains of GCV treated TRAMP tk, TRAMP GK1 and TRAMP GK2 tumor slices. At approximately day 38-41 at treatment termination, tumor samples from the responding mice were fixed in formalin for H&E staining. Arrows are indicative of apoptosis

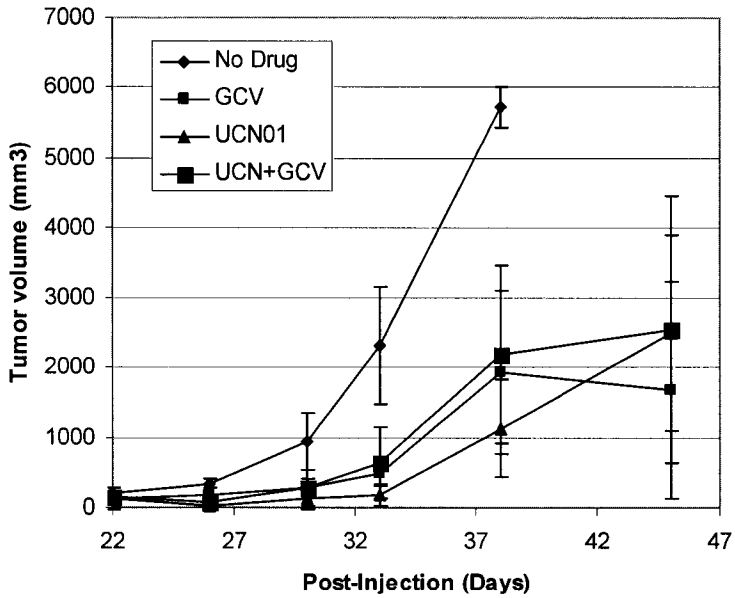

Fig. 39. TRAMP ectopic tumor model evalution of GCV, UCN, and U+G. Twenty C57/BL6 mice were injected ectopically (into the chest wall) with $5X10^6$ cells comprised of 90% parent TRAMP-C1P3 and 10% TRAMP-TkK cells. Tumors were allowed to grow for 22 days, and then mice were randomized into 4 groups of 5 mice each. Drug treatments: GCV: 70mg/kg GCV once daily for five days (day 22-26). UCN-01: 2mg/kg UCN-01 for 5 days. U+G: the combination of 70mg/kg GCV once daily for five days and 2mg/kg UCN-01 for 5 days. Each point is an average of at least 5 mice per condition.

no treatment. Tumor volumes were determined at day 22 and every 3-4 days thereafter until termination. As shown in Figure 39, the doses tested were effective at reducing the tumor burden, however, the combination with UCN-01 did not produce significantly enhanced tumor reduction compared to GCV alone. *In vitro* studies with TRAMP-tk cells revealed that these cells have a particularlyhigh bystander effect, which is not necessarily representative of true *in vivo* effects. (data not shown) Animals were not observed at later time points after treatments as they were all harvested by day 45.

Discussion

The generation of GCV-kinases has helped define the role of GCV metabolism on cell cycle and cell death. The HSV-tk variants are very promising for the manipulation of therapy based upon the different types of cell death they may be signaling. Table 9 shows the cumulative descriptive data we have on the variants thus far. Because we believe that the deliberate induction of a non-apoptotic cell death could make a significant contribution to over therapeutic efficacy, it will be interesting to determine if the altered metabolism of N7530 or N30-3 HSV-tk variant will translate into differences in the *in vivo* immune response in animal tumor models. We are looking forward to testing the variants more extensively *in vitro* and *in vivo* with UCN-01. The successful completion of several animal studies using the TRAMP model boosts our confidence in subsequent studies that will be more in depth. A summary of future experiments is suggested in *Chapter VI: Conclusions.*

CHAPTER VI

CONCLUSIONS

The combination of UCN-01 and HSV-TK/GCV represents a new lead strategy for improving current cancer gene therapy protocols, regardless of p53 status, via alternative and additional DNA damage pathways. It was important to characterize these pathways such that existing treatments can be more fully exploited and optimized, and this information could also be utilized for the development of new chemotherapeutic drugs. Three diverse philosophies of methodology were used to benefit the best cancer therapeutic outcome using HSV-tk gene therapy combined with the chemotherapeutic drug UCN-01: 1) Cell cycle and death mechanism characterization 2) DNA damage signaling network delineation and 3) Therapeutic modality evaluation *in vitro* and *in vivo.* All of these approaches combined provided both a molecular basis guide for future experiments and a foundation for more in depth *in vivo* studies. UCN-01 is a very exciting and intriguing compound that tested our knowledge of signal transduction (specifically DNA damage and cell death pathways), as most clinical studies and *in vitro* studies have shown that it is an excellent therapeutic partner with other modalities. The new pathways identified and the unique properties of UCN-01 in our system could lead to novel directions of study and provide new therapeutic targets and directions of study. The following pages include conclusions of the results presented in Chapters III-V and suggested future directions:

Chapter III: Conlusions and future directions

Conclusions:

1. GCV treated HSV-tk expressing cells undergo an S-phase arrest.
2. UCN-01 has variable effects on the cell cycle, possibly inducing a decrease in S-phase cell population, although cells continue to cycle through more quickly than control. UCN-01 causes mitotic proteins to degrade as detected by western blot.
3. The combination of U+G allows the cells to progress through the cell cycle initially; however undergo an S-phase specific cell death in the end. Concommitently, key mitotic proteins are degraded but at a slower rate than cells treated with UCN-01 only.
4. Order of addition of the two drugs resulted in UCN-01 dominating the effects whenever it was added. Changing the order of addition of our treatments has not yet affected tumor cell toxicity. This remains to be tested more thoroughly in an animal model.
5. Distinct SELDI-TOF generated, low mass protein signatures for each drug treatment were detected in whole cell and nuclear lysates. Identification of these differentially expressed proteins could provide a new way to evaluate molecular mechanisms and treatment efficacies of cancer therapeutics.
6. Two dimensional gel electrophoresis is a powerful tool in discovering components of the GCV/UCN-01 mechanism of cell death and will be the subject of future in depth studies of this system.

Future directions

We originally hypothesized that the targeted destruction of key mitotic proteins by UCN-01 contributed significantly to its cytotoxicity with GCV. Although gene array analyses were performed (data not shown), we never observed levels of the transcripts of those mitotic genes to be significantly reduced. Prior to initiating more protein studies, the effects of UCN-01 and U+G treatments on the suppression of transcripts should be done using methods other than gene arrays. Reverse transcriptase PCR (RT-PCR) is a powerful tool to look for the transcripts after isolating mRNA from cells treated with the drugs and harvested at multiple time points. Primers for Cdc25C, cyclin B, CDK1, and others could be used to determine the levels of these transcript levels. However, it is also possible that these events are occurring at the protein level, in which case we have considered pulse chase radiolabeling of proteins coupled with immunoprecipitation of the same mitotic proteins to see if indeed they are going through drug dependent targeted degradation. This might also help us zero in on the particular mode of cell death such as autophagy or mitotic catastrophe.

Another possibility is that the protein levels are purely indicative of cell cycle phases. We would address this by coupling propidium iodide or 7-AAD staining for cell cycle analysis and using an antibody for the cell cycle protein of interest. We would not need to synchronize cells, and we would have valuable data giving us the phase of the cell cycle and if the cell cycle protein was being expressed. Also, the active mitotic indicator histone 2B could be used to help define the G_2/M boundary and identify cells undergoing mitosis. ApopTag™

could be combined with any of these stains or antibodies to also quantitate numbers of apoptotic cells.

With the acquisition of new imaging equipment, duel fluorescent stains, a gel spot picker, and GE Amersham Decyder software, future experiments can be planned for more thorough studies and identification of proteins of interest from 2D gels. Total protein measurements as well as phosphorylated and glycosylated proteins methods of detection are also now available in our laboratories. Cell lines and treatments are recommended in Table 10.

Furthermore, in depth 2-dimensional gel electrophoresis analysis of the UCN-01 interactome would be carried out by coupling UCN-01 to an epoxy-sepharose column to isolate all UCN-01 interacting proteins. Spots identified by PD Quest Software from BioRad would be used to select spots of interest to be sequenced by the Eastern Virginia Medical School protein sequencing facility.

Chapter IV: Conlusions and future directions

Conclusions:

1. Treatment of cells with UCN-01 results in DNA double strand breaks
2. Cumulative data indicate that UCN-01 may be directly causing physical damage to DNA systematic fashion, and base excision repair could be involved in its repair. The combination of the base excision repair inhibitor and methoxyamine and UCN-01 caused sub-additive potentiation of cell killing.

3. The cumulative effects of UCN-01 treatment are very complex involving cell cycle checkpoints, survival pathway proteins, apoptotic proteins, DNA damage signaling and repair proteins resulting in equilibrium shifts between apoptosis, survival, cell cycle progression and arrest. The underlying mechanism that allows UCN-01 to significantly improve the therapeutic window of DNA damaging drugs and other chemotherapeutic agents already available as treatment options may be due to its ability to damage the DNA itself while launching a multi-tiered assault on the tumor cells survival network.

The exact sequence of events leading to cell death after treatment of cells with UCN-01 is largely unknown. We have hypothesized in general that the physical interaction of UCN-01 with DNA causes a cascade of DNA damage signaling while also causing replication stress leading to stalled replication forks during S-phase. Also, the incompletion of base excision repair that is believed to be involved in the repair of UCN-01 induced lesions causes single strand breaks in the DNA. The cell cycle data presented in Chapter III have indicated interesting and non-classical responses to DNA damage after UCN-01 treatment, but this could be due to the fact that UCN-01 can abrogate the arrest induced by Chk1 in S and G2 phases of the cell cycle, and of several BER single strand break intermediates converting into DSBs. Detection of the double strand break marker γH2AX in S-phase could represent double strand breaks from stalled replication forks while γH2AX detection in G1 or G2 could be due to immediate damage or repair. Persistance of γH2AX is indicative of a lesion that remains

unrepaired. High induction of H2AX phosphorylation has been detected in S-phase cells treated with UV irradiation (169). It would be interesting to correlate the phase of the cell cycle with H2AX phosphorylation via flow cytometry after UCN-01 treatment.

Figure 40 is a suggested depiction of the many effects (including DNA binding) and interactions that UCN-01 has within DNA damage signaling network. The interaction mapped out in blue includes how GCV incorporation might fit into the over mechanism.

Future Directions

The interaction of UCN-01 with DNA could be tested a number of different ways. Another indolocarbozole antibiotic (AT2433-B1) structurally related to rebeccamycin and staurosporine was shown to bind strongly to DNA (170). Carrasco *et al.* determined this interaction using DNase 1 footprinting complimented with BiaCor Surface Plasmon Resonance measurements (170). Another approach would be to use absorption spectroscopy combined with equilibrium dialysis. Bible *et al* used this method to compare the binding of flavopiridol DNA binding to known intercalators doxorubicin and pyrazoloacridine, and they further investigated the binding properties with Nuclear Magnetic Resonance Spectroscopy (171). Equilibrium dialysis and enzymatic cleavage of the DNA are both methods that are easily accessible, and collaborations could be sought in the other areas (NMR and Surface Plasmon Resonance) if we determine they are necessary.

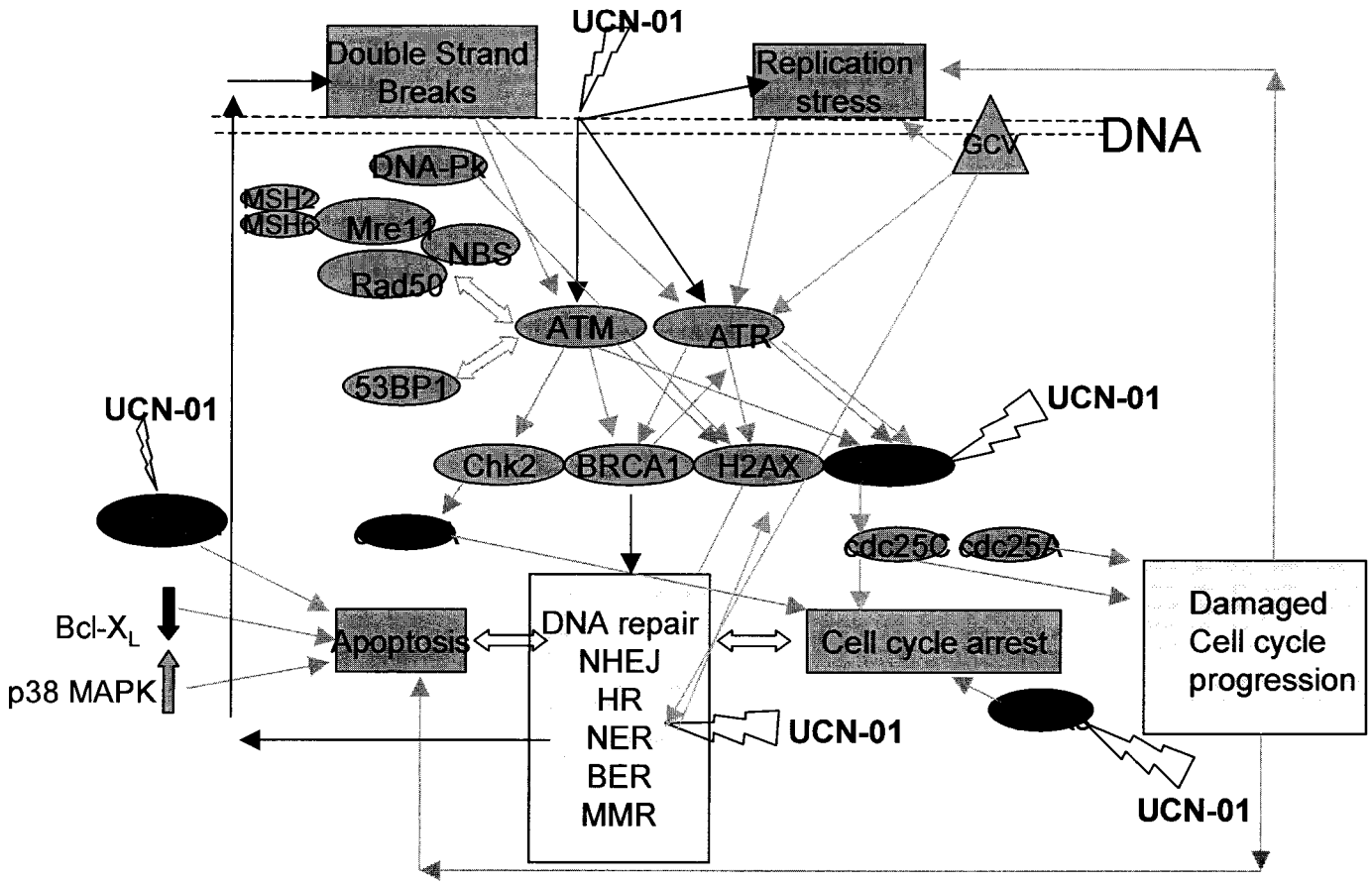

Fig 40. Suggested Summary of UCN-01 and GCV mediated Effects on DNA damage signaling pathways. Active proteins, phosphorylation, or interactions are indicated in green. Inactive proteins or processes are indicated in red. Both DNA repair and cell cycle progression are yellow because activation and inactivation may be occuring. GCV mediated effects are indicated in blue.

Chapter V: Conclusions and future directions

Conclusions

1. The best GCV specific kinase, GK1 (Q7530), had the highest GCV incorporation into the DNA, the most rapid S-phase arrest, and one of the best killing efficacies *in vitro* and *in vivo*. HSV-tk variants have different GCV metabolic properties, and we believe these may be exploited for the best tumor cell killing combination by possibly inducing several complimentary modes of cell death.
2. The TRAMP model is useful for evaluating HSV-tk/GCV gene therapy and revealed that the therapy can be successful at reducing tumor burden
3. HSV-tk variants delivered by an adenovirus combined with GCV, ACV, and UCN-01 in an *in vivo* model is the most promising approach for our lab to contribute to the growing need for improved HSV-tk gene therapy schemes.

Future Directions

The core strategy for future aims in the therapeutic branch of our research includes a larger scale animal model study where multiple facets of the therapy will be tested and evaluated. This includes extensive proteomic analysis of serum and tumor homogenate from mice within the study and other methods listed in Table 11. Data gathered from the animal model will include animals treated with titrated concentrations of both UCN-01 and GCV to determine the lowest effective dose. Order of addition of the drugs will be tested to determine if

either can sensitize the tumor to further treatments. Those experiments will aid us in the future planning of experiments that will include an immune component such as the FLT-3 ligand or cytokines such as IL-2. The distant bystander effect is one of the most promising angles for the further improvement of HSV-tk/GCV gene therapy through multiple modalities. Vile *et al.* in their 1997 review summarized it best when they claimed:

> In effect, if an immune response can be effectively activated against tumor cells, the burden of gene delivery efficiency, specificity and inadvertent toxicity should be transferred from the gene therapist onto the immune system. (45)

The outcome of our preliminary animal data was very promising and an outline of suggested future animal model studies is outlined in Table 10. Parallel experiments in the TRAMP-TK expressing cell lines, as outlined in Table 11, could also be done to further support these suggested *in vivo* studies.

The combination of results, conclusions, and future directions from Chapters III-V come together for suggesting an interesting and a full-scale approach for characterization of multiple cell lines with diverse molecular backgrounds after UCN-01 and other drug treatments. It would be especially of interest to determine the mechanism of resistance or sensitivity to the drug schemes tested in these diverse cell lines. In addition to investigating the discrepancies between SW620s and HT29 sporadic cell lines to drug treatments, a variety of DNA damage signaling repair knockout pairs could be further tested such as HCT116 colon cancer cells which are already MMR deficient, HCT116

Table 10 *Suggested future animal studies in the TRAMP model*

Animal Studies	Treatment schemes	Analysis Methods
TRAMP wild type and HSV variants	Adenoviral tk delivery	Tumor measurements
	Concentration titration and drug order of addition: GCV, ACV, and UCN-01	Immune cell infiltrate Flow cytometry Immunofluorescence H&E staining
	Immunotherapy such as Flt-3 ligand	ApopTag™
		SELDI and 2D Gels Tumor homogenate Mouse sera Laser Capture Microdissection

Table 11 *Summary of Future in vitro Experiments*

Cell Lines	Treatments	Analysis Methods
SW620	None	2D gels Silver staining
HT29	GCV (if expressing TK)	SYPRO Ruby ProQ Diamond
DU145		Emerald Green Differential In Gel
	ACV	Electrophoresis (DIGE)
MCF-7		
	UCN-01	
NCM460		Flow Cytometry
CSC-1	NU7026	BrDU labeling; cell cycle; cell cycle proteins; Apoptosis
MDA-345	Methoxyamine	(markers and $SubG_1$)
M095J/K	Proteasome Inhibitors	Western blots and Confocal Microscopy
HCT116 p53 -/- and +/+ p21 -/- and +/+ Chk2 -/- and +/+ UCN-01 resistant TK variants	Caspase Inhibitors	Chk1; Chk2; BRCA; ATM/ATR; H2AX; H2B; 53BP1; phospho cdc25C and cdc25A; pRb
	Concentration ranges, combinations, and order of addition of all drugs tested	PFGE (neutral and alkaline)
TRAMP tk variants		SELDI-TOF
		MTT and
		Clonal Survival assays

p21-/+, HCT116 p53-/+, and HCT116 Chk2-/-, and MO95K/J glioma cells (proficent and deficient in DSB repair). Breast cancer cell lines (MDA-345 and MCF-7) could be also be subjected to a panel of treatments and analyzed as outlined in Table 11. The BER inhibitor methoxyamine and the DSB repair inhibitor NU7026 would be used cooperatively in our in methods investigating the DNA damage signallig pathways. Finally, a UCN-01 resistant HCT116 cell has been developed in our laboratory, and in depth investigations using the proposed analysis methods in Table 11 could also reveal the mechanism of damage by UCN-01.

All of the cell lines suggested in Table 11 are already currently available for these suggested studies and are part of our well -defined cell culture repertoire. However, we have also considered using Chinese Hampster Ovary (CHO) cells for assessment of DNA repair pathway components. There are several DNA repair protein knockouts that are available and well described for DNA damage repair studies.

Concluding remarks

Many treatment schemes for cancers have had profound and positive consequences for the lives of patients; however, many therapies are limited because of side effects on normal tissue and cells and drug resistance of tumors. Elucidation of pathways could provide new targets for effective cancer therapies and for design of rational strategies to target resistant cancers. Examples of the recent progress made in molecular cancer therapeutics include Herceptin,

Gleevec, and Iressa. These are powerful anti-cancer therapeutics for specific cancers as reviewed in (172). Our molecular and therapeutic aims join to contribute to these types of therapeutics and for answering the call for innovative strategies that will benefit patients with cancers that are not responsive to current treatments.

HSV-tk/GCV gene therapy is still providing hope for patients with devastating cancers that do not have effective treatments. For example, in November 2004 it was reported that adenoviral HSV-tk gene therapy with intranvenous ganciclovir produced a clinically and statistically significant increase in mean survival in malignant glioma patients (173). However improving gene therapy delivery is currently the largest hurdle for gene therapy researchers to overcome. We have begun studies using adenoviruses in our own laboratory and are looking forward to testing their efficacy in the animal model. Another research angle being conducted by another graduate student in the Drake laboratory ties in tumor specific expression of HSV-tk in colon cancer cells. It is this project combined with the research stated within that will specifically and aggressively evaluate gene therapy for colon cancers.

We are confident that with the data presented herein and our suggested future studies that HSV-tk/GCV combined multiple approaches like UCN-01 will make a significant contribution to the successful implementation of molecular based therapies for cancers such as colon, breast, and prostate.

REFERENCES

1. Zwacka, R. M., and Dunlop, M. G. Gene therapy for colon cancer. Hematol. Oncol. Clin. North Am., *12:* 595-615, 1998.
2. Lengauer, C., Kinzler, K. W., and Vogelstein, B. Genetic instability in colorectal cancers. Nature, *386:* 623-627, 1997.
3. Lengauer, C., Kinzler, K. W., and Vogelstein, B. DNA methylation and genetic instability in colorectal cancer cells. Proc. Natl. Acad. Sci. U S A, *94:* 2545-2550, 1997.
4. Burt, R. W. Colon cancer screening. Gastroenterology, *119:* 837-853, 2000.
5. Kim, H., Jen, J., Vogelstein, B., and Hamilton, S. R. Clinical and pathological characteristics of sporadic colorectal carcinomas with DNA replication errors in microsatellite sequences. Am. J. Pathol., *145:* 148-156, 1994.
6. Aaltonen, L. A., Peltomaki, P., Mecklin, J. P., Jarvinen, H., Jass, J. R., Green, J. S., Lynch, H. T., Watson, P., Tallqvist, G., Juhola, M., and et al. Replication errors in benign and malignant tumors from hereditary nonpolyposis colorectal cancer patients. Cancer Res., *54:* 1645-1648, 1994.
7. Aaltonen, L. A., Peltomaki, P., Leach, F. S., Sistonen, P., Pylkkanen, L., Mecklin, J. P., Jarvinen, H., Powell, S. M., Jen, J., Hamilton, S. R., and et al. Clues to the pathogenesis of familial colorectal cancer. Science, *260:* 812-816, 1993.

8. Ionov, Y., Peinado, M. A., Malkhosyan, S., Shibata, D., and Perucho, M. Ubiquitous somatic mutations in simple repeated sequences reveal a new mechanism for colonic carcinogenesis. Nature, *363:* 558-561, 1993.

9. Thibodeau, S. N., Bren, G., and Schaid, D. Microsatellite instability in cancer of the proximal colon. Science, *260:* 816-819, 1993.

10. Mitchell, R. J., Farrington, S. M., Dunlop, M. G., and Campbell, H. Mismatch repair genes hMLH1 and hMSH2 and colorectal cancer: a HuGE review. Am. J. Epidemiol., *156:* 885-902, 2002.

11. Peltomaki, P. Role of DNA mismatch repair defects in the pathogenesis of human cancer. J. Clin. Oncol., *21:* 1174-1179, 2003.

12. Kamory, E., Kolacsek, O., Otto, S., and Csuka, O. hMLH1 and hMSH2 somatic inactivation mechanisms in sporadic colorectal cancer patients. Pathol. Oncol. Res., *9:* 236-241, 2003.

13. Gomez-Navarro, J., Curiel, D. T., and Douglas, J. T. Gene therapy for cancer. Eur. J. Cancer, *35:* 2039-2057, 1999.

14. Freeman, S. M., Whartenby, K. A., Freeman, J. L., Abboud, C. N., and Marrogi, A. J. In situ use of suicide genes for cancer therapy. Semin. Oncol., *23:* 31-45, 1996.

15. Klatzmann, D., Cherin, P., Bensimon, G., Boyer, O., Coutellier, A., Charlotte, F., Boccaccio, C., Salzmann, J. L., and Herson, S. A phase I/II dose-escalation study of herpes simplex virus type 1 thymidine kinase "suicide" gene therapy for metastatic melanoma. Study Group on Gene Therapy of Metastatic Melanoma. Hum. Gene Ther., *9:* 2585-2594, 1998.

16. Bonini, C., Ferrari, G., Verzeletti, S., Servida, P., Zappone, E., Ruggieri, L., Ponzoni, M., Rossini, S., Mavilio, F., Traversari, C., and Bordignon, C. HSV-TK gene transfer into donor lymphocytes for control of allogeneic graft-versus-leukemia. Science, *276:* 1719-1724, 1997.

17. Shand, N., Weber, F., Mariani, L., Bernstein, M., Gianella-Borradori, A., Long, Z., Sorensen, A. G., and Barbier, N. A phase 1-2 clinical trial of gene therapy for recurrent glioblastoma multiforme by tumor transduction with the herpes simplex thymidine kinase gene followed by ganciclovir. GLI328 European-Canadian Study Group. Hum. Gene Ther., *10:* 2325-2335, 1999.

18. Sterman, D. H., Treat, J., Litzky, L. A., Amin, K. M., Coonrod, L., Molnar-Kimber, K., Recio, A., Knox, L., Wilson, J. M., Albelda, S. M., and Kaiser, L. R. Adenovirus-mediated herpes simplex virus thymidine kinase/ganciclovir gene therapy in patients with localized malignancy: results of a phase I clinical trial in malignant mesothelioma. Hum. Gene Ther., *9:* 1083-1092, 1998.

19. Rubsam, L. Z., Davidson, B. L., and Shewach, D. S. Superior cytotoxicity with ganciclovir compared with acyclovir and 1-beta-D-arabinofuranosylthymine in herpes simplex virus-thymidine kinase-expressing cells: a novel paradigm for cell killing. Cancer Res., *58:* 3873-3882, 1998.

20. Rubsam, L. Z., Boucher, P. D., Murphy, P. J., KuKuruga, M., and Shewach, D. S. Cytotoxicity and accumulation of ganciclovir triphosphate in bystander cells cocultured with herpes simplex virus type 1 thymidine kinase-expressing human glioblastoma cells. Cancer Res., *59:* 669-675, 1999.

21. Halloran, P. J., and Fenton, R. G. Irreversible G2-M arrest and cytoskeletal reorganization induced by cytotoxic nucleoside analogues. Cancer Res., *58:* 3855-3865, 1998.

22. Moolten, F. L. and Wells, J. M. Curability of tumors bearing herpes thymidine kinase genes transferred by retroviral vectors. J. Natl. Cancer Inst., *82:* 297-300, 1990.

23. Drake, R. R., Wilbert, T. N., Hinds, T. A., and Gilbert, K. M. Differential ganciclovir-mediated cell killing by glutamine 125 mutants of herpes simplex virus type 1 thymidine kinase. J. Biol. Chem., *274:* 37186-37192, 1999.

24. Wu, Q., Moyana, T., and Xiang, J. Cancer gene therapy by adenovirus-mediated gene transfer. Curr. Gene Ther., *1:* 101-122, 2001.

25. Soling, A., Theiss, C., Jungmichel, S., and Rainov, N. G. A dual function fusion protein of Herpes simplex virus type 1 thymidine kinase and firefly luciferase for noninvasive in vivo imaging of gene therapy in malignant glioma. Genet. Vaccines Ther., *2:* 7, 2004.

26. French gene therapy group reports on the adverse event in a clinical trial of gene therapy for X-linked severe combined immune deficiency (X-SCID). Position statement from the European Society of Gene Therapy. J. Gene Med., *5:* 82-84, 2003.

27. Brand, K., Arnold, W., Bartels, T., Lieber, A., Kay, M. A., Strauss, M., and Dorken, B. Liver-associated toxicity of the HSV-tk/GCV approach and adenoviral vectors. Cancer Gene Ther., *4:* 9-16, 1997.

28. Yee, D., McGuire, S. E., Brunner, N., Kozelsky, T. W., Allred, D. C., Chen, S. H., and Woo, S. L. Adenovirus-mediated gene transfer of herpes simplex virus thymidine kinase in an ascites model of human breast cancer. Hum. Gene Ther., *7:* 1251-1257, 1996.

29. Melcher, A., Gough, M., Todryk, S., and Vile, R. Apoptosis or necrosis for tumor immunotherapy: what's in a name? J. Mol. Med., *77:* 824-833, 1999.

30. Ilsley, D. D., Lee, S. H., Miller, W. H., and Kuchta, R. D. Acyclic guanosine analogs inhibit DNA polymerases alpha, delta, and epsilon with very different potencies and have unique mechanisms of action. Biochemistry, *34:* 2504-2510, 1995.

31. Thust, R., Tomicic, M., Klocking, R., Voutilainen, N., Wutzler, P., and Kaina, B. Comparison of the genotoxic and apoptosis-inducing properties of ganciclovir and penciclovir in Chinese hamster ovary cells transfected with the thymidine kinase gene of herpes simplex virus-1: implications for gene therapeutic approaches. Cancer Gene Ther., *7:* 107-117, 2000.

32. Tomicic, M. T., Bey, E., Wutzler, P., Thust, R., and Kaina, B. Comparative analysis of DNA breakage, chromosomal aberrations and apoptosis induced by the anti-herpes purine nucleoside analogues aciclovir, ganciclovir and penciclovir. Mutat. Res., *505:* 1-11, 2002.

33. Tomicic, M. T., Thust, R., Sobol, R. W., and Kaina, B. DNA polymerase beta mediates protection of mammalian cells against ganciclovir-induced cytotoxicity and DNA breakage. Cancer Res., *61:* 7399-7403, 2001.

34. Wei, S. J., Chao, Y., Hung, Y. M., Lin, W. C., Yang, D. M., Shih, Y. L., Ch'ang, L. Y., Whang-Peng, J., and Yang, W. K. S- and G2-phase cell cycle arrests and apoptosis induced by ganciclovir in murine melanoma cells transduced with herpes simplex virus thymidine kinase. Exp. Cell Res., *241:* 66-75, 1998.

35. Thust, R., Tomicic, M., Klocking, R., Wutzler, P., and Kaina, B. Cytogenetic genotoxicity of anti-herpes purine nucleoside analogues in CHO cells expressing the thymidine kinase gene of herpes simplex virus type 1: comparison of ganciclovir, penciclovir and aciclovir. Mutagenesis, *15:* 177-184, 2000.

36. Moolten, F. L. Tumor chemosensitivity conferred by inserted herpes thymidine kinase genes: paradigm for a prospective cancer control strategy. Cancer Res., *46:* 5276-5281, 1986.

37. Freeman, S. M., Abboud, C. N., Whartenby, K. A., Packman, C. H., Koeplin, D. S., Moolten, F. L., and Abraham, G. N. The "bystander effect": tumor regression when a fraction of the tumor mass is genetically modified. Cancer Res., *53:* 5274-5283, 1993.

38. Culver, K. W. and Blaese, R. M. Gene therapy for cancer. Trends Genet., *10:* 174-178, 1994.

39. van Dillen, I. J., Mulder, N. H., Vaalburg, W., de Vries, E. F., and Hospers, G. A. Influence of the bystander effect on HSV-tk/GCV gene therapy. A review. Curr. Gene Ther., *2:* 307-322, 2002.

40. McMasters, R. A., Saylors, R. L., Jones, K. E., Hendrix, M. E., Moyer, M. P., and Drake, R. R. Lack of bystander killing in herpes simplex virus thymidine kinase-transduced colon cell lines due to deficient connexin43 gap junction formation. Hum. Gene Ther., *9:* 2253-2261, 1998.

41. Drake, R. R., Pitlyk, K., McMasters, R. A., Mercer, K. E., Young, H., and Moyer, M. P. Connexin-independent ganciclovir-mediated killing conferred on bystander effect-resistant cell lines by a herpes simplex virus-thymidine kinase-expressing colon cell line. Mol. Ther., *2:* 515-523, 2000.

42. Kianmanesh, A. R., Perrin, H., Panis, Y., Fabre, M., Nagy, H. J., Houssin, D., and Klatzmann, D. A "distant" bystander effect of suicide gene therapy: regression of nontransduced tumors together with a distant transduced tumor. Hum. Gene Ther., *8:* 1807-1814, 1997.

43. Wei, M. X., Bougnoux, P., Sacre-Salem, B., Peyrat, M. B., Lhuillery, C., Salzmann, J. L., and Klatzmann, D. Suicide gene therapy of chemically induced mammary tumor in rat: efficacy and distant bystander effect. Cancer Res., *58:* 3529-3532, 1998.

44. Vile, R. G., Nelson, J. A., Castleden, S., Chong, H., and Hart, I. R. Systemic gene therapy of murine melanoma using tissue specific expression of the HSVtk gene involves an immune component. Cancer Res., *54:* 6228-6234, 1994.

45. Vile, R. G., Castleden, S., Marshall, J., Camplejohn, R., Upton, C., and Chong, H. Generation of an anti-tumour immune response in a non-immunogenic tumour: HSVtk killing in vivo stimulates a mononuclear cell infiltrate and a Th1-like profile of intratumoural cytokine expression. Int. J. Cancer, *71:* 267-274, 1997.

46. Bi, W., Kim, Y. G., Feliciano, E. S., Pavelic, L., Wilson, K. M., Pavelic, Z. P., and Stambrook, P. J. An HSVtk-mediated local and distant antitumor bystander effect in tumors of head and neck origin in athymic mice. Cancer Gene Ther., *4:* 246-252, 1997.

47. Kuriyama, S., Kikukawa, M., Masui, K., Okuda, H., Nakatani, T., Akahane, T., Mitoro, A., Tominaga, K., Tsujinoue, H., Yoshiji, H., Okamoto, S., Fukui, H., and Ikenaka, K. Cancer gene therapy with HSV-tk/GCV system depends on T-cell-mediated immune responses and causes apoptotic death of tumor cells in vivo. Int. J. Cancer, *83:* 374-380, 1999.

48. Hall, S. J., Sanford, M. A., Atkinson, G., and Chen, S. H. Induction of potent antitumor natural killer cell activity by herpes simplex virus-thymidine kinase and ganciclovir therapy in an orthotopic mouse model of prostate cancer. Cancer Res., *58:* 3221-3225, 1998.

49. Ramesh, R., Munshi, A., Marrogi, A. J., and Freeman, S. M. Enhancement of tumor killing using a combination of tumor immunization and HSV-tk suicide gene therapy. Int. J. Cancer, *80:* 380-386, 1999.

50. Black, M. E., Kokoris, M. S., and Sabo, P. Herpes simplex virus-1 thymidine kinase mutants created by semi-random sequence mutagenesis improve prodrug-mediated tumor cell killing. Cancer Res., *61:* 3022-3026, 2001.

51. Pantuck, A. J., Matherly, J., Zisman, A., Nguyen, D., Berger, F., Gambhir, S. S., Black, M. E., Belldegrun, A., and Wu, L. Optimizing prostate cancer suicide gene therapy using herpes simplex virus thymidine kinase active site variants. Hum. Gene Ther., *13:* 777-789, 2002.

52. Mercer, K. E., Ahn, C. E., Coke, A., Compadre, C. M., and Drake, R. R. Mutation of herpesvirus thymidine kinase to generate ganciclovir-specific kinases for use in cancer gene therapies. Protein Eng., *15:* 903-911, 2002.

53. Beltinger, C., Fulda, S., Walczak, H., and Debatin, K. M. TRAIL enhances thymidine kinase/ganciclovir gene therapy of neuroblastoma cells. Cancer Gene Ther., *9:* 372-381, 2002.

54. Wildner, O., Blaese, R. M., and Morris, J. C. Synergy between the herpes simplex virus tk/ganciclovir prodrug suicide system and the topoisomerase I inhibitor topotecan. Hum. Gene Ther., *10:* 2679-2687, 1999.

55. Chhikara, M., Huang, H., Vlachaki, M. T., Zhu, X., Teh, B., Chiu, K. J., Woo, S., Berner, B., Smith, E. O., Oberg, K. C., Aguilar, L. K., Thompson, T. C., Butler, E. B., and Aguilar-Cordova, E. Enhanced therapeutic effect of HSV-tk+GCV gene therapy and ionizing radiation for prostate cancer. Mol. Ther., *3:* 536-542, 2001.

56. Kanazawa, T., Mizukami, H., Okada, T., Hanazono, Y., Kume, A., Nishino, H., Takeuchi, K., Kitamura, K., Ichimura, K., and Ozawa, K. Suicide gene therapy using AAV-HSVtk/ganciclovir in combination with irradiation results in regression of human head and neck cancer xenografts in nude mice. Gene Ther., *10:* 51-58, 2003.

57. Warren, P., Song, W., Holle, E., Holmes, L., Wei, Y., Li, J., Wagner, T., and Yu, X. Combined HSV-TK/GCV and secondary lymphoid tissue chemokine gene therapy inhibits tumor growth and elicits potent antitumor CTL response in tumor-bearing mice. Anticancer Res., *22:* 599-604, 2002.

58. Boucher, P. D., Ostruszka, L. J., and Shewach, D. S. Synergistic enhancement of herpes simplex virus thymidine kinase/ganciclovir-mediated cytoxicity by hydroxyurea. Cancer Res., *60:* 1631-1636, 2000.

59. Castleden, S. A., Chong, H., Garcia-Ribas, I., Melcher, A. A., Hutchinson, G., Roberts, B., Hart, I. R., and Vile, R. G. A family of bicistronic vectors to enhance both local and systemic antitumor effects of HSVtk or cytokine expression in a murine melanoma model. Hum. Gene Ther., *8:* 2087-2102, 1997.

60. McMasters, R. A., Wilbert, T. N., Jones, K. E., Pitlyk, K., Saylors, R. L., Moyer, M. P., Chambers, T. C., and Drake, R. R. Two-drug combinations that increase apoptosis and modulate bak and bcl-X(L) expression in human colon tumor cell lines transduced with herpes simplex virus thymidine kinase. Cancer Gene Ther., *7:* 563-573, 2000.

61. Omura, S., Iwai, Y., Hirano, A., Nakagawa, A., Awaya, J., Tsuchya, H., Takahashi, Y., and Masuma, R. A new alkaloid AM-2282 OF Streptomyces origin. Taxonomy, fermentation, isolation and preliminary characterization. J. Antibiot. (Tokyo), *30:* 275-282, 1977.

62. Bertrand, R., Solary, E., O'Connor, P., Kohn, K. W., and Pommier, Y. Induction of a common pathway of apoptosis by staurosporine. Exp. Cell Res., *211:* 314-321, 1994.

63. Takahashi, I., Kobayashi, E., Asano, K., Yoshida, M., and Nakano, H. UCN-01, a selective inhibitor of protein kinase C from Streptomyces. J. Antibiot. (Tokyo), *40:* 1782-1784, 1987.

64. Jarvis, W. D., and Grant, S. Protein kinase C targeting in antineoplastic treatment strategies. Invest. New Drugs, *17:* 227-240, 1999.

65. Kurata, N., Matsushita, S., Nishi, K., Watanabe, H. H., Kobayashi, S., Suenaga, A., and Otagiri, M. Characterization of a binding site of UCN-01, a novel anticancer drug on alpha-acid glycoprotein. Biol. Pharm. Bull., *23:* 893-895, 2000.

66. Sparreboom, A., Chen, H., Acharya, M. R., Senderowicz, A. M., Messmann, R. A., Kuwabara, T., Venzon, D. J., Murgo, A. J., Headlee, D., Sausville, E. A., and Figg, W. D. Effects of alpha1-acid glycoprotein on the clinical pharmacokinetics of 7-hydroxystaurosporine. Clin. Cancer Res., *10:* 6840-6846, 2004.

67. Gescher, A. Staurosporine analogues - pharmacological toys or useful antitumour agents? Crit. Rev. Oncol. Hematol., *34:* 127-135, 2000.

68. Zhou, B. B. and Sausville, E. A. Drug discovery targeting Chk1 and Chk2 kinases. Prog. Cell Cycle Res., *5:* 413-421, 2003.

69. Sanchez, Y., Wong, C., Thoma, R. S., Richman, R., Wu, Z., Piwnica-Worms, H., and Elledge, S. J. Conservation of the Chk1 checkpoint pathway in mammals: linkage of DNA damage to Cdk regulation through Cdc25. Science, *277:* 1497-1501, 1997.

70. Peng, C. Y., Graves, P. R., Thoma, R. S., Wu, Z., Shaw, A. S., and Piwnica-Worms, H. Mitotic and G2 checkpoint control: regulation of 14-3-3 protein binding by phosphorylation of Cdc25C on serine-216. Science, *277:* 1501-1505, 1997.

71. Dalal, S. N., Schweitzer, C. M., Gan, J., and DeCaprio, J. A. Cytoplasmic localization of human cdc25C during interphase requires an intact 14-3-3 binding site. Mol. Cell Biol., *19:* 4465-4479, 1999.

72. Ohi, R. and Gould, K. L. Regulating the onset of mitosis. Curr. Opin. Cell Biol., *11:* 267-273, 1999.

73. Busby, E. C., Leistritz, D. F., Abraham, R. T., Karnitz, L. M., and Sarkaria, J. N. The radiosensitizing agent 7-hydroxystaurosporine (UCN-01) inhibits the DNA damage checkpoint kinase hChk1. Cancer Res., *60:* 2108-2112, 2000.

74. Graves, P. R., Yu, L., Schwarz, J. K., Gales, J., Sausville, E. A., O'Connor, P. M., and Piwnica-Worms, H. The Chk1 protein kinase and the Cdc25C regulatory pathways are targets of the anticancer agent UCN-01. J. Biol. Chem., *275:* 5600-5605, 2000.

75. Jackson, J. R., Gilmartin, A., Imburgia, C., Winkler, J. D., Marshall, L. A., and Roshak, A. An indolocarbazole inhibitor of human checkpoint kinase (Chk1) abrogates cell cycle arrest caused by DNA damage. Cancer Res., *60:* 566-572, 2000.

76. Komander, D., Kular, G. S., Bain, J., Elliott, M., Alessi, D. R., and Van Aalten, D. M. Structural basis for UCN-01 (7-hydroxystaurosporine) specificity and PDK1 (3-phosphoinositide-dependent protein kinase-1) inhibition. Biochem. J., *375:* 255-262, 2003.

77. Sato, S., Fujita, N., and Tsuruo, T. Interference with PDK1-Akt survival signaling pathway by UCN-01 (7-hydroxystaurosporine). Oncogene, *21:* 1727-1738, 2002.

78. Jia, W., Yu, C., Rahmani, M., Krystal, G., Sausville, E. A., Dent, P., and Grant, S. Synergistic antileukemic interactions between 17-AAG and UCN-01 involve interruption of RAF/MEK- and AKT-related pathways. Blood, *102:* 1824-1832, 2003.

79. Jiang, H. and Yang, L. Y. Cell cycle checkpoint abrogator UCN-01 inhibits DNA repair: association with attenuation of the interaction of XPA and ERCC1 nucleotide excision repair proteins. Cancer Res., *59:* 4529-4534, 1999.

80. Yang, L. Y., Jiang, H., Rangel, K. M., and Plunkett, W. Cisplatin-induced ubiquitination of RNA polymerase II large subunit and suppression of induction by 7-hydroxystaurosporine (UCN-01). Oncol. Rep., *10:* 1489-1495, 2003.

81. Chan, U. P., Lee, J. F., Wang, S. H., Leung, K. L., and Chen, G. G. Induction of colon cancer cell death by 7-hydroxystaurosporine (UCN-01) is associated with increased p38 MAPK and decreased Bcl-xL. Anticancer Drugs, *14:* 761-766, 2003.

82. Jones, C. B., Clements, M. K., Redkar, A., and Daoud, S. S. UCN-01 and camptothecin induce DNA double-strand breaks in p53 mutant tumor cells, but not in normal or p53 negative epithelial cells. Int. J. Oncol., *17:* 1043-1051, 2000.

83. Wilson, W. H., Sorbara, L., Figg, W. D., Mont, E. K., Sausville, E., Warren, K. E., Balis, F. M., Bauer, K., Raffeld, M., Senderowicz, A. M., and Monks, A. Modulation of clinical drug resistance in a B cell lymphoma patient by the protein kinase inhibitor 7-hydroxystaurosporine: presentation of a novel therapeutic paradigm. Clin. Cancer Res., *6:* 415-421, 2000.

84. Abe, S., Kubota, T., Saikawa, Y., Otani, Y., Furukawa, T., Watanabe, M., Kumai, K., and Kitajima, M. Independent antitumor spectrum of UCN-01 (7-hydroxystaurosporine) against gastric and colorectal cancers as detected by MTT assay. Anticancer Res., *22:* 3605-3610, 2002.

85. Shi, Z., Azuma, A., Sampath, D., Li, Y. X., Huang, P., and Plunkett, W. S-Phase arrest by nucleoside analogues and abrogation of survival without cell cycle progression by 7-hydroxystaurosporine. Cancer Res., *61:* 1065-1072, 2001.

86. Bunch, R. T. and Eastman, A. Enhancement of cisplatin-induced cytotoxicity by 7-hydroxystaurosporine (UCN-01), a new G2-checkpoint inhibitor. Clin. Cancer Res., *2:* 791-797, 1996.

87. Lee, S. I., Brown, M. K., and Eastman, A. Comparison of the efficacy of 7-hydroxystaurosporine (UCN-01) and other staurosporine analogs to abrogate cisplatin-induced cell cycle arrest in human breast cancer cell lines. Biochem. Pharmacol., *58:* 1713-1721, 1999.

88. Shao, R. G., Cao, C. X., Shimizu, T., O'Connor, P. M., Kohn, K. W., and Pommier, Y. Abrogation of an S-phase checkpoint and potentiation of camptothecin cytotoxicity by 7-hydroxystaurosporine (UCN-01) in human cancer cell lines, possibly influenced by p53 function. Cancer Res., *57:* 4029-4035, 1997.

89. Sugiyama, K., Shimizu, M., Akiyama, T., Tamaoki, T., Yamaguchi, K., Takahashi, R., Eastman, A., and Akinaga, S. UCN-01 selectively enhances mitomycin C cytotoxicity in p53 defective cells which is mediated through S and/or G(2) checkpoint abrogation. Int. J. Cancer, *85:* 703-709, 2000.

90. Wang, S., Wang, Z., and Grant, S. Bryostatin 1 and UCN-01 potentiate 1-beta-D-arabinofuranosylcytosine-induced apoptosis in human myeloid leukemia cells through disparate mechanisms. Mol. Pharmacol., *63:* 232-242, 2003.

91. Shao, R. G., Cao, C. X., and Pommier, Y. Abrogation of Chk1-mediated S/G2 checkpoint by UCN-01 enhances ara-C-induced cytotoxicity in human colon cancer cells. Acta Pharmacol. Sin., *25:* 756-762, 2004.

92. Dai, Y., Dent, P., and Grant, S. Tumor necrosis factor-related apoptosis-inducing ligand (TRAIL) promotes mitochondrial dysfunction and apoptosis induced by 7-hydroxystaurosporine and mitogen-activated protein kinase kinase inhibitors in human leukemia cells that ectopically express Bcl-2 and Bcl-xL. Mol. Pharmacol., *64:* 1402-1409, 2003.

93. Dai, Y., Yu, C., Singh, V., Tang, L., Wang, Z., McInistry, R., Dent, P., and Grant, S. Pharmacological inhibitors of the mitogen-activated protein kinase (MAPK) kinase/MAPK cascade interact synergistically with UCN-01 to induce mitochondrial dysfunction and apoptosis in human leukemia cells. Cancer Res., *61:* 5106-5115, 2001.

94. Hsueh, C. T., Wu, Y. C., and Schwartz, G. K. UCN-01 suppresses E2F-1 mediated by ubiquitin-proteasome-dependent degradation. Clin. Cancer Res., *7:* 669-674, 2001.

95. Yamauchi, T., Keating, M. J., and Plunkett, W. UCN-01 (7-hydroxystaurosporine) inhibits DNA repair and increases cytotoxicity in normal lymphocytes and chronic lymphocytic leukemia lymphocytes. Mol. Cancer Ther., *1:* 287-294, 2002.

96. Dasmahapatra, G. P., Didolkar, P., Alley, M. C., Ghosh, S., Sausville, E. A., and Roy, K. K. In vitro combination treatment with perifosine and UCN-01 demonstrates synergism against prostate (PC-3) and lung (A549) epithelial adenocarcinoma cell lines. Clin. Cancer Res., *10:* 5242-5252, 2004.

97. Koh, J., Kubota, T., Koyama, T., Migita, T., Hashimoto, M., Hosoda, Y., and Kitajima, M. Combined antitumor activity of 7-hydroxystaurosporine (UCN-01) and tamoxifen against human breast carcinoma in vitro and in vivo. Breast Cancer, *10:* 260-267, 2003.

98. Mack, P. C., Jones, A. A., Gustafsson, M. H., Gandara, D. R., Gumerlock, P. H., and Goldberg, Z. Enhancement of Radiation Cytotoxicity by UCN-01 in Non-small Cell Lung Carcinoma Cells. Radiat. Res., *162:* 623-634, 2004.

99. Yokoyama, Y., Shinohara, A., Takahashi, Y., Wan, X., Takahashi, S., Niwa, K., and Tamaya, T. Synergistic effects of danazol and mifepristone on the cytotoxicity of UCN-01 in hormone-responsive breast cancer cells. Anticancer Res., *20:* 3131-3135, 2000.

100. Bhoumik, A., Gangi, L., and Ronai, Z. Inhibition of melanoma growth and metastasis by ATF2-derived peptides. Cancer Res., *64:* 8222-8230, 2004.

101. Stewart, Z. A. and Pietenpol, J. A. p53 Signaling and cell cycle checkpoints. Chem. Res. Toxicol., *14:* 243-263, 2001.

102. Rich, T., Allen, R. L., and Wyllie, A. H. Defying death after DNA damage. Nature, *407:* 777-783, 2000.

103. de Laat, W. L., Jaspers, N. G., and Hoeijmakers, J. H. Molecular mechanism of nucleotide excision repair. Genes Dev., *13:* 768-785, 1999.

104. Wallace, S. S. DNA damages processed by base excision repair: biological consequences. Int. J. Radiat. Biol., *66:* 579-589, 1994.

105. Sancar, A., Lindsey-Boltz, L. A., Unsal-Kacmaz, K., and Linn, S. Molecular mechanisms of mammalian DNA repair and the DNA damage checkpoints. Annu. Rev. Biochem., *73:* 39-85, 2004.

106. Jacob, S., Aguado, M., Fallik, D., and Praz, F. The role of the DNA mismatch repair system in the cytotoxicity of the topoisomerase inhibitors camptothecin and etoposide to human colorectal cancer cells. Cancer Res., *61:* 6555-6562, 2001.

107. Habraken, Y., Jolois, O., and Piette, J. Differential involvement of the hMRE11/hRAD50/NBS1 complex, BRCA1 and MLH1 in NF-kappaB activation by camptothecin and X-ray. Oncogene, *22:* 6090-6099, 2003.

108. Jackson, S. P. Detecting, signalling and repairing DNA double-strand breaks. Biochem. Soc. Trans., *29:* 655-661, 2001.

109. Li, Z., Otevrel, T., Gao, Y., Cheng, H. L., Seed, B., Stamato, T. D., Taccioli, G. E., and Alt, F. W. The XRCC4 gene encodes a novel protein involved in DNA double-strand break repair and V(D)J recombination. Cell, *83:* 1079-1089, 1995.

110. Grawunder, U., Wilm, M., Wu, X., Kulesza, P., Wilson, T. E., Mann, M., and Lieber, M. R. Activity of DNA ligase IV stimulated by complex formation with XRCC4 protein in mammalian cells. Nature, *388:* 492-495, 1997.

111. Jeggo, P. A. DNA-PK: at the cross-roads of biochemistry and genetics. Mutat. Res., *384:* 1-14, 1997.

112. Lieber, M. R., Grawunder, U., Wu, X., and Yaneva, M. Tying loose ends: roles of Ku and DNA-dependent protein kinase in the repair of double-strand breaks. Curr. Opin. Genet. Dev., *7:* 99-104, 1997.

113. Rothkamm, K. and Lobrich, M. Misrepair of radiation-induced DNA double-strand breaks and its relevance for tumorigenesis and cancer treatment (review). Int. J. Oncol., *21:* 433-440, 2002.

114. Helleday, T. Pathways for mitotic homologous recombination in mammalian cells. Mutat. Res., *532:* 103-115, 2003.

115. Wang, B., Matsuoka, S., Carpenter, P. B., and Elledge, S. J. 53BP1, a mediator of the DNA damage checkpoint. Science, *298:* 1435-1438, 2002.

116. Narod, S. A. and Foulkes, W. D. BRCA1 and BRCA2: 1994 and beyond. Nat. Rev. Cancer, *4:* 665-676, 2004.

117. Hartman, A. R. and Ford, J. M. BRCA1 and p53: compensatory roles in DNA repair. J. Mol. Med., *81:* 700-707, 2003.

118. Burma, S., Chen, B. P., Murphy, M., Kurimasa, A., and Chen, D. J. ATM phosphorylates histone H2AX in response to DNA double-strand breaks. J. Biol. Chem., *276:* 42462-42467, 2001.

119. Anderson, L., Henderson, C., and Adachi, Y. Phosphorylation and rapid relocalization of 53BP1 to nuclear foci upon DNA damage. Mol. Cell Biol., *21:* 1719-1729, 2001.

120. Rappold, I., Iwabuchi, K., Date, T., and Chen, J. Tumor suppressor p53 binding protein 1 (53BP1) is involved in DNA damage-signaling pathways. J. Cell Biol., *153:* 613-620, 2001.

121. Weinert, T. A DNA damage checkpoint meets the cell cycle engine. Science, *277:* 1450-1451, 1997.

122. Nurse, P. Checkpoint pathways come of age. Cell, *91:* 865-867, 1997.

123. Matsuoka, S., Huang, M., and Elledge, S. J. Linkage of ATM to cell cycle regulation by the Chk2 protein kinase. Science, *282:* 1893-1897, 1998.

124. Iwabuchi, K., Basu, B. P., Kysela, B., Kurihara, T., Shibata, M., Guan, D., Cao, Y., Hamada, T., Imamura, K., Jeggo, P. A., Date, T., and Doherty, A. J. Potential role for 53BP1 in DNA end-joining repair through direct interaction with DNA. J. Biol. Chem., *278:* 36487-36495, 2003.

125. Celeste, A., Fernandez-Capetillo, O., Kruhlak, M. J., Pilch, D. R., Staudt, D. W., Lee, A., Bonner, R. F., Bonner, W. M., and Nussenzweig, A. Histone H2AX phosphorylation is dispensable for the initial recognition of DNA breaks. Nat. Cell Biol., *5:* 675-679, 2003.

126. Lees-Miller, S. P. and Meek, K. Repair of DNA double strand breaks by non-homologous end joining. Biochimie, *85:* 1161-1173, 2003.

127. Modesti, M., Hesse, J. E., and Gellert, M. DNA binding of Xrcc4 protein is associated with V(D)J recombination but not with stimulation of DNA ligase IV activity. Embo. J., *18:* 2008-2018, 1999.

128. Park, E. J., Chan, D. W., Park, J. H., Oettinger, M. A., and Kwon, J. DNA-PK is activated by nucleosomes and phosphorylates H2AX within the nucleosomes in an acetylation-dependent manner. Nucleic Acids Res., *31:* 6819-6827, 2003.

129. Alley, M. C., Scudiero, D. A., Monks, A., Hursey, M. L., Czerwinski, M. J., Fine, D. L., Abbott, B. J., Mayo, J. G., Shoemaker, R. H., and Boyd, M. R. Feasibility of drug screening with panels of human tumor cell lines using a microculture tetrazolium assay. Cancer Res., *48:* 589-601, 1988.

130. Fan, M., Du, L., Stone, A. A., Gilbert, K. M., and Chambers, T. C. Modulation of mitogen-activated protein kinases and phosphorylation of Bcl-2 by vinblastine represent persistent forms of normal fluctuations at G2-M1. Cancer Res., *60:* 6403-6407, 2000.

131. Murray, D., Simpson, R., Rosenberg, E., Carraway, A., and Britten, R. Correlation between gamma-ray-induced DNA double-strand breakage and cell killing after biologically relevant doses: analysis by pulsed-field gel electrophoresis. Int. J. Radiat. Biol., *65:* 419-426, 1994.

132. Friedmann, B., Caplin, M., Hartley, J. A., and Hochhauser, D. Modulation of DNA repair in vitro after treatment with chemotherapeutic agents by the epidermal growth factor receptor inhibitor gefitinib (ZD1839). Clin. Cancer Res., *10:* 6476-6486, 2004.

133. Olnes, M. I. and Kurl, R. N. Isolation of nuclear extracts from fragile cells: a simplified procedure applied to thymocytes. Biotechniques, *17:* 828-829, 1994.

134. Somers, K. D., Brown, R. R., Holterman, D. A., Yousefieh, N., Glass, W. F., Wright, G. L., Jr., Schellhammer, P. F., Qian, J., and Ciavarra, R. P. Orthotopic treatment model of prostate cancer and metastasis in the immunocompetent mouse: efficacy of flt3 ligand immunotherapy. Int. J. Cancer, *107:* 773-780, 2003.

135. Akiyama, T., Yoshida, T., Tsujita, T., Shimizu, M., Mizukami, T., Okabe, M., and Akinaga, S. G1 phase accumulation induced by UCN-01 is associated with dephosphorylation of Rb and CDK2 proteins as well as induction of CDK inhibitor p21/Cip1/WAF1/Sdi1 in p53-mutated human epidermoid carcinoma A431 cells. Cancer Res., *57:* 1495-1501, 1997.

136. Kawakami, K., Futami, H., Takahara, J., and Yamaguchi, K. UCN-01, 7-hydroxyl-staurosporine, inhibits kinase activity of cyclin-dependent kinases and reduces the phosphorylation of the retinoblastoma susceptibility gene product in A549 human lung cancer cell line. Biochem. Biophys. Res. Commun, *219:* 778-783, 1996.

137. De Clercq, E., Descamps, J., De Somer, P., Barr, P. J., Jones, A. S., and Walker, R. T. (E)-5-(2-Bromovinyl)-2'-deoxyuridine: a potent and selective anti-herpes agent. Proc. Natl. Acad. Sci. U S A, *76:* 2947-2951, 1979.

138. Hsueh, C. T., Kelsen, D., and Schwartz, G. K. UCN-01 suppresses thymidylate synthase gene expression and enhances 5-fluorouracil-induced apoptosis in a sequence-dependent manner. Clin. Cancer Res., *4:* 2201-2206, 1998.

139. Aghi, M., Kramm, C. M., Chou, T. C., Breakefield, X. O., and Chiocca, E. A. Synergistic anticancer effects of ganciclovir/thymidine kinase and 5-fluorocytosine/cytosine deaminase gene therapies. J. Natl. Cancer Inst., *90:* 370-380, 1998.

140. Hutchens, T. W., Yip TT. New desorption strategies for the mass spectrometric analysis of macromolecules. Rapid Communications Mass Spectrom., *7:* 576-580, 1993.

141. Wright, G. L., Jr. SELDI proteinchip MS: a platform for biomarker discovery and cancer diagnosis. Expert. Rev. Mol. Diagn., *2:* 549-563, 2002.

142. Wang, T. H., Wang, H. S., and Soong, Y. K. Paclitaxel-induced cell death: where the cell cycle and apoptosis come together. Cancer, *88:* 2619-2628, 2000.

143. Milross, C. G., Mason, K. A., Hunter, N. R., Chung, W. K., Peters, L. J., and Milas, L. Relationship of mitotic arrest and apoptosis to antitumor effect of paclitaxel. J. Natl. Cancer Inst., *88:* 1308-1314, 1996.

144. Corban-Wilhelm, H., Hull, W. E., Becker, G., Bauder-Wust, U., Greulich, D., and Debus, J. Cytosine deaminase and thymidine kinase gene therapy in a Dunning rat prostate tumour model: absence of bystander effects and characterisation of 5-fluorocytosine metabolism with 19F-NMR spectroscopy. Gene Ther., *9:* 1564-1575, 2002.

145. Donzelli, M., Squatrito, M., Ganoth, D., Hershko, A., Pagano, M., and Draetta, G. F. Dual mode of degradation of Cdc25 A phosphatase. Embo. J., *21:* 4875-4884, 2002.

146. Hassepass, I., Voit, R., and Hoffmann, I. Phosphorylation at serine 75 is required for UV-mediated degradation of human Cdc25A phosphatase at the S-phase checkpoint. J. Biol. Chem., *278:* 29824-29829, 2003.

147. Jin, J., Shirogane, T., Xu, L., Nalepa, G., Qin, J., Elledge, S. J., and Harper, J. W. SCFbeta-TRCP links Chk1 signaling to degradation of the Cdc25A protein phosphatase. Genes Dev., *17:* 3062-3074, 2003.

148. Mailand, N., Podtelejnikov, A. V., Groth, A., Mann, M., Bartek, J., and Lukas, J. Regulation of G(2)/M events by Cdc25A through phosphorylation-dependent modulation of its stability. Embo. J., *21:* 5911-5920, 2002.

149. Zhao, B., Bower, M. J., McDevitt, P. J., Zhao, H., Davis, S. T., Johanson, K. O., Green, S. M., Concha, N. O., and Zhou, B. B. Structural basis for Chk1 inhibition by UCN-01. J. Biol. Chem., *277:* 46609-46615, 2002.

150. Singh, S. V., Herman-Antosiewicz, A., Singh, A. V., Lew, K. L., Srivastava, S. K., Kamath, R., Brown, K. D., Zhang, L., and Baskaran, R. Sulforaphane-induced G2/M phase cell cycle arrest involves checkpoint kinase 2 mediated phosphorylation of Cdc25C. J. Biol. Chem., 2004.

151. Tyagi, A., Agarwal, C., Harrison, G., Glode, L. M., and Agarwal, R. Silibinin causes cell cycle arrest and apoptosis in human bladder transitional cell carcinoma cells by regulating CDKI-CDK-cyclin cascade, and caspase 3 and PARP cleavages. Carcinogenesis, 2004.

152. Raj, K., Ogston, P., and Beard, P. Virus-mediated killing of cells that lack p53 activity. Nature, *412:* 914-917, 2001.

153. Chen, F., Zhang, Z., Bower, J., Lu, Y., Leonard, S. S., Ding, M., Castranova, V., Piwnica-Worms, H., and Shi, X. Arsenite-induced Cdc25C degradation is through the KEN-box and ubiquitin-proteasome pathway. Proc. Natl. Acad. Sci. U S A, *99:* 1990-1995, 2002.

154. Redon, C., Pilch, D., Rogakou, E., Sedelnikova, O., Newrock, K., and Bonner, W. Histone H2A variants H2AX and H2AZ. Curr. Opin. Genet. Dev., *12:* 162-169, 2002.

155. Birren, B. and Lai, E. Rapid pulsed field separation of DNA molecules up to 250 kb. Nucleic. Acids Res., *22:* 5366-5370, 1994.

156. Willmore, E., de Caux, S., Sunter, N. J., Tilby, M. J., Jackson, G. H., Austin, C. A., and Durkacz, B. W. A novel DNA-dependent protein kinase inhibitor, NU7026, potentiates the cytotoxicity of topoisomerase II poisons used in the treatment of leukemia. Blood, *103:* 4659-4665, 2004.

157. Rogakou, E. P., Nieves-Neira, W., Boon, C., Pommier, Y., and Bonner, W. M. Initiation of DNA fragmentation during apoptosis induces phosphorylation of H2AX histone at serine 139. J. Biol. Chem., *275:* 9390-9395, 2000.

158. Ward, I. M. and Chen, J. Histone H2AX is phosphorylated in an ATR-dependent manner in response to replicational stress. J. Biol. Chem., *276:* 47759-47762, 2001.

159. Ward, I. M., Minn, K., Jorda, K. G., and Chen, J. Accumulation of checkpoint protein 53BP1 at DNA breaks involves its binding to phosphorylated histone H2AX. J. Biol. Chem., *278:* 19579-19582, 2003.

160. Chan, D. W., Gately, D. P., Urban, S., Galloway, A. M., Lees-Miller, S. P., Yen, T., and Allalunis-Turner, J. Lack of correlation between ATM protein expression and tumour cell radiosensitivity. Int. J. Radiat. Biol., *74:* 217-224, 1998.

161. Sancar, A. DNA excision repair. Annu. Rev. Biochem., *65:* 43-81, 1996.

162. Horton, J. K., Prasad, R., Hou, E., and Wilson, S. H. Protection against methylation-induced cytotoxicity by DNA polymerase beta-dependent long patch base excision repair. J. Biol. Chem., *275:* 2211-2218, 2000.

163. Liu, L., Nakatsuru, Y., and Gerson, S. L. Base excision repair as a therapeutic target in colon cancer. Clin. Cancer. Res., *8:* 2985-2991, 2002.

164. Canman, C. E., Lawrence, T. S., Shewach, D. S., Tang, H. Y., and Maybaum, J. Resistance to fluorodeoxyuridine-induced DNA damage and cytotoxicity correlates with an elevation of deoxyuridine triphosphatase activity and failure to accumulate deoxyuridine triphosphate. Cancer Res., *53:* 5219-5224, 1993.

165. Kaneko, Y. and Tsukamoto, A. Gene therapy of hepatoma: bystander effects and non-apoptotic cell death induced by thymidine kinase and ganciclovir. Cancer Lett., *96:* 105-110, 1995.

166. Tomicic, M. T., Thust, R., and Kaina, B. Ganciclovir-induced apoptosis in HSV-1 thymidine kinase expressing cells: critical role of DNA breaks, Bcl-2 decline and caspase-9 activation. Oncogene, *21:* 2141-2153, 2002.

167. Greenberg, N. M., DeMayo, F., Finegold, M. J., Medina, D., Tilley, W. D., Aspinall, J. O., Cunha, G. R., Donjacour, A. A., Matusik, R. J., and Rosen, J. M. Prostate cancer in a transgenic mouse. Proc. Natl. Acad. Sci. U S A, *92:* 3439-3443, 1995.

168. Foster, B. A., Gingrich, J. R., Kwon, E. D., Madias, C., and Greenberg, N. M. Characterization of prostatic epithelial cell lines derived from transgenic adenocarcinoma of the mouse prostate (TRAMP) model. Cancer Res., *57:* 3325-3330, 1997.

169. Halicka, H. D., Huang, X., Traganos, F., King, M. A., Dai, W., and Darzynkiewicz, Z. Histone H2AX Phosphorylation After Cell Irradiation with UV-B: Relationship to Cell Cycle Phase and Induction of Apoptosis. Cell Cycle, *4*, 2005.

170. Carrasco, C., Facompre, M., Chisholm, J. D., Van Vranken, D. L., Wilson, W. D., and Bailly, C. DNA sequence recognition by the indolocarbazole antitumor antibiotic AT2433-B1 and its diastereoisomer. Nucleic Acids Res., *30:* 1774-1781, 2002.

171. Bible, K. C., Bible, R. H., Jr., Kottke, T. J., Svingen, P. A., Xu, K., Pang, Y. P., Hajdu, E., and Kaufmann, S. H. Flavopiridol binds to duplex DNA. Cancer Res., *60:* 2419-2428, 2000.

172. Tsuruo, T., Naito, M., Tomida, A., Fujita, N., Mashima, T., Sakamoto, H., and Haga, N. Molecular targeting therapy of cancer: drug resistance, apoptosis and survival signal. Cancer Sci., *94:* 15-21, 2003.

173. Immonen, A., Vapalahti, M., Tyynela, K., Hurskainen, H., Sandmair, A., Vanninen, R., Langford, G., Murray, N., and Yla-Herttuala, S. AdvHSV-tk gene therapy with intravenous ganciclovir improves survival in human malignant glioma: a randomised, controlled study. Mol. Ther., *10:* 967-972, 2004.

VITA

Christina Elizabeth Ahn

Education

Ph.D. Biomedical Sciences
Eastern Virginia Medical School and Old Dominion University, 2005
Department of Microbiology and Immunology
700 W. Olney Rd.
Norfolk, VA 23507

B.A. Biology and Classics
Austin College, 1999

Home address:

910 Constitution Dr. Apt 218
Durham, NC 27705